



Norwegian University of
Science and Technology

Experimental and Numerical Study of Oil- Water Dispersions at the Inlet of a Pipe Separator

Ellen Kristine Knudsen Ellertsen

Petroleum Geoscience and Engineering

Submission date: June 2018

Supervisor: Milan Stanko, IGP

Norwegian University of Science and Technology
Department of Geoscience and Petroleum

Summary

In the production of petroleum, it is normal to not only produce oil and gas, but also to produce water. Over the lifetime of the fields, the amount of water produced will normally increase. The additional water will later have to be separated from the oil and gas, either at the surface or down on the seabed. If the processing facilities cannot handle these higher rates of water, the producing line has to be choked back, which will result in a lower production of oil. Increasing the efficiency of oil-water separators and develop subsea separation solutions will therefore allow to maintain, or increase the fields production rate, hence reducing cost. The separation performance is affected, among other things by the droplet size. This thesis is focused on studying the characteristics of oil-water flow and droplet size distribution at the inlet of an oil-water pipe separator for varying rates of oil and water.

Experimental tests were performed at the inlet section of an inline oil-water pipe separator developed at NTNU (SUBPRO project 2.9). Four main tasks were performed. First, measurements of the physical properties of the oil and water were performed. Second, the flow pattern map of the system was determined varying the flow rates and water cuts. Third, the droplet size distribution was computed by analyzing and processing pictures of the flow taken with a PVM probe. The analyzing of the images were performed manually and automatically using a computational routine written in Matlab. The droplet size distribution was quantified for several flow rate combinations, two water cuts, two probe positions and two valve openings. Additionally, the droplet size distribution data was compared with four statistical distributions and models; Log-Normal Distribution, Upper-Limit Log-Normal Distribution, and different breakage models.

It was found that the flow system with the valve fully open had larger droplet sizes for flow rates in the higher range. However, with the valve 50% open the droplet sizes got smaller for flow rates in the higher range. With more water present in the system the droplet size decreased. The droplet sizes for oil-in-water were smaller than the droplet sizes for water-in-oil. The Brauner breakage model and the Upper-Limit Log-Normal Distribution gave the best representation of the data. The experimental data gathered has a great value for future validation of multiphase and dispersion models, thus improving their predictability and quantifying and reducing their inaccuracies.

Sammendrag

Ved produksjon av petroleum er det vanlig at det blir produsert vann i tillegg til den ønskede oljen og gassen. I løpet av et felts levetid, vil mengden vann som produseres ofte øke. Det produserte vannet må separeres fra oljen og gassen. Separasjonen kan enten gjøres på plattform eller på havbunnen. Dersom utstyret som skal prosessere oljen ikke har tilstrekkelig kapasitet til å håndtere de store vannmengdene, må produksjonsstrømmen strupes. Dette vil resultere i en lavere produksjon av olje. Ved å øke effektiviteten til olje-vann separatorer og ved å videreutvikle subsea separasjonsmetoder vil kostnadene kunne reduseres, samt bidra til å opprettholde eller øke feltets produksjonsrate. Separasjonstiden for to væsker er blant annet avhengig av dråpestørrelsen til de dispergerte dråpene i den kontinuerlige fasen. Denne masteroppgaven har i all hovedsak fokus på karakteriseringen av olje-vann strømning. Dråpestørrelsesfordelingen ved innløpet til en olje-vann rørseparator ved forskjellige rater for olje og vann har også blitt undersøkt.

De eksperimentelle testene ble utført ved innløpet til en olje-vann rørseparator, utviklet på NTNU (SUBPRO prosjekt 2.9). Fire oppgaver ble gjennomført. Først ble de fysiske egenskapene til oljen og vannet bestemt. Videre ble det laget et strømningskart for ulike strømningsrater og vannkutt. Deretter ble dråpestørrelsesfordelingen beregnet ved å prosessere og analysere bilder tatt med et PVM-kamera. Bildene ble tatt ved innløpet til rørseparatoren. Analysen av bildene ble gjort manuelt, men også automatisk ved å bruke et dataprogram som er skrevet i Matlab. Dråpestørrelsesfordelingen ble funnet ved ulike strømningsrater, to vannkutt, to kameraposisjoner og ved to ventilåpninger. I tillegg ble data fra dråpestørrelsesfordelingen sammenlignet med fire statistiske distribusjoner og modeller: Log-normal fordeling, øvre-grense log-normal fordeling og forskjellige dråpebrytningsmodeller.

Funnene viste at fluidsyste­met med ventilen fullstendig åpen hadde voksende dråpefordelinger ved økende strømningsrate. Den motsatte trenden ble funnet for fluidsyste­met der ventilen var 50% åpen. Da ble dråpestørrelsen mindre for økende strømningsrater. Resultatet viste også at dråpestørrelsen ble mindre med økte mengder vann tilstede i syste­met. Dråpestørrelsen for olje i vann var mindre enn dråpestørrelsen for vann i olje. Dataene ble best presentert ved å benytte Brauners brytningsmodell samt den øvre-grense log-normal fordelingen. De eksperimentelle dataene som ble funnet har en verdi for videre validering av disperger­te- og flerfase-modeller da de kan brukes til å forbedre modellenes forutsigbarhet og nøyaktighet.

Acknowledgements

This master thesis has been written under the Department of Geoscience and Petroleum at NTNU, Trondheim, spring 2018. The master thesis is the final product to be delivered as a part of the Petroleum Geosciences and Engineering 5 years Master's degree program, where the specialization has been Petroleum Production.

First of all, I will thank my supervisor Milan Stanko for letting me work on a very interesting project, the SUBPRO project 2.9. Your help and guidance with the thesis work has been highly appreciated. Thank you to PhD candidate Håvard Skjefstad for letting me work with him on this interesting project. I really appreciate all the time, help and guidance you have contributed to the thesis work.

I will send a special thanks to Heiner Schümann for the help and time he has invested on the project. You have been a great help! For this, I am very grateful.

A great thanks to Roger Overå for all the help with the experiments that have been performed in the Reservoir Lab. And thank you to Noralf Vedvik and the others at the work-shop for always finding solutions to my problems and always being so welcoming and happy.

And finally I would like to thank my Family for all of the support and motivation you have given me throughout my studies. Thank you to my friends that make the busy and stressful days easier and more fun. Last but not least, I would like to give thanks to Josh for all the support and motivation, and for the help you have given me with my work.

Ellen Kristine K. Ellertsen
Trondheim, June 2018

Contents

Summary	i
Sammendrag	iii
Acknowledgements	v
List of Figures	xi
List of Tables	xiii
Nomenclature	xviii
1 Introduction	1
1.1 Previous work	2
1.1.1 Literature	2
1.1.2 Experiments performed at SINTEF facilities	3
1.2 Objectives	3
1.3 Thesis Overview	4
2 Theory	7
2.1 Separation of Oil and Water	7
2.1.1 SUBPRO Project 2.9	9
2.2 Droplet Size	10
2.2.1 Droplet diameter	12
2.2.2 Droplet size distribution	13
2.2.3 Droplet break-up over valves	15
2.2.4 Parameters that effect droplet size	16
2.3 Droplet Size Measurement Methods	16
2.4 Horizontal Flow Patterns for oil-water flow	19
2.4.1 Stratified flow	19
2.4.2 Dispersed flow	20
2.4.3 Annular flow	21
2.4.4 Plug and Bubble flow	21
2.5 Flow Pattern Maps for Oil and Water Flow	22

2.6	Numerical models	23
2.6.1	Log-Normal Distribution	23
2.6.2	Upper-Limit Log-Normal Distribution	24
2.6.3	Hinze and Brauner - breakage models	25
2.6.4	Droplet breakup over restrictions	26
2.7	Error estimation	27
3	Experiment setup	29
3.1	Separator Loop	29
3.2	Mounting of PVM	30
3.3	Calibration errors	31
3.4	Image processing	32
3.4.1	Matlab routine	32
3.4.2	Manual counting	33
4	Experiment Execution	35
4.1	Fluid properties	35
4.1.1	Density	35
4.1.2	Viscosity	36
4.1.3	Interfacial tension	38
4.2	Flow Pattern Mapping	41
4.2.1	Method	41
4.2.2	Result and Discussion	42
4.2.3	Sources of error	45
4.3	Characterizing Droplet Size Distribution	46
4.3.1	Method	46
4.3.2	Improvement to Matlab code	49
4.3.3	Result and discussion	55
4.3.4	Sources of error	71
5	Numerical Modeling	73
5.1	Method	73
5.1.1	Log-Normal Distribution	73
5.1.2	Upper-Limit Log-Normal Distribution	73
5.1.3	Hinze and Brauner - breakage models	75
5.1.4	Droplet breakup over restrictions	75
5.2	Results and discussion	75
5.2.1	SINTEF Data	75
5.2.2	NTNU Data	78
6	Conclusion	83
7	Recommendations for Further Work	85
	Bibliography	87
	Appendices	95

A Pictures of Flow	95
B User manuals	103
B.1 Matlab program	103
B.2 Edited part of the Matlab code	103
C Matlab Code	105
C.1 Matlab routine that was edited	106
C.2 Function to get data from flow rates	107
C.3 Log-Normal Distribution	108
C.4 Upper-Limit Log-Normal Distribution	109
C.5 Hinze and Brauner breakage models	111
C.6 Droplet breakup over restrictions	113
D Density experiment	115
E PDF's	117
E.1 Risk Assessment	118
E.2 Hagenbach constant	120
E.3 Camera mount	121
E.4 Capillary Viscometer Certificate	123

List of Figures

2.1.1	Gravitational separator for gas, oil and water	7
2.1.2	Forces acting on an oil droplet dispersed in water	8
2.2.1	Surface tension and pressure acting on a droplet	10
2.2.2	Different ways of plotting the droplet size distributions	14
2.2.3	Number and volume weighted distribution	15
2.3.1	PVM with dimensions	17
2.3.2	PVM probe with a 4 mm "hat"	18
2.3.3	PVM placed at a 45° angle	18
2.4.1	Stratified flow patterns	19
2.4.2	Dispersed flow patterns	20
2.4.3	Annular flow patterns	21
2.4.4	Bubble flow patterns	21
2.5.1	Different flow pattern maps for oil-water flow	22
2.6.1	Orifice illustration with flow and pressure field	27
3.1.1	Flow and instrumentation diagram for the SUBPRO rig	29
3.2.1	PVM camera mount	30
3.4.1	Processed images from running Matlab routine	32
3.4.2	Matlab program interface	33
3.4.3	Manually counting using ImageJ	34
4.1.1	Cannon-Fenske capillary viscometer filled with oil	36
4.1.2	Image of the droplet where tests were performed	38
4.1.3	Pendant drop on needle used to calculate IFT	39
4.1.4	Plot for number of measurements vs. IFT	40
4.2.1	Horizontal oil-water flow patterns	42
4.2.2	Images of the different flow patterns that were characterized	43
4.2.3	Flow pattern map plotted for superficial velocities	44
4.2.4	Flow pattern map plotted for water cut and mixed flow velocity	44
4.2.5	Flow pattern map plotted for water cut and mixed flow rate	45
4.3.1	Images of the flow used to find how far down in the pipe the probe should be placed	46
4.3.2	Measured heights to find the distance to place the PVM in the pipe	47
4.3.3	Tested flow rates and water cut	48

4.3.4	Droplets from valve 50% open counted manually	49
4.3.5	Unwanted droplet placement scenarios	50
4.3.6	Example of an overestimated droplet	50
4.3.7	Matlab routine compared with manual counting	51
4.3.8	Example of Matlab detecting and creating an overestimated droplet	52
4.3.9	Example of number of droplets recognized by Matlab	53
4.3.10	Comparison of measurements performed manually with measure- ments using Matlab routine	54
4.3.11	Images of the flow taken with the PVM at the top part of the pipe	56
4.3.12	Images of the flow taken with the PVM at the bottom part of the pipe	57
4.3.13	Different types of DSD plot	58
4.3.14	WC30 bottom of pipe for all flow rates, Dw/o	59
4.3.15	WC70 bottom of pipe for all flow rates, Do/w	60
4.3.16	WC30 top of pipe for all flow rates, Dw/o	61
4.3.17	WC70 top of pipe for all flow rates, Do/w	62
4.3.18	Cumulative log-plot of all test points for each flow rate	63
4.3.19	Total flow rate plotted against d_{max}	65
4.3.20	Total flow rate plotted against d_{32}	66
4.3.21	Change in flow system when using ball valve 50% open	67
4.3.22	Images taken of the flow with the PVM, 50% valve opening	68
4.3.23	DSD for valve 50% and 100% open counted manually	69
4.3.24	Comparing how the droplet size distributions vary for 50% and 100% valve opening	70
5.1.1	Cubic equation crossing the 90th percentile in two points	74
5.2.1	Comparing Log-Normal Distribution with real data	76
5.2.2	Best LND fit for 100 mbar and 500 mbar	76
5.2.3	Cubic fitted curve to droplet diameter vs $100v$	77
5.2.4	Best and worst fit using ULLN	77
5.2.5	Best and worst fit using LND	79
5.2.6	Comparing quadratic and cubic fit to data	79
5.2.7	Best and worst fit using ULLN	80
D.0.1	Pycnometer filled with oil	115

List of Tables

4.1.1	Results from viscosity experiment	37
4.1.2	Result from pendant drop measurements	39
4.2.1	Test matrix for flow pattern map	41
4.3.1	Test matrix for DSD measurements	47
4.3.2	Description of different droplet placements	49
4.3.3	d_{max} and d_{32} results from Matlab routine from tests with valve 50% open	54
4.3.4	Numbers of droplets counted using Matlab routine	58
4.3.5	Results for d_{max} for all test points	64
4.3.6	Results for d_{32} for all test points	66
4.3.7	d_{max} and d_{32} from manual counting droplets from experiment with valve 50% open	70
5.2.1	Comparison of maximum droplet diameters	78
5.2.2	Maximum droplet diameter using Hinze and Brauner model	80
D.0.1	Results from density measurements	116

Nomenclature

Abbreviations

Do/w	Dispersed oil-in-water
Do/w + Dw/o	Dispersed layer of oil-in-water coexisting with a dispersed layer of water-in-oil
Do/w + w	Dispersed oil-in-water with a layer of water at the bottom of the pipe
DSD	Droplet size distribution
Dw/o	Dispersed water-in-oil
Dw/o + o	Dispersed water-in-oil with a layer of oil at the top of the pipe
FBRM	Focused Beam Reflectance Measurements
ID	Inner diameter
IFT	Interfacial Tension
LND	Log-Normal Distribution
o/w	Oil-in-water
OD	Outer diameter
PVM	Particle Vision Microscope
SM	Stratified flow with mixing on the interface
ULLN	Upper-Limit Log-Normal Distribution
w/o	Water-in-oil
WC	Water cut/Water fraction

Greek Symbols

α	The probability that the mean will fall outside the confidence interval	
β	Uncertainty	
δ	Size distribution parameter	[–]

ϵ_d	Fraction of the dispersed phase	
γ	Mean of the population	
μ	Viscosity	[p]
ν	Dimensionless function of droplet diameter	[-]
ω	Intervals for variables when calculating uncertainty	[-]
ρ	Density	[kg/m^3]
σ	Surface tension	[N/m]
τ	Student-t distribution	
θ	The "width" of the Log-Normal Distribution	[-]
ε	Energy dissipation rate	[m^2/s^3]
ϑ_x	Hagenbach correction constant	[s]

Other

$100v$	$100 \times v$	
\bar{x}	Mean value	
Δp_{perm}	The permanent pressure drop	[Pa]
Δx_{perm}	The length of the orifice zone	[m]
U_p	Mean velocity in the restriction	[m/s]
OH	Distance along the outside of the pipe	[m]
Re	Reynolds number	[-]
We	Weber number	[-]
We_{crit}	Critical Weber number	[-]

Roman Symbols

ℓ_k	Kolmogotov microscale	[m]
\tilde{C}_H	Tunable constant	[-]
b	Parameter in Log-Normal Distribution	
v	The volume fraction of droplets having diameter < d	
x	Values of a sample data	
A	Cross section area	[m^2]
a	Parameter in Upper-Limit Log-Normal Distribution	[-]
C	Constant in Brauner breakage model	[-]

c	Instrumental error	
D	Pipe diameter	[m]
d	Droplet diameter	[m]
f	Wall friction factor	[-]
g	Gravitational constant	[m/s ²]
H	Vertical distance inside pipe	[m]
K	Measuring sphere constant	[mm ² /s ²]
L	Distance between centre of droplet one and two	[m]
l	Distance between measuring point and needle point	[m]
N	Finite number of elements for a population	
n	Constant in Brauner breakage model	[-]
n	Number of measurements	
p	Pressure	[Pa]
q	Flow Rate	[m ³ /s]
R	A linear function of <i>n</i> independent variables	
r	Radius of sphere/droplet	[m]
S	Sample standard deviation	
T	Temperature	[°C]
t	Time	[s]
U	Velocity in the system	[m/s]
u	Velocity of the fluid/droplet in the system	[m/s]
V	Volume of a sphere/ volume of a droplet	[m ³]
v	Independent variables in R	
z	Parameter in Upper-Limit Log-Normal Distribution	[-]

Subscripts

0	Reference diameter
10	10th percentile
32	The Sauter mean diameter
43	De Brouckere mean diameter
50	50th percentile

90	90th percentile
c	Continuous phase
d	Dispersed phase
m	Mixed phase
o	Oil
s	Superficial
w	Water

Chapter 1: Introduction

In the production of oil and gas from the reservoirs it is common to not only get the petroleum products, but also to produce water. In fields that have not been producing for long, the produced water comes from water that already exists in the reservoirs, like water from aquifers. During the production of oil and gas from the fields, the pressure in the reservoir will drop. To maintain the pressure in the reservoir water can be injected, which in addition can increase the recovery of oil from the reservoir. The injected water will after some time "break through" the reservoir, and the additional water will be a part of the oil production (Norsk olje og gass 2017). The production of water will therefore increase for more mature fields. Norsk olje og gass (2017) have published numbers showing that the ratio of the produced water, to produced oil on the Norwegian continental shelf has increased over the years, due to production from more mature fields. The production was more than two times more water to oil in 2015, but the ratio decreased in 2016 possibly due to the opening of new fields.

The additional volumes of water that are produced from the reservoirs require the processing facilities to handle larger volumes of produced fluids. These additional water volumes and higher rates could therefore bottleneck the separators, which would result in choking back the liquid production, hence, a lower production of oil (Skjefstad & Stanko 2017). After the water is separated from the oil it can be re-injected into the reservoir, or discharged into the sea. There are strict purity requirements to the water that is going to be discharged into the sea. The Norwegian government has a requirement of less than 30 ppm oil in the discharged water (Norsk olje og gass 2017). To invest in equipment to handle the large volumes of water, and to process and clean the water to meet the restrictions is an expensive part of petroleum production. It costs the petroleum industry billions of NOK (Norsk olje og gass 2017).

When water and oil flow together in the production lines they can start to mix and create a dispersion of droplets of oil-in-water or water-in-oil. For higher water cuts and flow rates, the flow will be more dominated by dispersed oil-in-water (Van der Zande & Van den Broek 1998). In the transportation line, from the well to the separators the producing liquids will pass tubing, connections, valves and pumps which will contribute to droplet break-up resulting in smaller droplets (Van der Zande & Van den Broek 1999). These small droplets dispersed in the fluid are

more difficult, and take a long time to separate due to the need of long residence time in the separator. This will affect the separation efficiency for the topside and subsea oil-water separators. The knowledge of the sizes of these droplets and the droplet distribution in a dispersion is therefore an important parameter to determine when designing oil-and water separators (Fossen & Schümann 2017, Van der Zande & Van den Broek 1998). Models and commercial simulators used to predict droplet sizes normally works well within the range of measurements. When tested outside the range of measurements, there might be a deviation from the measured data. Due to this, there is a need for experimental data measured in a controlled environment that can be later used to validate and improve models.

1.1 Previous work

1.1.1 Literature

Since the droplet size distribution (DSD) is such an important parameter regarding separation of water and oil, there are several authors that have done research on this topic. Brauner (2003) wrote a thorough description of liquid-liquid flow. She described different flow patterns, and how the liquids behaved. She also introduced several models, where for this thesis the model to predict the largest droplet size in a dense dispersion is the most relevant. The model was based on the model for dilute dispersions, made by Hinze in 1995 (Brauner 2003).

Different measurement methods have been used to find the droplet size distribution. Mugele & Evans (1951) looked at droplet size distributions in sprays. They looked at different distribution equations, and formulated a new equation; the Upper-limit equation. The equation was applied for a wide variety of data for sprays, but also tested for other dispersions. They found that the model worked better, than other models. Angeli & Hewitt (2000*b*) performed an experimental study of dispersions of kerosene (Exxol D80) and water. The droplet distribution was found with a video-recording technique using an endoscope. Both the upper-limit log-normal distribution and the Rosin–Rammler distribution were used, where the Rosin–Rammler distribution gave the best fit.

Fossen & Schümann (2017) used a Cauty InFlow camera to study droplet breakup in a two-phase (mineral-)oil and water flow. It was found that the pressure drop determined the droplet size downstream of the valve more than the flow rate, which had much less effect. Two models for droplet breakup were also compared. The model based on turbulence in the dissipation zone gave the best fit. Ellertsen (2017) did also find the droplet size distribution using a Cauty InFlow camera. The droplet size distribution for oil (Exxol D60) and water (mix of glycerol and water) was determined downstream of a valve. It was found that the droplet sizes got smaller for higher pressure drops, and larger with increasing water cuts.

1.1.2 Experiments performed at SINTEF facilities

Ellertsen (2017) performed experiments to measure the droplet size distribution of oil-water mixtures at the SINTEF Multiphase Flow Laboratory at Tiller. In this thesis work the data that was found will be compared with statistical distributions and models in chapter 5. The experimental setup and results are explained below.

The experiments performed at SINTEF were executed at a small scale mini-flow loop (12 mm ID) using Exxol D60 and water (a mix of glycerol and water with 20 cp at 23°C). The oil and water were mixed at the inlet, before passing a valve that worked as a shear zone, and created a higher pressure drop where droplet break-up appeared. Images of the flow were recorded using a Cauty InFlow camera that was connected to the loop (the fluid flows in a gap in the camera, between the camera lens and a light source). Tests were performed at different pressure drops (25, 100 and 500 mbar) and water cuts. The DSD was found by counting droplets manually, using ImageJ. For each test 500 droplets were counted to find the droplet size distribution. It was found that both the pressure drop and water cut affect the droplet size distribution. The droplet sizes got smaller for higher pressure drops, and larger for increasing water cuts. It was found that to count 500 droplets was sufficient to get a good measurements of d_{32} , but it should be counted more for good d_{max} measurements.

1.2 Objectives

The research done in this thesis is performed to give a deeper understanding of the fluid system used in a rig build for SUBPRO research activities of project 2.9. The results can be used for calculations, a deeper understanding of the properties and behaviors of the fluid system in the rig and for further research. The thesis has four objectives. The first objective is to measure physical properties (density, viscosity and interfacial tension) of the oil and water used for the experimental tests. The second objective is to characterize the flow patterns of the oil-water mixture at the inlet of the separator for different flow velocities and water cuts. This will be used to determine the flow pattern map. The third, and main objective, is to characterize the droplet dispersion of oil-in-water and water-in-oil at the inlet of the inline separator. This will be performed by counting and measuring droplets from images of the flow taken with a PVM camera probe. Two methods will be employed to process the images, manual counting and automatic counting using a computational routine. The results of the two methods will be compared and studied. The tests will be performed at two different water cuts (30% and 70%), two different valve openings (100% and 50% open), at two positions in the pipe and for nine different mixed flow rates between 300-700 L/min. The last objective is to compare the results with numerical functions and models. Two sets of data will be compared with the numerical models and functions; data from tests performed at SINTEF and data from the tests performed at the rig at NTNU. Four statistical distributions and models will be compared; Log-Normal Distribution, Upper-Limit Log-Normal Distribution, and different breakage models.

1.3 Thesis Overview

This master thesis is made up of seven chapters. A description of the set-up of the chapter and the main topics for each chapter is written below.

Chapter 1 is an introduction chapter. Previous work done by other researches are introduced, and the work that was performed at SINTEF in the fall of 2017 is presented.

Chapter 2 is a theory chapter where the reader will get an introduction to the necessary background knowledge needed to understand the thesis. The chapter will introduce theory about droplets and a droplet measuring method. The PVM that will be used to record pictures of the flow in chapter 4 will be presented. Flow patterns and flow pattern maps will be described, and the four statistical distributions and models that will be tested in chapter 5 will be described. Some sections in the chapter have been taken from the Specialization project report, Ellertsen (2017), that was written in the fall of 2017. The sections taken from the report are:

- Section 2.1 Separation of Oil and Water - only minor editing.
- Section 2.2 Droplet Size - Here about 50% is taken from the report.
- Section 2.2.1 Droplet Diameter - The parts about De Brouckere mean is new.
- Section 2.2.2 Droplet size distribution - About 50% is taken from the report.
- Section 2.2.3 Droplet break-up over valves - only minor editing.
- Section 2.2.4 Parameters that effect droplet size - only minor editing.
- Section 2.3 Droplet Size Measurement Methods - about 50% is taken from the report.
- Section 2.4 Horizontal Flow Patterns for oil-water flow - only minor editing.

Chapter 3 explains the setup for the experiments that will be performed in chapter 4. The rig where the experiments will be performed is explained, with the setup for the PVM camera. The different instruments used to measure different flow parameters will be introduced, and calibration equations will be given. Two different ways to process the images recorded by the PVM camera of the flow will be described. An automatically counting using a computational routine written in Matlab and manual counting.

Chapter 4 presents all the experiments that were performed in the thesis. The chapter is divided into three sections where each section describes an experiment. Each experiment is divided into parts with first describing the method used in the experiment, before the result are presented and discussed. Section 4.1 present the experiments performed to find the fluid properties (density, viscosity and interfacial tension). Section 4.2 present the experiment to find the flow pattern map, and

section 4.3 present the experiment to find the droplet size distribution using the rig described in chapter 3.

Chapter 5 present the results for the statistical distributions and models that were modeled for two sets of data. First, the method used to test the different models in Matlab is explained. Then comes the result and discussion part, which is further divided in two parts. First the result of the data from the SINTEF experiment, presented in chapter 1 will be presented. Three distributions and models are tested: Log-Normal Distribution, Upper-Limit Log-Normal Distribution and the Droplet breakup over restriction model. Secondly, the results from the tests performed on the data from the rig at NTNU, presented in chapter 4, will be presented. Three distributions and models are tested here as well: Log-Normal Distribution, Upper-Limit Log-Normal Distribution and the Hinze and Brauner breakage models.

Chapter 6 presents the conclusion of the thesis work.

Chapter 7 propose some recommendations for further work.

Chapter 2: Theory

The droplet size is an important parameter to consider when designing oil-water separators. This chapter is written to give a better understanding of why this is. It will also give the reader an introduction to the necessary theory needed to understand the thesis.

2.1 Separation of Oil and Water

The gravity force can be used to separate different fluids that are not miscible. The fluids are separated because of their difference in density and weight, so liquids with the same density will be separated in a layer. The heaviest liquid will settle on the bottom, and lighter liquids will separate over top. The different liquids can then be tapped out in different parts of a separator. For a water and oil separator the oil will settle on top of the water because the oil has a lower density. An example of this can be seen in Fig. 2.1.1. The separator can either be a two-phase separator that separates oil-water, oil-gas or water-gas, or a three-phase separator that separates both liquids and gas. It is also possible to have a four-phase flow with sand in the fluid system, which would also have to be separated out.

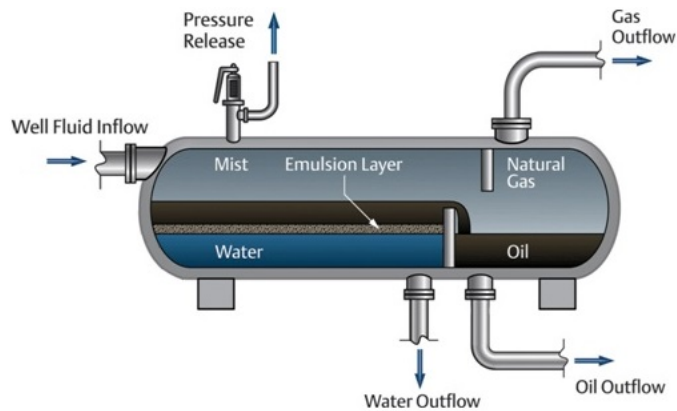


Figure 2.1.1: Gravitational separator for gas, oil and water ¹

For separation processes with water and oil, the water droplets that are dispersed in oil will sink through the oil-layer and create a water layer underneath. The oil droplets that are dispersed in the water layer will rise through the water-layer and create an oil layer above. The time it takes for the droplets to travel through the other phase is called settling time.

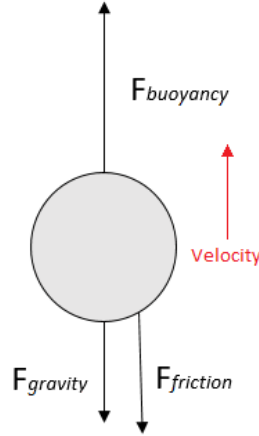


Figure 2.1.2: Forces acting on an oil droplet dispersed in water

At a steady state settling velocity there will be three forces acting on the droplet, which can be seen in Fig. 2.1.2. The gravity is working with a downward force, the buoyant force is working with an upwards force and there is a shear force between the two liquids. Balancing these three forces and solving for the friction force, gives an equation known as Stokes law which is applicable for laminar flows (Cengel & Cimbala 2014). Solving Stokes law in terms of the velocity will give the speed of a droplet rising or sinking in a fluid. For an oil droplet rising in a water layer, the velocity of the droplet, u_o , can be expressed as:

$$u_o = \frac{gd^2}{18} \frac{(\rho_w - \rho_o)}{\mu_w} \quad (2.1.1)$$

The sinking velocity of a water droplet, u_w , dispersed in oil can be expressed as:

$$u_w = \frac{gd^2}{18} \frac{(\rho_w - \rho_o)}{\mu_o} \quad (2.1.2)$$

in the equations g is the gravity force, d is the droplet diameter, μ is the viscosity of either water or oil, and ρ is the density of either water or oil.

¹Modified picture from Emerson (2014)

Eq. (2.1.1) and (2.1.2) can be used to determine the time it will take for droplets to rise or sink when being dispersed in a layer of the other fluid. The settling time will be dependant on the distance the drop has to travel, and the diameter of the droplet. Knowing the settling time can further be used to find the residence time (the time liquids have to remain in a separator for the fluids to separate) which can be used to determine the dimensions of a separator. In the equations (Eq. (2.1.1) and (2.1.2)) the diameter is squared, which means it will have a large impact on the settling time. Large droplets will travel faster through the fluid layer, and will be separated faster, than the smaller droplets. Knowing the size of the droplets dispersed in a fluid, will therefore be essential when finding the residence time.

The vertical distance in a separator will also effect the settling time of the liquids. The larger the vertical distance of the layer a droplet has to travel through, the longer time it will take to separate the liquids. For an inline separator the diameter of the pipe will be the maximum distance the drop needs to rise or sink. This distance is relatively small compared to large tank separators, resulting in the need of a lower separation time for an inline separator. Because of this, the separation can be done at higher flow velocities for the inline separator. The inline separator also favours a more compact design (Skjefstad & Stanko 2017) which can be integrated as a part of the already existing transportation line or subsea structure. This will favor weight reduction and lower cost (FMC Technologies 2018). The rig that is used for experiments in this thesis consists of a multi-branch pipe separator, which will favor the conditions mentioned.

2.1.1 SUBPRO Project 2.9

The main objective of project 2.9 is to study experimentally, and with models, the performance of a multi-branch pipe separator. It is going to separate the produced water from the producing oil (Skjefstad & Stanko 2017). The PhD candidate responsible for the project is Håvard Skjefstad.

SUBPRO stands for Subsea Production and Processing, and is a research centre for innovative-based research within subsea-research and production. SUBPRO combine competence from the industry with research performed at NTNU (SUBPRO 2017).

2.2 Droplet Size

When two immiscible liquids flow in the same pipe, an interface or membrane between the two liquids will be created. The pulling force that works on the membrane is created by the attractive forces between the different molecules that are creating a tension between the two liquids (Cengel & Cimbala 2014). This tension force acting per unit length across the created membrane, is defined as the surface tension (Frohn & Roth 2000). The surface tension, σ , therefore represents the force needed to stretch or contract a surface area by a unit amount.

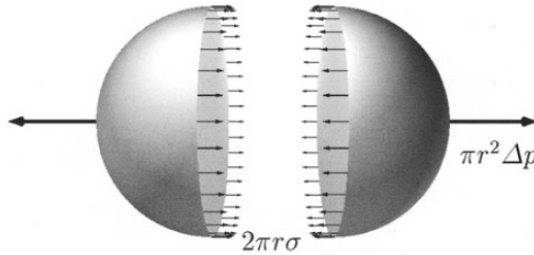


Figure 2.2.1: Surface tension acting on the circumference in equilibrium with the force created by pressure difference inside and outside the drop ²

The forces acting on a single drop can be seen in Fig. 2.2.1. If a force balance is performed on the droplet it will give an equilibrium between the pressure forces and the surface tension forces known as the Young and Laplace Equation (2.2.1). Assuming the two radii are equal to each other (spherical surface) will give a special case of the equation, see Eq. (2.2.2) (Sahimi 2012).

$$\Delta p = \sigma \left(\frac{1}{r_1} + \frac{1}{r_2} \right) \quad (2.2.1)$$

$$\text{for } r_1 = r_2$$

$$\Delta p = \frac{2\sigma}{r} \quad (2.2.2)$$

Here Δp is the pressure difference between the two mediums. r_1 and r_2 are the principal radii of curvature.

A spherical shape has the minimum surface area that can be created for a given volume, and this shape is created in a droplet by the forces seen in Eq. (2.2.1). On the surface of a liquid is a net attractive force acting on the molecules that will try to pull the molecules on the surface towards the interior of the liquid. The molecules below the surface creates a repulsive force from being compressed. These two forces will balance each other out, resulting in a minimizing of the surface area and create a spherical shape (Cengel & Cimbala 2014).

²Picture from (Frohn & Roth 2000)

For a droplet to stay intact, the surface tension force has to overcome the external shear forces that are trying to deform and break up the droplet into two or more daughter droplets. The maximum droplet size found in the system, will appear when the surface tension is still larger than the break-up forces. When external break-up forces are larger than the surface tension force, the droplet will break up. The ratio between the forces trying to break up the drop, and the restoring forces is known as the Weber number (Van der Zande & Van den Broek 1999, Walsh 2016). It is given as:

$$We = \frac{\rho U^2 d}{\sigma} \quad (2.2.3)$$

where U is the velocity in the system, d is the drop diameter, ρ is the density of the solution and σ is the interfacial tension.

Break-up of a drop will eventually happen for all droplets in a system if $We > We_{crit}$. The critical Weber number, We_{crit} , is the largest Weber number the drop can have before it will break up. When breaking up, the droplet diameter will decrease along with the Weber number. The breaking of droplets will continue until $We < We_{crit}$ for all droplets in the system (Van der Zande & Van den Broek 1999).

The mechanism that will make the droplet resist to break-up, as mentioned, is the surface tension. When droplets of the same fluid collide droplets will start to coalesce to create larger droplets. This happens if the droplets (of the dispersed phase) that collide get to be in contact long enough for the trapped fluid of the continuous phase to drain to a thickness where it will rupture (Angeli & Hewitt 2000a). The droplet size and amount of droplets in a system will be determined by a balance between the mechanisms that cause coalescence and breakup. These mechanisms are therefore important to understand when looking at droplet size distributions in a dispersed flow (Angeli & Hewitt 2000a). Mechanisms that deform droplets and create droplet break-up are large shear stresses, turbulent flow in the continuous phase and rapid accelerations in the flow (Brauner 2003). A turbulent flow is a chaotic flow with velocity fluctuations, which normally occurs at high flow velocities in pipes or from pumps and valves. The flow normally exist of different sized eddies, which are regions of rapid fluctuations and swirling fluid (Cengel & Cimbala 2014). It is the small-scale eddies that is a large contributor to the break up of the droplets in a flow. The eddies collide into the droplets which break them up to smaller droplets. The frequency of the eddy collisions and the energy dissipated in each collision might vary, and this together with the drop-drop collision frequency can determine the amount of droplet break-up that will appear (Walsh 2016).

In a dispersed flow these two opposite mechanisms will work alongside to either create larger droplets or break-up droplets into smaller ones. For a system with many droplets there will be a larger chance for droplets to meet and collide, which will lead to a higher coalescence frequency. Hence, the turbulent eddies in the system might separate the colliding drops, which will prevent the coalescence (Angeli & Hewitt 2000a). It is therefore a balance between the coalescence forces and the

break-up forces in the system, and at the same time a function of the amount of droplets in the system that will determine what droplet size distribution that will be found in the system.

2.2.1 Droplet diameter

The volume of a sphere is given by Eq. (2.2.4) and uses the sphere diameter (d) as input:

$$V = \frac{1}{6} \Pi d^3 \quad (2.2.4)$$

Here V is the volume of the sphere and d is the diameter.

In a dispersed flow the dispersed liquid will appear in the form of droplets, typically exhibiting multiple droplet sizes. As seen from Eq. (2.2.4), knowing the diameter distribution of the droplets will allow to estimate the liquid volume transported in the dispersed flow (Lovick et al. 2005). As mentioned in sec. 2.1, the size of a droplet will affect the time it takes to separate the droplet from the dispersed liquid. If the settling time of droplets is known and the length of time the fluid will be in a separator, then this can be used to find a critical droplet diameter of the fluid that will not be separated in time. This can then be used to find the volume of the liquid that is still dispersed in the fluid flow.

There are many ways to represent the characteristic droplet diameter from a measured distribution. In literature d_{min} , d_{max} and different types of mean diameters have been used. Some examples of mean diameters are De Brouckere mean diameter (Fossen & Schümann 2017), arithmetic mean diameter (Boxall et al. 2010) and Sauter mean diameter.

As seen above the maximum diameter, d_{max} , that can be seen in a flow, reflect the forces that is working in the system. The d_{max} can therefore be related to the characteristics of the system and how strong the internal forces in the fluids are.

When finding the mean of a distribution, there are many different ways this can be done. The simplest means, like adding all diameters and dividing by the number of droplets in the distribution, requires counting large numbers of droplets. When working with large volumes, the counting of all the droplets in the distribution will be very time consuming. Means that does not take into account the numbers of droplets measured are moment means, which is weighted towards the properties of the droplets. Two of the most known moment means are the Sauter mean and the De Brouckere mean (Rawle 2017).

Sauter mean distribution, d_{32} , has been used by several authors, Boxall et al. (2010), Fossen & Schümann (2017) and Angeli & Hewitt (2000b) to compare the droplet size distribution. It is often used in the case of oil-water dispersed flow.

The Sauter mean diameter is defined as:

$$d_{32} = \frac{\sum_{i=1}^n d_i^3}{\sum_{i=1}^n d_i^2} \quad (2.2.5)$$

where n is the number of drops counted in the distribution and d_i is the diameter of the drop i in the measured distribution.

The Sauter mean diameter can also be referred to as the surface area mean or the surface-volume mean. As the name indicates, it is the average diameter calculated as the volume-to-surface ratio. The physical meaning of this is that the Sauter mean diameter for a distribution of spherical droplets with different diameters, will be equal to the diameter of a droplet from an equal distribution with identical spherical droplets. The number of droplets for the two systems are different, but the total area and volume of the two systems will be the same (Kowalczyk & Drzymala 2016).

The De Brouckere mean, d_{43} , can also be referred to as the volume or mass moment mean. As the name indicates the De Brouckere mean diameter take the volume or weight of the spheres into account. It express the size of the droplets that account for the bulk of the volume (Malvern-Instruments 2015). The De Brouckere mean diameter is not as commonly reported as the Sauter mean diameter, but Schümann et al. (2015) have reported and compared values in their report. The De Brouckere mean can be expressed as:

$$d_{43} = \frac{\sum_{i=1}^n d_i^4}{\sum_{i=1}^n d_i^3} \quad (2.2.6)$$

The volume weight distribution is more sensitive to the larger droplets in the size distribution. The Sauter mean distribution on the other hand, is more sensitive to the smaller droplets in the size distribution (Malvern-Instruments 2015)

2.2.2 Droplet size distribution

The properties of a dispersion can be described by a droplet size distribution. A droplet size distribution shows how the droplet size varies for a system, and how frequent each droplet size appears. Examples of some different ways to show droplet size distributions can be seen in Fig. 2.2.2

A good way to show how the size of droplets are distributed in a system, is by using a histogram, or droplet distribution curves (Kowalczyk & Drzymala 2016). On the x-axis it is normal to plot the droplet diameter (in μm), and how frequent the

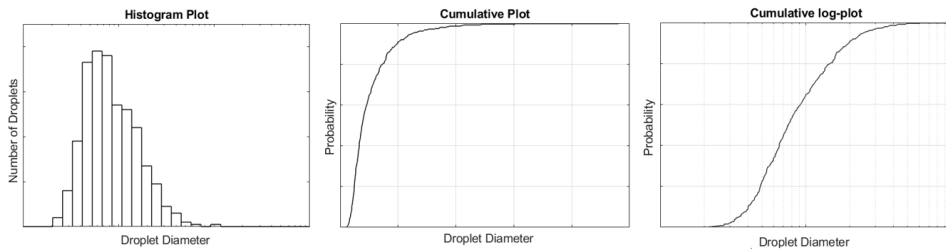


Figure 2.2.2: Different ways of plotting the droplet size distributions

diameter appears in a system can be read on the y-axis. The distribution can be represented using logarithmic axis, where it often resembles a normal distribution. The droplet distribution curve has been used by several authors to display the droplet distribution, which can be seen in the work of Schümann et al. (2015), Ward & Knudsen (1967) and Fossen & Schümann (2017). The distribution that is used most often is the cumulative distribution. The distribution shows the probability of a droplet to be less or equal to a certain size. The distribution is good for i.e. to see the percentage of droplets that is still in a system, and has not been separated out. If the smallest droplet that can be separated is known, the percentage of droplets that is smaller than this, which will still be in the system, can be read from the cumulative graph. Contrary, if a separator that separates a certain percentage of the liquid mix is going to be designed, then the largest droplet diameter that equals this percentage can be found from the graph.

There are also different ways to represent the composition of a distribution. Some of the different ways to represent or weight the distribution, is around the numbers of droplets, the surface area of the droplets or the volume of the droplets. Which parameter the distributions are weighted around, will give very different distributions and results. An example of this can be seen when comparing the volume and number weighted distributions (Malvern-Instruments 2015). For a number weighted distribution each droplet size is weighted equally. The number of droplets having the same diameter will be reported. This means that droplets that are common in the distribution will have a higher peak, and droplets that are not well represented will have a smaller peak in the plot. When looking at a volume weighted distribution the volume the droplets occupy out of the total volume, will be presented. The distribution is therefore weighed around the volume of the droplets in the distribution. The large droplets in the distribution have a larger effect on the total volume, compared to the smaller droplets, even though it might be a larger number of smaller droplets in the distribution.

A short example to show the difference in the two weighted distributions is to look at a droplet distribution consisting of 10 droplets. Out of the ten droplets 7 droplets are $1\ \mu\text{m}$, 2 droplets are $2\ \mu\text{m}$ and 1 droplet is $10\ \mu\text{m}$. The number weighted distribution and volume weighted distribution is plotted with histogram plots in Fig. 2.2.3. It can be seen from the figure that the number weighted distribution is

shifted more towards the left, to smaller droplet sizes, while the volume weighted distribution is shifted more towards the right and larger droplet sizes.

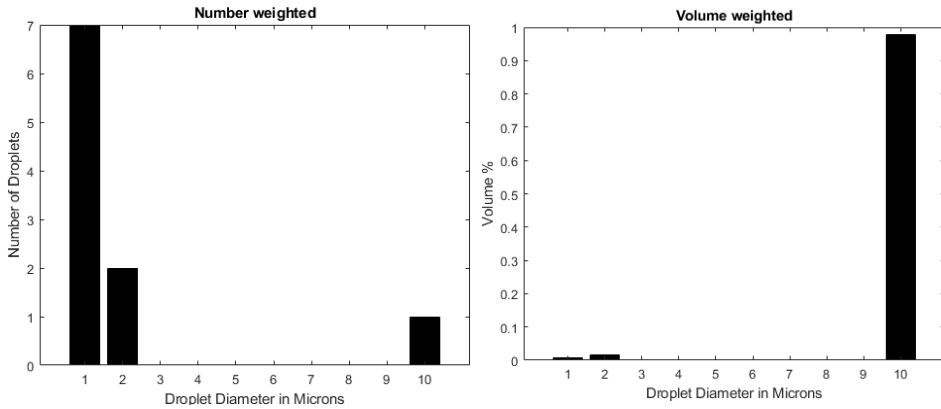


Figure 2.2.3: Number and volume weighted distribution

2.2.3 Droplet break-up over valves

The use of valves are common in the petroleum industry, for instance to control the production rate or the system pressure. Different types of valves can be used, but they work by the same principle; fluid is forced through a smaller restriction, creating an increased flow speed, with an associated pressure drop. When fluids are exposed to a large enough shear a dispersion will be created. The higher the shear stress, the smaller the droplets will be created. This leads to a slower separation, due to the smaller diameter of the droplet (Walsh 2016), see Eq. (2.1.1) and Eq. (2.1.2). There are a few options described by Walsh (2016) on how to reduce the shear stress to avoid creation of small droplets. It is the high-intensity turbulence created by the valve that break up the droplets to smaller drops. In pipes and flow lines, the flow changes to a mild turbulence flow, which can promote drop-drop coalescence that will increase the average drop size. By increasing the length from the valve to the separator could therefore enhance the time for coalescence to occur. Chemicals can also be added to the system to reduce the fluids sensitivity to shear (Walsh 2016), but this could also change the properties of the flow, so this has to be done with caution.

For more aged or stable droplets (droplets that are not expected to change their diameter over time) the droplet break-up from a valve could be beneficial. The aged droplets are more stable, and might not coalesce with other droplets. After passing the higher shear zone, the droplets might break up to smaller droplets that could more easily coalesce, resulting in an increase in the total surface area of the droplets (Fossen & Schümann 2017).

2.2.4 Parameters that effect droplet size

There are several parameters that can affect the droplet size, and break-up of droplets. Walsh (2016) found that there was a trend of smaller droplets in the flow when there was an increase in shear rate. This was also seen in the experiments performed by Schümman et al. (2015), where the droplet size decreased for a higher mixing intensity (a higher shear force).

Fossen & Schümman (2017) studied droplet sizes downstream a restriction. They found that the droplet size is reduced with the pressure drop, while the flow rate had a smaller effect. Van der Zande & Van den Broek (1998) found that in a turbulent pipe flow, the droplet size decreased with increasing flow rates. They also noticed that the maximum stable droplet size, for an oil-water mixture, increased for higher oil viscosity.

Both Schümman et al. (2015) and Paolinelli et al. (2017) found that for increasing water cuts (ratio of produced water volume to total volume produced) and water-volume fraction or dispersed- volume fraction, the max and mean droplet size increased. The increase in water fraction did not only create larger droplet sizes, but the whole droplet distribution was also found to be broadened.

2.3 Droplet Size Measurement Methods

Characterizing oil-water dispersion and droplet size distributions can be done by using different kinds of apparatuses. The apparatuses use different techniques for the measurements, for instance measuring electrical properties, pressure drops, or taking pictures or recording videos of the flow. The cameras used for recording can either take pictures inside the flow, in-situ, or record through a transparent section. Some of the equipment that can be used to measure the droplets and give real time measurements are Canty InFlow and FBRM (Focused Beam Reflectance Measurements), which are further explained in the report Ellertsen (2017). In this thesis a PVM camera will be used to find the DSD of the flow. The following section will therefore give a more thorough description of the PVM camera.

PVM – Particle Vision Microscope

Particle Vision Microscope (PVM³) is an in-situ probe camera that takes real time images of a flow. The PVM has been used by several researchers to characterize droplet sizes where some are Greaves et al. (2008), Schümman et al. (2015) and Boxall et al. (2010). The probe can be used for environmental temperatures of 5 to 30°C for the housing/CCD camera, and -80 to 120°C for the probe. Field of view is 1075x825 μm , with a resolution of 2 μm (for more details see Mettler-Toledo (2009)). The output image from using the PVM camera is (1024 \times 1360) pixels

with a picture resolution of $0.8 \mu\text{m}/\text{pixel}$. A description of the apparatus with dimensions is shown in Fig. 2.3.1.

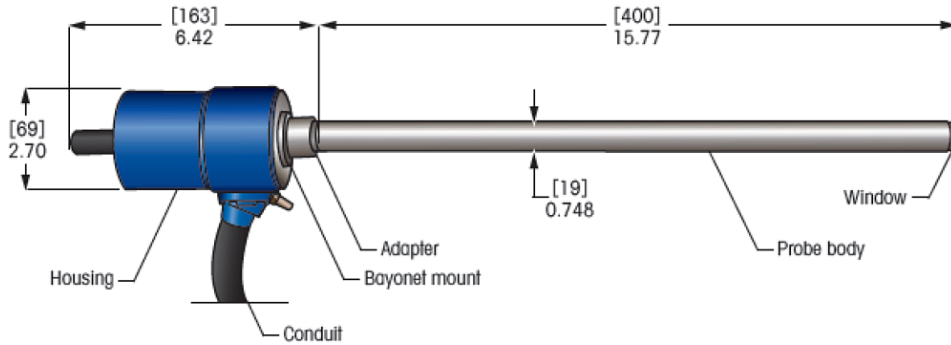


Figure 2.3.1: PVM with dimensions where units in brackets are in mm^3

The PVM consists of a long probe with a camera at the end. Around the camera independent laser sources are placed that send out light to illuminate the fluid around the camera to get a clear image. Due to these lasers, the PVM can be used for dark emulsions, and still get a pretty clear image (Schümann et al. 2015). For light solutions and emulsions it can be difficult to get clear images, since the solution reflects little light back to the camera. To get a better image small "hats" can be put on the tip of the camera. Fig. 2.3.2 shows the PVM with a white hat placed on the tip of the probe. The fluid flows through the small gap and the light is reflected back from the white tip of the "hat" to the camera. Different "hat" lengths (where the length between the camera lens and the reflective part vary) can be used for different flow systems.

The PVM captures images in-situ, which gives an accurate description of what is happening in the system. This makes it easy to notice changes appearing in the flow (Mettler-Toledo 2017). One downside of having the PVM inside the flow, is that it could affect the flow characteristics and change the droplet size downstream of the probe. This is due to the shear force created from droplets colliding with the probe, which would give a different flow and droplet distribution than originally occurred. The placement and the angle of where the probe is put in the flow is therefore important to take into consideration, to try to avoid disturbances. To avoid this, the probe should be connected to the pipe in a way that it shows the upstream flow, where the flow has not yet been affected by the probe. The system manual Mettler-Toledo (2009) reports that the optimum angle of the probe to direct the flow to the surface glass of the PVM, is to mount the PVM at a 45° angle to the flow. This will give a continuous flow of fluid past the camera lens and lead to less buildup of fluid on the screen. Fig. 2.3.3 shows how the liquid will pass the probe using an angle of 45° to the flow.

³Mettler-Toledo (2009)

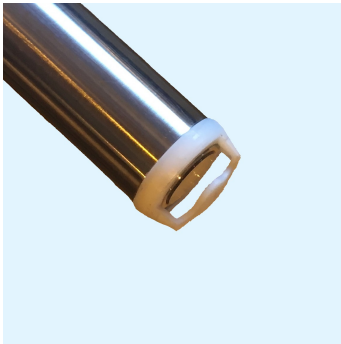


Figure 2.3.2: PVM probe with a 4 mm "hat"

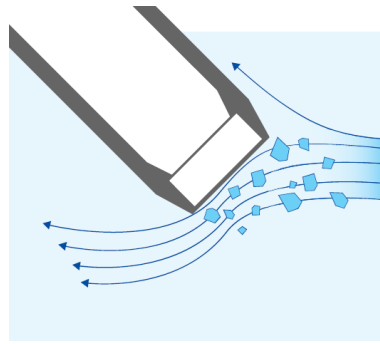


Figure 2.3.3: PVM placed at a 45° angle³

The placement of the probe in a system should be three-to-five pipe diameters to the last upstream disturbance (Mettler-Toledo 2009). It is recommended to place the PVM in an upward-oriented pipe due to good mixing conditions. Placements in horizontal or down-flow pipe will affect the analysis due to the large changes in flow speed, dispersion and density of the flow. The variation in measurements might therefore not be due to the change of droplet size or amount of droplets in the flow, but due to the placement of the PVM. This has to be taken into account when placing the PVM, to try to avoid these variations.

For experiments run below temperatures of 20°C some condensation of the gas within the PVM probe can appear. To avoid condensation, purge gas can be used by connecting it to the PVM unit. The purge gas might contain some small oil droplets, so a pressure resistant filter should be used. The gas must be run for a minimum of ten minutes before the probe is put into the cold temperature system. Different criteria for the gas that should be used can be found in the system manual Mettler-Toledo (2009).

When using the PVM, some "probe coating" can be experienced, where droplets stick to the PVM camera lense when running experiments. This was experienced by Schümann et al. (2015) for tests performed with high viscous oil that was rotated at a low speed in a beaker glass. The probe coating will result in the same drops being repeatedly counted, and the resulting droplet distribution will be incorrect. To avoid this, the images from the recordings have to be monitored so the probe can be cleaned when it is noticed that some of the droplets are stuck on the camera. The use of different chemicals that will prevent the droplets to settle on the glass can also be used, if these will not affect other properties of the flow.

2.4 Horizontal Flow Patterns for oil-water flow

A flow regime or a flow pattern is "a description of the geometrical distribution of a multiphase fluid moving through a pipe" Schlumberger (2017). This multiphase fluid can consist of a two-phase, three-phase or a four-phase flow. In the rig built for project 2.9 a liquid-liquid flow consisting of water and oil will be used. Oil and water are immiscible liquids with densities close to each other with oil density varying from around 800 kg/m^3 to 1000 kg/m^3 , and water density around 1000 kg/m^3 . The viscosity on the other hand might have a larger difference where water viscosity is around 1 cp, while oil viscosity can vary from 1 cp to thousands of cp (Speight 2014). Because of the similarity in density the flow pattern seen in an oil-water flow will differ from the flow patterns seen in a gas-liquid flow. The flow pattern will also change for different inclinations of the pipe. The present study will focus on horizontal liquid-liquid flow, since this is what will be seen in the built rig. The four basic horizontal flow patterns will be introduced. Flow patterns can also co-exist, and be a combination of these four basic patterns.

2.4.1 Stratified flow

A stratified flow is characterized by a smooth interface between two segregated fluid layers. The fluid velocities are low, so the gravity force will be the most dominant force to act on the system. Due to this, the oil layer, which has a lower density, will be occupying the top part of the pipe, while the water that has a higher density, will occupy the bottom part of the pipe. With an increase in velocity the interface will become more wavy, and because of shear between the two fluids, droplets can start to break out from one layer and settle in the other layer. This results in small droplets on the interface between the layers (Brauner 2003). Examples of the different types of stratified layers can be seen in Fig. 2.4.1, where the oil phase is black and the water phase is white.

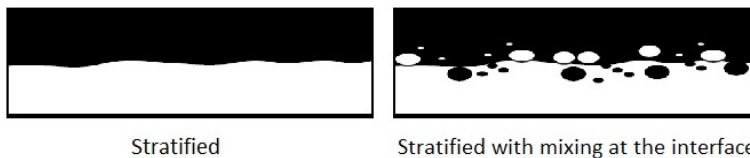


Figure 2.4.1: Stratified flow patterns ⁴

⁴Pictures taken from Brauner (2003)

2.4.2 Dispersed flow

For increasing fluid velocities the interfacial shear will increase, resulting in droplet creation at the interface. At sufficiently high shear all liquid of one phase will be entrained, losing its continuity. The flow will be fully dispersed where water is dispersed in the oil phase, or opposite where oil is dispersed in the water phase. Different types of dispersion and dispersed flow can be seen in Fig. 2.4.2. If the flow is not fully dispersed, it can look like there is three different layers in the flow, with a continuous oil layer at the top and a continuous water layer on the bottom separated by a dispersed layer. If the dispersion is stable, which means droplets will not separate out for a long period of time, the flow is called an emulsion. A dispersed flow might be produced in a turbulent flow and from pressure drops in devices like pumps, valves or bends (Fossen & Schümann 2017).

Oil-water dispersions can often exhibit a phenomena called phase inversion (Brauner 2003, Trallero et al. 1997, Schümann 2016). At a certain volume fraction the continuous and the dispersed phases will swap places (e.g. a dispersion of oil in a continuous matrix of water will become a dispersion of water in a continuous matrix of oil). This change is associated with a sudden pressure drop in, or around the inversion point. The changes in properties of the flow, and the large pressure drop that appear at the inversion point are important parameters to consider when looking at transportation of oil and water (Brauner 2003).

A dispersion can be divided into two categories, dense dispersion and dilute dispersion. In a dilute system the dominating mechanisms is droplet break-up, which results in smaller droplets. In dense dispersion it will be more coalescence that leads to larger droplet sizes (Brauner 2003). The mechanisms which determine this break-up and coalescence are explained more in detail in sec. 2.2.

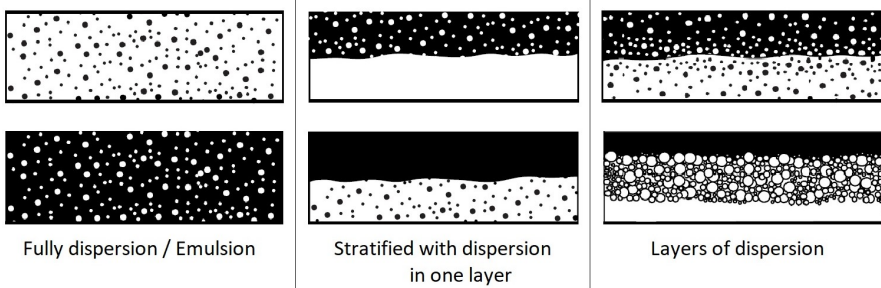


Figure 2.4.2: Dispersed flow patterns ⁴

2.4.3 Annular flow

In an annular flow pattern one of the liquids in the system creates a core inside the pipe, while the other creates a lubricating transport layer around the inside pipe wall, see Fig. 2.4.3. It is common to see an annular flow pattern when the density of the two liquids are equal or one liquid has a much larger viscosity (Angeli & Hewitt 2000a). For high viscous oils that flow slowly in a pipe, the water can work as a lubricant to transport the heavy oil in the annulus. Water creates a smaller friction force on the wall, resulting in a lower pressure drop than if the oil was transported alone in the pipe. This transport phenomena is the most attractive when looking at pressure drop reduction and saving power in the transportation. When water creates the core and oil is the outside layer, it is called an "inverted" annular flow (Brauner 2003).

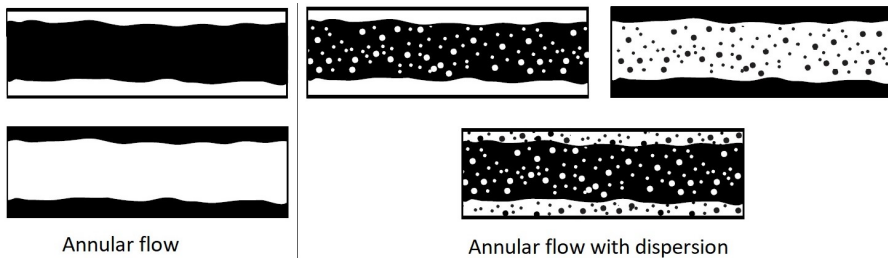


Figure 2.4.3: Annular flow patterns ⁴

2.4.4 Plug and Bubble flow

If the velocities of the fluids in an annular flow is increased, the core can break and create large bubbles or slugs of one liquid in the other. This will create a plug or bubble flow that is characterized by droplets, plugs or slugs of oil that flow in the top part of the pipe (Amundsen 2011). The annular flow could also turn into a dispersed flow (Brauner 2003). The plug flow pattern is not mentioned and seen as much in the literature, as the other flow patterns. A figure of large bubbles of oil and water flowing in a pipe can be seen in Fig. 2.4.4.

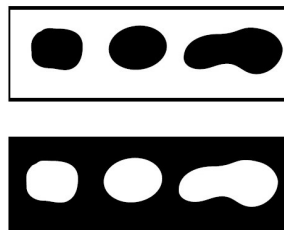


Figure 2.4.4: Bubble flow patterns ⁴

2.5 Flow Pattern Maps for Oil and Water Flow

The different flow patterns that appear in a flow system can be plotted in a diagram, called a flow pattern map. The flow pattern map shows the transition boundaries between different flow patterns. These boundaries occur because of instability in the current flow, which makes the flow pattern transition to another flow pattern. The flow pattern boundaries are therefore more transition zones rather than clear distinctive lines (Brennen 2005). Due to this, the flow map can be used to find for which properties a change in the flow patterns can be expected, hence a change in the properties of the flow. Each flow map is unique for a certain flow system. The map will depend on the pipe inclination, pipe diameter and the properties of the fluids. The properties that are plotted on the different coordinate axis can vary from author to author (Brennen 2005). For liquid-liquid flow superficial velocities, u_s , is often used, i.e. by Rivera (2011), Brauner (2003) and Trallero et al. (1997). The superficial velocities are not a real fluid velocity, but a parameter that is often used for multiphase flow, which shows the velocity the fluid would have if it was the only fluid occupying the pipe. It can be defined as:

$$u_{is} = \frac{q_i}{A} \quad (2.5.1)$$

where q_i is the volumetric flow rate and A is the cross section area of the pipe. Another way of creating flow maps is to plot the water fraction or water cut, WC, against the total flow velocity, or mixed flow velocity u_m (velocity of the oil and water when flowing together). This has been done by Arirachakaran et al. (1989), Nädler & Mewes (1995) and Trallero et al. (1997). The water cut is defined as:

$$WC = \frac{q_w}{q_w + q_o} \quad (2.5.2)$$

An example of a flow pattern map can be seen in Fig. 2.5.1.

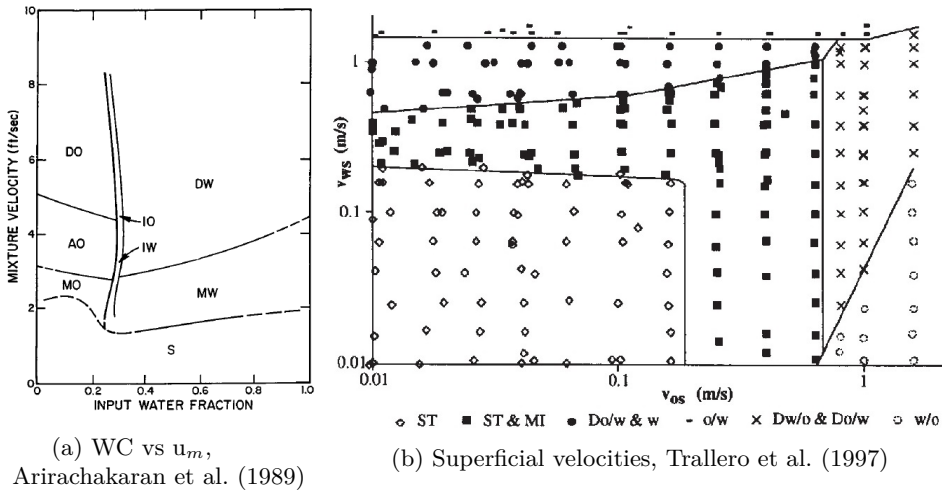


Figure 2.5.1: Different flow pattern maps for oil-water flow

2.6 Numerical models

Different distribution functions exist that can be used to describe a droplet size distribution. Some of the different distributions that exist are the Rosin-Rammler distribution, the upper-limit log-normal function and the log-normal distribution (Simmons & Azzopardi 2001, O'Rourke & MacLoughlin 2005, Boxall et al. 2010, Schümann et al. 2015, Farr 2013, Mugele & Evans 1951). As written by Simmons & Azzopardi (2001) the Rosin-Rammler distribution does not contain a mathematical upper limit cut-off. This means it will find infinite droplet sizes, which is unrealistic since there will always exist a maximum stable droplet size in a system. Due to this, this distribution is not going to be considered further.

Different models can be used to find the maximum droplet diameter in a fluid system. Models exist for dilute and dense dispersions, and for break-up over valves. Summary of some of the different distribution functions and models are presented below.

2.6.1 Log-Normal Distribution

The Log-Normal Distribution (LND) was used by Schümann et al. (2015) in their work. The distribution is described in Farr (2013) and can be used to describe the logarithmic distribution for volume-, number-, diameter and surface-weighted distributions. The distribution is dependant on already measured data to create a continuous function, and can be expressed as:

$$f(d) = \frac{1}{d\theta\sqrt{2\pi}} \exp\left\{-\frac{[\ln(d/d_0)]^2}{2\theta^2}\right\} \quad (2.6.1)$$

$f(d)$ is the log-normal distribution for the diameter d . The parameters θ is the "width" of the distribution, and d_0 is a reference diameter. Both θ and d_0 can be found using surface weighted mean diameter (Eq. (2.2.5)) and volume-weighted mean diameter (Eq. (2.2.6)) using the equations below.

$$d_0 = (d_{32} d_{43})^{1/2} (d_{32}/d_{43})^b \quad (2.6.2)$$

$$\theta = \sqrt{\ln\left(\frac{d_{43}}{d_{32}}\right)} \quad (2.6.3)$$

The reference diameter can be expressed for different types of distributions, where each distribution has a different variable of b . b can take the value 0, 1, 2 or 3 referring to volume-, surface-, diameter-, and number-weighted distributions respectively.

2.6.2 Upper-Limit Log-Normal Distribution

The upper limit function (ULLN) was used in the work by Simmons & Azzopardi (2001), Karabelas (1978). A thorough description of the function can be found in Mugele & Evans (1951). The cumulative volume fraction of droplets smaller than size d can be described by:

$$f(d) = 1 - \frac{1}{2}[1 - \operatorname{erf}(\delta z)] \quad (2.6.4)$$

where the different parameters can be determined from the equations:

$$a = \frac{d_{max} - d_{50}}{d_{50}} \quad (2.6.5)$$

$$\nu_i = \frac{d_i}{d_{max} - d_i} \quad (2.6.6)$$

$$z = \ln \left[\frac{ad}{d_{max} - d} \right] \quad (2.6.7)$$

$$\delta = \frac{0.394}{\log_{10} \left[\frac{\nu_{90}}{\nu_{50}} \right]} \quad (2.6.8)$$

The maximum diameter d_{max} can be found by trial and error to find the best fit with the data when plotting $100 \times v$ (will be written $100v$) against ν , which is shown in Mugele & Evans (1951). The parameter v is defined as "the volume fraction of droplets having diameter $< d$ " (Mugele & Evans 1951). A direct approximation can also be found by; first plot the diameters against $100v$ (creating a cumulative distribution) and draw a smooth curve that best fit the points. (In this thesis v is calculated by dividing the sum of the volume of drops with diameter smaller than d , by the total volume of all droplets, see Eq. (5.1.1)). Secondly, from the fitted curve, read off the different percentiles, d_{10} , d_{50} and d_{90} (the 10th, 50th and 90th percentiles respective) to be used in Eq. (2.6.9) to find d_{max} (Mugele & Evans 1951).

$$\frac{d_{max}}{d_{50}} = \frac{d_{50}(d_{90} + d_{10}) - 2d_{90}d_{10}}{d_{50}^2 - d_{90}d_{10}} \quad (2.6.9)$$

The d_{32} can also be found using the parameters above:

$$d_{32} = \frac{d_{max}}{1 + a \times \exp\left[\frac{1}{4\delta^2}\right]} \quad (2.6.10)$$

It was found when comparing the models from Simmons & Azzopardi (2001) with the equations from Mugele & Evans (1951) that Simmons & Azzopardi has reported ν_{90}/ν_{10} , rather than ν_{90}/ν_{50} for Eq. (2.6.8). This would give an different result, than if the ν_{90}/ν_{50} is used, as written by Mugele & Evans.

2.6.3 Hinze and Brauner - breakage models

Both the Hinze model and the Brauner model are predicting the maximum size of a droplet in a turbulent flow field. These predictive models to find d_{max} can be compared with the d_{max} found from the curve-fit functions, written above, and the real data to see if they give a good match and apply to the measured data.

Hinze dilute model

The Hinze model can be used for dilute dispersions. "The model is based on a static force balance between the eddy dynamic pressure and the counteracted surface tension force" and does not take into account the coalescence (Brauner 2003).

The model can be written as:

$$\left[\frac{d_{max}}{D} \right]_{dilute} = 0.55 W e_c^{-0.6} f^{-0.4} ; \quad \ell_k \ll d_{max} < \ell_{max} \quad (2.6.11)$$

ℓ_k is the Kolmogorov microscale, which represent the smallest eddies found in the continuous phase, and can be seen below where ε is the energy dissipation rate.

$$\ell_k = \left(\frac{\mu_c^3}{\rho_c \varepsilon} \right)^{\frac{1}{4}} \quad (2.6.12)$$

ℓ_{max} represents the length scale of the largest eddies, and for pipe flow, the value has been reported to be approximately $0.1D$, where D is the pipe diameter (Paolinelli et al. 2017). $W e_c$ is the Weber number for the continuous phase, see Eq. (2.2.3). f is the wall friction factor and can be found by:

$$f = C R e_m^{-n} \quad (2.6.13)$$

where C and n are constants and can vary for different systems. Xu et al. (2010) posted a list with C and n found by different authors. $R e_m$ is the Reynolds number for the mixed phase and is expressed as:

$$R e_m = \frac{\rho_m u_m D}{\mu_c} \quad (2.6.14)$$

where u_m is the mixed flow velocity and μ_c is the dynamic viscosity of the continuous phase. The mixed density can be found by $\rho_m = \rho_d \epsilon_d + \rho_c (1 - \epsilon_d)$. ϵ_d is the fraction of the dispersed phase (equivalent to the water fraction or oil fraction).

Brauner dense model

A model to find the largest droplet size for dense dispersions was found by Brauner and is explained in Brauner (2003). The model is an extension of the Hinze model, and takes the coalescence into account. The model can be expressed as:

$$\left[\frac{d_{max}}{D} \right]_{dense} = 2.22 \tilde{C}_H W e_c^{-0.6} \left[\frac{\rho_m}{\rho_c(1-\epsilon_d)} f \right]^{-0.4} \left(\frac{\epsilon_d}{1-\epsilon_d} \right) \quad (2.6.15)$$

\tilde{C}_H is a tunable constant, $\tilde{C}_H = O(1)$. For a dense system $(d_{max})_{dense} > (d_{max})_{dilute}$.

2.6.4 Droplet breakup over restrictions

Van der Zande & Van den Broek (1998) proposed a relation for the largest droplet that can be found after a restriction in the turbulent field by using the Weber number. This relation was used by Fossen & Schümann (2017) in their work. The equation for the largest stable drop diameter in a turbulent zone was expressed as:

$$d_{max} \propto \left(\frac{\sigma}{\rho_c} \right)^{0.6} \varepsilon^{-0.4} \quad (2.6.16)$$

where ε is the energy dissipation rate. Van der Zande & Van den Broek (1998) approximated ε by the mean energy dissipation rate $\bar{\varepsilon}$, expressed as:

$$\bar{\varepsilon} = \frac{\Delta p_{perm} U_p}{\rho_c \Delta x_{perm}} \quad (2.6.17)$$

σ is the interfacial tension and Δp_{perm} is the permanent pressure drop. Δx_{perm} is the length of the orifice zone (distance between where the pressure first starts to decrease, to where the pressure is recovered (Van der Zande & Van den Broek 1998)) and can be related to 2.5D (Fossen & Schümann 2017). U_p is the mean velocity in the restriction, which can be found by $U_p = U_{mix}(D_{pipe}/D_{orifice})^2$. Fig. 2.6.1 is a schematic representation of an orifice area with the flow and pressure fields.

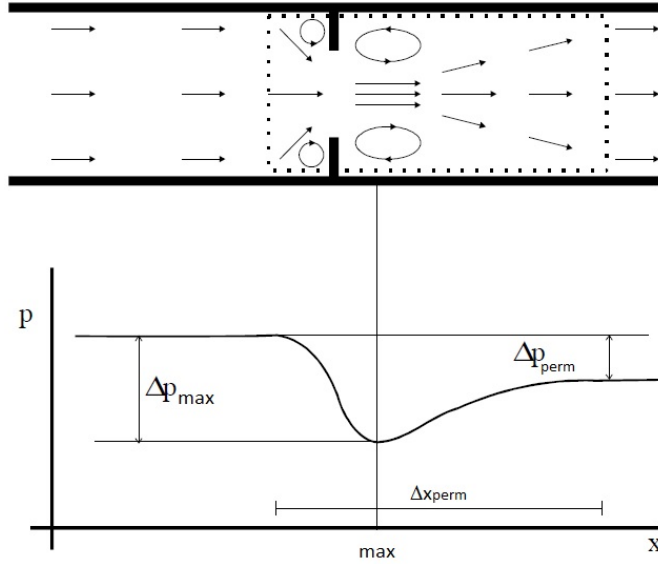


Figure 2.6.1: Illustration of an orifice with flow and pressure field ⁵

2.7 Error estimation

When performing experiments, errors may occur. It is therefore important to do an error estimation, to find the error. An introduction to different equations and parameters used to find the error is described below.

For equations with several components, where each component has its own error, the total error can be found with the following equation:

$$\omega_R = \sqrt{\left(\frac{\partial R}{\partial v_1}\omega_1\right)^2 + \left(\frac{\partial R}{\partial v_2}\omega_2\right)^2 + \dots + \left(\frac{\partial R}{\partial v_n}\omega_n\right)^2} \quad (2.7.1)$$

here R is a linear function of n independent variables v . ω_i is the error for the variables, while ω_R is the error for the result (Kline & McClintock 1953).

In this thesis experiments will be performed where errors could occur from the used instruments and from variation in measurements. To find the error that accounts for both of these errors, the following equation can be used:

$$\text{error} = \sqrt{S_{\bar{x}}^2 + c^2} \quad (2.7.2)$$

where c is the error from the instrument $S_{\bar{x}}$ is the standard deviation of the mean value of the measurements. It can be found by using the equations below. (The definitions are taken from Wheeler (2010).)

⁵Modified picture taken from Van der Zande & Van den Broek (1998)

The mean value of the performed measurements can be found by:

$$\bar{x} = \sum_{i=1}^n \frac{x_i}{n} \quad (2.7.3)$$

where x_i are the values of the sample data. The standard deviation of a sample can be defined as:

$$S = \sqrt{\sum_{i=1}^n \frac{(x_i - \bar{x})^2}{(n-1)}} \quad (2.7.4)$$

The probability that a calculated population mean will fall within a specified interval, within a certain percentage of the measurements, is called a confidence level. It can be expressed as:

$$\text{confidence level} = P(\bar{x} - \beta \leq \gamma \leq \bar{x} + \beta) \quad (2.7.5)$$

where β is the uncertain, \bar{x} is the sample mean and γ is the mean of the population. The confidence level can also be expressed as $1 - \alpha$ where α is the probability that the mean will fall outside the confidence interval. The confidence interval is the interval from $\bar{x} - \beta$ to $\bar{x} + \beta$.

The *central limit theorem* can be used to make an estimate of the confidence interval. For a population of the random variable x , having a mean value γ and a standard deviation S , if several tests are performed on the sample (each of size n), each test would have a mean \bar{x}_i . It is not expected that each mean will have the same value. The theorem states that if n is sufficiently large, the \bar{x}_i will follow a normal distribution where the standard deviation of the means will be given by:

$$S_{\bar{x}} = \frac{S}{\sqrt{n}} \quad (2.7.6)$$

(The population does not have to be normally distributed for the means to be normally distributed.) To find an estimate for the confidence interval, the student-t distribution can be used. It can be expressed as

$$\tau = \frac{\bar{x} - \gamma}{S/\sqrt{n}} \quad (2.7.7)$$

With some calculations, the confidence interval becomes:

$$\gamma = \bar{x} \pm \tau \times \frac{S}{\sqrt{n}} \quad \text{with confidence level } 1 - \alpha \quad (2.7.8)$$

which can be written as

$$\gamma = \bar{x} \pm \tau \times S_{\bar{x}} \quad (2.7.9)$$

A student-t table (an example can be seen in (Table 2018)) can be used to find the different t-values valid for a certain confidence interval. For a confidence interval of 95%, the t-value is 1.984 for 100 elements, while it is 1.962 for a thousand elements.

Chapter 3: Experiment setup

3.1 Separator Loop

The rig that will be used for the experiments in chapter 4 is build for the SUBPRO project 2.9 (Skjefstad & Stanko 2017). Measurements are performed using the liquids in the rig. Flow pattern maps and DSD are found at the inlet pipe of the compact separator. A flow and instrumentation diagram of the setup of the rig can be seen in Fig. 3.1.1. The section where the PVM and flow map measurements will be performed are marked in red. The setup consists of a large storage tank containing Exxol D60 with added red coloring (Merck 2018), and distilled water with 3.5 wt% salt. Four centrifugal pumps for boosting are connected, where two are used at a time. For the water phase the allowed flow rate is 100-2100 L/min while for the oil it is 100-1700 L/min. The pump speed is regulated with frequency converters, and flow meters are installed to get the desired water cut. To determine the fluid properties two Coriolis meters and a temperature sensor will be used. The equations given from calibration of the instrument to be used to find the fluid properties will be explained in sec. 3.3.

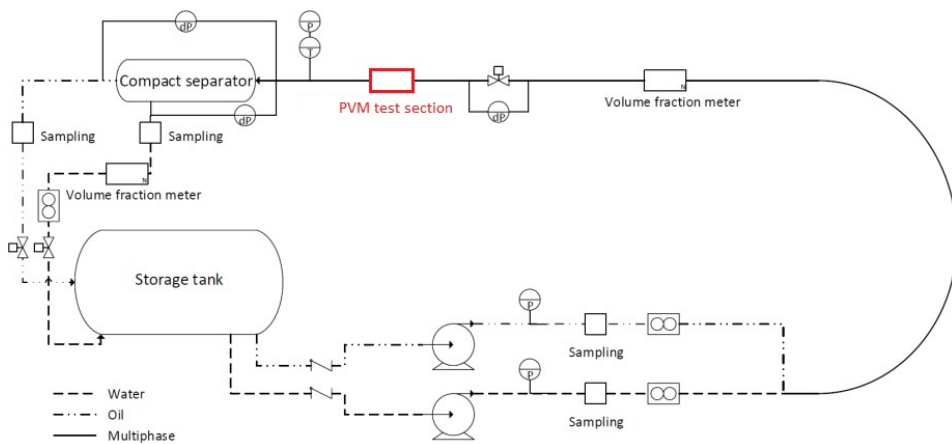
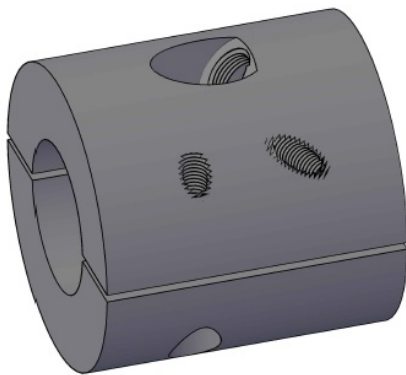


Figure 3.1.1: Flow and instrumentation diagram for the SUBPRO rig⁶

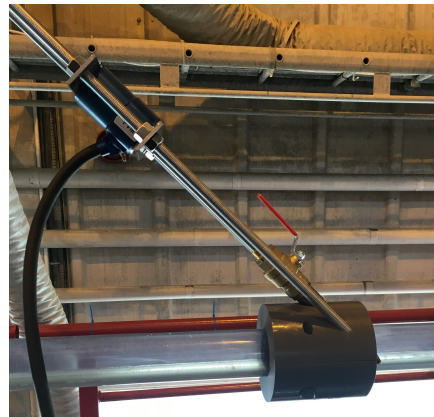
The oil and water are mixed at a commingling point and flow in a 12 m long (75 mm OD, 67.8 mm ID) transparent PVC pipe before entering the compact separator. The pipe can withstand a maximum pressure of 10 bar. An electrical ball valve and a PVM camera are mounted on the pipe. The ball valve can be used to create different pressure drops, and to create different flow regimes. The PVM can be used to record films of the in-situ flow, as discussed in sec. 2.3, to be able to determine the droplet size distribution. More specifics about the placement and mounting of the PVM can be seen in sec. 3.2.

3.2 Mounting of PVM

The guidelines mentioned in sec. 2.3 is used when mounting the PVM camera. The PVM is mounted at a 45° angle to the flow, to get a continuous flow of fluid past the camera. The inlet where measurements will be performed is horizontal, which is not an ideal measurement placement. To try to avoid this unwanted placement the probe will be placed at the top of the pipe to allow the probe to move up and down, to enter different layers of the flow. The probe mount is placed 81 cm from the inlet and 106 cm to the middle of the upstream valve, which is aligned with the recommended distance to upstream disturbances.



(a) Mechanical drawing of PVM-camera mold. Image: Noralf Vedvik



(b) PVM placed in camera mount on pipe

Figure 3.2.1: PVM camera mount

To support the inlet pipe and make it possible to adjust the PVM up and down a supporting mount is created. The mount design was made by Noralf Vedvik. The mount is made from a PVC-block that was machined by a CNC. Pictures of the camera mount can be seen in Fig. 3.2.1. Technical drawings can be found in

⁶Modified picture taken from Skjefstad & Stanko (2017)

Appendix E.3. To fasten the camera setup, first a hole was drilled through the inlet pipe, drilling with the camera mount on for guidance. Then the camera mount is glued to the pipe and fastened with two screws. A valve is fastened on the top of the camera mount to make it impenetrable to the oil and water and allow to run experiments without the PVM in the system. Further, two supporting beams are screwed in the mount. Hexagon nuts are used to regulate the position of the PVM, where two metal plates are used to support the PVM.

3.3 Calibration errors

In the rig, two different instruments will be used to measure the different properties. Two Coriolis meters (Micro Motion F200) are used to measure the flow rate and density. A temperature probe (Ni1000 TK5000 resistance measurement element) is used to measure the temperature. Because of temperature variations in the rig, the instruments are calibrated before experiments are performed. The calibrations have been performed by PhD candidate Håvard Skjefstad. The calibration gave the following equations to correct for the temperature variation.

The temperature reading is varying with 0.5 degrees and has to be corrected using equation:

$$T_{corrected} = T_{measured} - 0.5 \quad (3.3.1)$$

To correct the density measurements the following equation should be used:

$$\rho_{w_{corrected}} = \rho_{w_{measured}} - (-0.1514\rho_{w_{measured}} + 3.0629) \quad (3.3.2)$$

$$\rho_{o_{corrected}} = \rho_{measured} - (-0.2774\rho_{o_{measured}} + 6.1817) \quad (3.3.3)$$

Using these equations, the reported density will equal the exact density measured, see sec. 4.1.1.

To correct the flow rate measurements the following equation should be used:

$$q_{corrected} = \frac{q_{measured} \times \rho_{measured}}{\rho_{corrected}} \quad (3.3.4)$$

The apparatus used to performed measurements have an error given by the producer. The error from the used apparatus are as follows:

- Temperature measurements = $\pm 0.3^{\circ}\text{C}$
- Density measurements = $\pm 0.54 \text{ kg/m}^3$
- Flow measurements = $\pm 0.15\%$ of actual value

This error will be the c value in Eq. (2.7.2) (in sec. 2.7) for calculations of the total error for the measurements.

3.4 Image processing

Different methods and softwares can be used to process pictures taken from the flow to determine the droplet size distribution. Some cameras, like the Canty camera (JM Canty Inc 2017), comes with a software. In this section two methods to process pictures will be described, a Matlab routine and manual counting.

3.4.1 Matlab routine

To process images that were taken from the flow with the PVM camera, a Matlab routine was used. The program code was made by Heiner Schümann, see Schümann et al. (2015). The routine works by first adjusting the contrast on the picture, binarizes, and doing edge detection before a Hough transformation is performed (Schümann et al. 2015). Images of the process can be seen in Fig. 3.4.1.

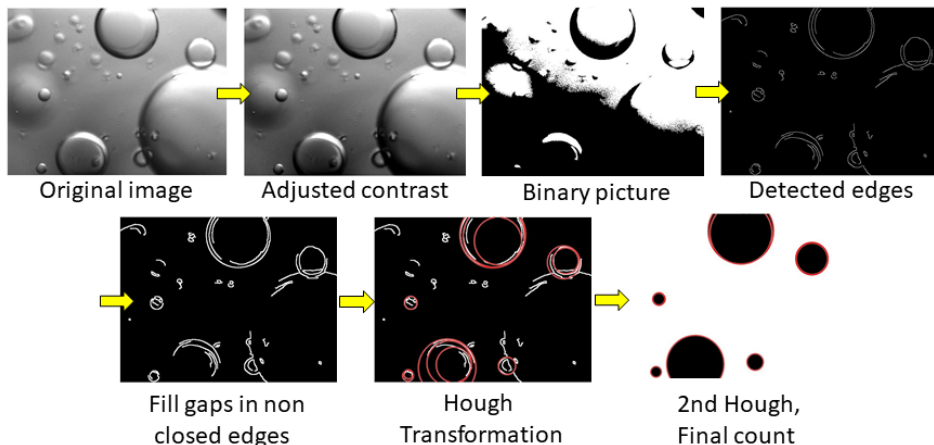


Figure 3.4.1: Processed images from running Matlab routine

The basic principle of the Hough transformation is that, it is a shape recognizing tool. It takes points from the original space and maps it into "Hough parameter space" where it plots points for all possible lines that could go through these points. Doing this for several points will give several curves, and the places where these curves intersect corresponds to the line that goes through all of these points. A more detailed explanation can be seen in the paper by Xu et al. (2013) and Ballard (1981). An example using the Matlab code can be seen in Corke (2011).

An image of the program interface can be seen in Fig. 3.4.2. The routine takes in a picture, with picture dimensions 680 x 512 pixels. The final output lists the number of droplets counted with the diameter in pixel and μm . Different statistics like d_{10} , d_{21} , d_{32} and d_{43} , and both weighted and non-weighted probability distributions together with cumulative distributions are also reported. The results

are displayed directly in the program, but an additional excel file containing the results (*Counted.xls*) is also created, which can be found in the Matlab folder. A more detailed explanation of the routine can be found in Appendix B.

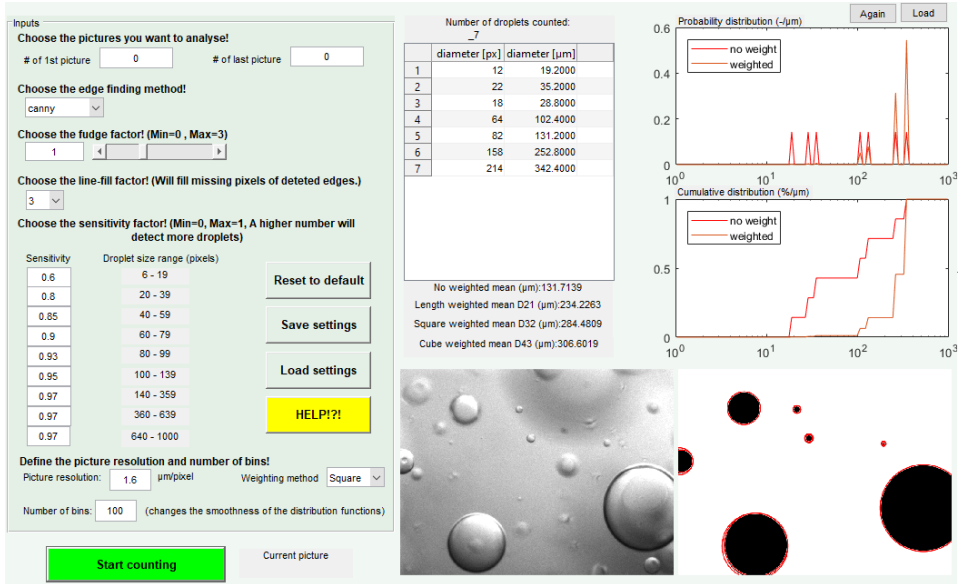


Figure 3.4.2: Matlab program interface

3.4.2 Manual counting

Counting and measuring droplets from pictures can also be done manually. In the project report by Ellertsen (2017) the DSD was found by counting manually, using the program ImageJ. A short summary of why and how to count manually is written below.

Counting manually is a time consuming procedure. Counting large numbers of droplets will give a more accurate DSD, but this will also be more time consuming. Identifying the smallest number of counts necessary to achieve good statistics can therefore reduce the time used when analyzing droplet data. Several authors (O'Rourke & MacLoughlin 2005, Schümann 2016, Fossen & Schümann 2017) found that counting (minimum) 500 droplets for each test, would give a meaningful result. In addition an error estimation should be performed, to see if the number of droplets counted is enough to give a correct result. ImageJ that was used for counting and measurements of the droplets worked by; marking and measuring the droplets (using the "stright" button), saving, and reporting the distance in pixels.

Some estimations were made when counting, to ensure the counting process was as similar as possible for each picture. The guidelines were: Droplets were assumed

to be 100% circular, and the diameter was (tried to be) placed through the center of the droplet. Only droplets that had a clear edge were counted. Droplets that were partly in the image were not counted due to the uncertainty of which outer points the diameter should be measured from. Both small droplets that were large enough to be measured, and large droplets were counted. An example can be seen in Fig. 3.4.3.

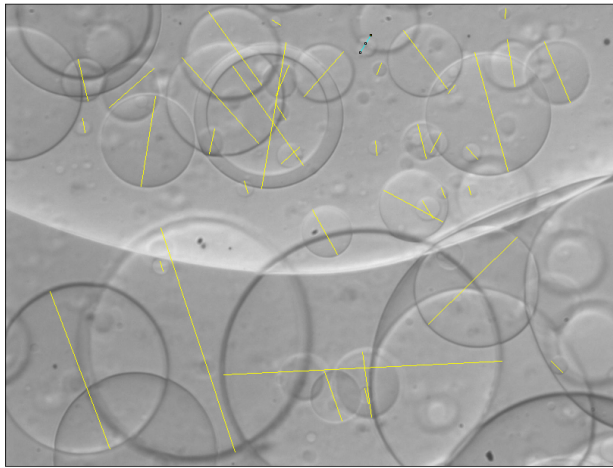


Figure 3.4.3: Manually counting using ImageJ

Chapter 4: Experiment Execution

4.1 Fluid properties

Fluid properties say something about the expected behavior of the fluids and can be used in different calculations, models and simulations. The fluid properties that will be found in this section is the density, viscosity and interfacial tension for both the oil and water solution. The experiments were performed in the Reservoir lab at NTNU.

4.1.1 Density

An experiment was performed in the Reservoir lab to find how the densities of the oil and distilled water with added salt changed with temperature. A pycnometer with a thermometer was used, but the errors were too large to find a linear equation on how the density changed with temperature (see Appendix D for full description of the experiment with results). Tests were therefore performed by the Chemical department at NTNU.

The reported equations for how the density vary with temperature [°C] is valid for 15–25°C and are reported below in units [kg/m³].

$$\rho_w = -0.004T^2 - 0.11T + 1025.4 \quad (4.1.1)$$

$$\rho_o = -0.732T + 806.29 \quad (4.1.2)$$

4.1.2 Viscosity

Tests were performed in the Reservoir lab at NTNU to find the viscosity of the oil and distilled water with added salt. The test samples were taken from the separator on the date 9-02-2018.

Method

The tests were performed at 22.8°C. To find the viscosity, a Cannon-Fenske capillary viscometer was used. Two different viscometers were used, one for measuring the oil and one for measuring the water. Both viscometers have a capillary number of 50. The liquid was filled in the larger reservoir of the capillary viscometer until the mark, before the viscometer was put on a stand. A figure of the viscometer filled with oil can be seen in Fig. 4.1.1. The liquid flowed from the large reservoir and start to fill up the measuring spheres. The time for the liquid to fill up the top two measuring spheres, named K_1 and K_2 , was registered.



Figure 4.1.1: Cannon-Fenske capillary viscometer filled with oil

To find the viscosities the following equation was used:

$$\mu_i = \rho \times K_i(t_i - \vartheta_i) \quad (4.1.3)$$

Here the subscript i stands for either 1 or 2, referring to the respective measuring sphere K_1 and K_2 . In the equation, K_1 and K_2 are a constant value that is given for each individual measuring sphere and reported for each viscometer. The t_x is the time it takes for the measuring sphere to be filled up. ϑ_x is the Hagenbach correction constant, which can be found from a table (see Appendix E.2). When both viscosities, μ_1 and μ_2 , are found an average viscosity of the two is calculated.

Result

Constants and results can be seen in Table. 4.1.1. The result match with the reported viscosities of water ~ 1 cp and Exxol D60 ~ 1.34 cp (kinematic viscosity = 1.7 cSt at 25 °C, $\rho = 0.788$ g/cm³ at 15.6°C), ExxonMobil (2016).

Table 4.1.1: Results from viscosity experiment

Parameter	Oil	Water	Unit
K_1	0.003667	0.003771	mm ² /s ²
K_2	0.002710	0.002763	mm ² /s ²
T_1	486.66	258.01	s
T_2	658.89	352.41	s
ϑ_1	-	0.08	s
ϑ_2	-	0.04	s
ρ	0.79	1.02	g/cm ³
μ_1	1.41	0.99	cp
μ_2	1.41	0.99	cp
μ_{avg}	1.41	0.99	cp

Sources of error

A potential source of error comes from, when the large reservoir in the oil test was filled up. The oil was filled past the marked line, so the capillary tube got filled with oil. This could have added some extra pressure due to the hydrostatic column with oil, but this would not affect the result much. The reported error for the viscometer constants were; "The relative uncertainty of the mentioned K_1 and K_2 comes to 1.2% at a confidence level of 95%" (taken from manufacturer's certificate, see Appendix E.4).

The largest error came from manually recording the time. The time could have been stopped or started a bit early, or a bit too late, which could give a small error in the measured time. Since the final viscosity is found using the average of two tests, and subtracting the Hagenbach constant, the error using manual measurement will be evened out. An error estimate was performed to see how the manually recording of time would affect the final result. To test the reaction time Human benchmark (2018) was used. Two tests were performed where the average of the tests were 0.265 s reaction time. To calculate the error Eq. (2.7.1) was used with the parameters in Eq. (4.1.3). The total error estimate gave the following error for the two viscosities: $\mu_o = 1.41 \pm 0.01$ cp, and $\mu_w = 0.99 \pm 0.01$ cp.

4.1.3 Interfacial tension

Tests were performed in the Reservoir lab at NTNU to find the interfacial tension (IFT) of the oil and distilled water with added salt. The test samples were taken from the separator on the date 9-02-2018.

Method

To perform the measurements a Drop Shape Analyzer from Krüss was used. The surrounding liquid, the distilled salt water, was put in a glass box and placed on the stand and the lid was screwed on. A syringe was filled with oil and placed in the stand. A J-shaped needle ($D = 1.047 \text{ mm}$) was placed on the tip of the syringe. The syringe and needle were then lowered into the water phase. At the end a temperature needle was put in the water phase to record at which temperatures the measurements were performed.

In the program controlling the apparatus, the properties of the different liquids were filled in, see table 4.1.2. The measurements use the pendant drop method to calculate the IFT, which takes in the difference in inner and outer pressure between the two liquids, see Laplace equation (2.2.1). The difference in pressure is found by $\Delta p = \Delta \rho g l$. g is the gravitational constant, and l is the difference between the measuring point and needle opening. The r_1 and r_2 is the radii of the horizontal and vertical circles of curvature (Krüss 2010). Fig. 4.1.2 show a picture of the droplet from the Krüss apparatus. The blue and green line are the r_1 and r_2 drawn on a curved surface segment. They define the surface curvature in the point where r_1 and r_2 intersect (Krüss 2010).

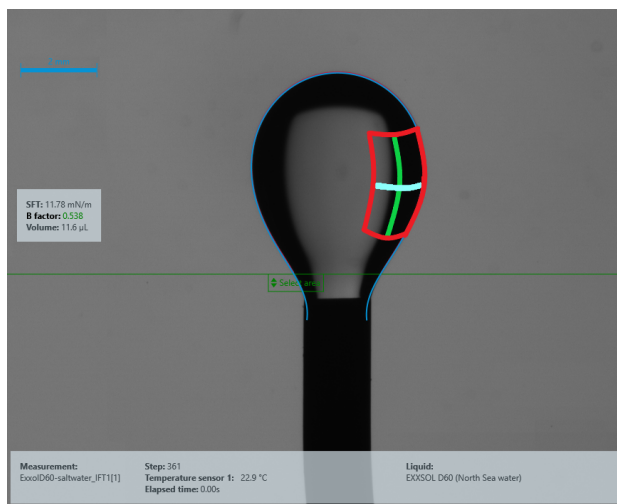


Figure 4.1.2: Image of the droplet where tests were performed. The blue and green line is the radii of the horizontal and vertical circles of curvature.

During the tests, the IFT showed a variation in time, as the one shown in Fig. 4.1.4, gradually stabilizing towards a constant value. Two tests were initially performed, but the duration used was not enough to ensure that the final value was fully stabilized. A third test was therefore performed where measurements were done every 20 s, and running for 3 hours were 540 tests (step numbers) were performed. An images of the droplet used to calculate the IFT can be seen in Fig. 4.1.3.

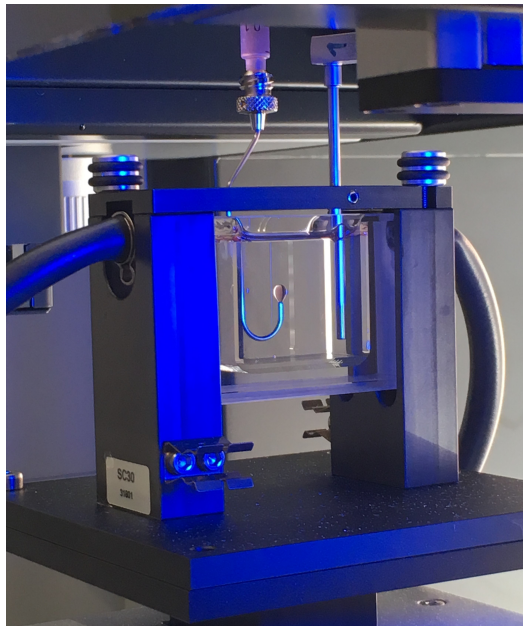


Figure 4.1.3: Pendant drop on needle used to calculate IFT

Results

The last ten values, where the graph flattens out, see Fig. 4.1.4, were used to find the average of the measurements. The results can be seen in table 4.1.2

Table 4.1.2: Result from pendant drop measurements

Test parameter	Average value
IFT	11.41 mN/m
Temperature	22.3 °C
Density oil	789.74 kg/m ³
Density water	1020.80 kg/m ³

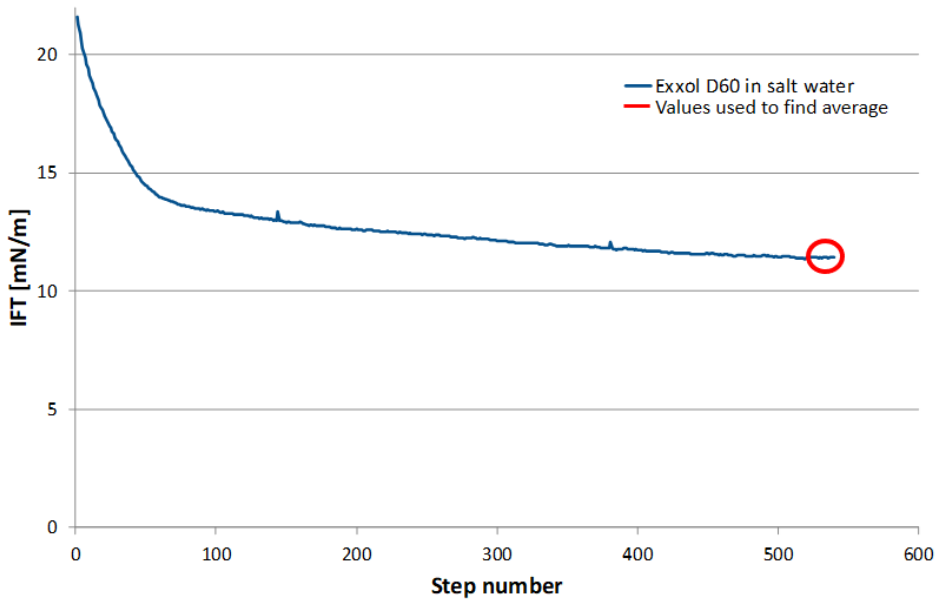


Figure 4.1.4: Plot for number of measurements vs. IFT

Sources of error

The density of the oil and water changes with temperature, see sec. 4.1.1. When inputting the densities in the instrument it was not possible to specify a temperature dependent trend. The densities for the room temperature at the time (22.6°C) was therefore used. Looking at the temperature from the last 10 measurements the average temperature was 22.3°C , see table 4.1.2 . A temperature of 22.3°C should give a density difference of 0.23 g/cm^3 . The used temperature gave a density difference of 0.23 g/cm^3 . This is the same density difference, so the results is therefore correct for the used temperature.

4.2 Flow Pattern Mapping

Flow patterns at the inlet of the separator were characterized for several combinations of water and oil flow rates, and a flow regime map was built. The determination of the flow patterns were performed to see for which flow rates and water cuts the different flow regimes appeared. Knowing this could be used to see how the different regimes affect the water separation, and how the droplet size distribution varies for different flow patterns.

4.2.1 Method

The tests were performed at the inlet of the pipe separator, running tests for different mixed flow rates and different water cuts. The tests were executed by keeping the flow rate fixed, while testing for different water cuts, before changing to a new rate. The test matrix for the experiment can be seen in Fig. 4.2.1.

Table 4.2.1: Test matrix for flow pattern map

Property	Test range	Step size
Mixed flow rate	250 - 700 L/min	50 L/min
Water cut	10 - 90%	10%

For each test a minimum of three pictures were taken using a single reflex camera (Canon EOS 70D). The cameras shutter time was put to a maximum (8000 UNIT) and used together with the highest possible ISO (12800). Two light sources were used to create better light for the image, where one source was placed behind the pipe and the other below. The camera was placed 20-30 cm away from the pipe. A paper ruler was taped on the pipe for reference and to be able to see how the interface between the water and oil change for different water cuts and flow rates. The flow data for each run is gathered for one minute logging 5 points per second.

To identify which flow pattern that is present in the flow, the flow patterns described by Trallero et al. (1997) are used for guidance, which can be seen in Fig. 4.2.1. Excel is used to plot the flow pattern maps.

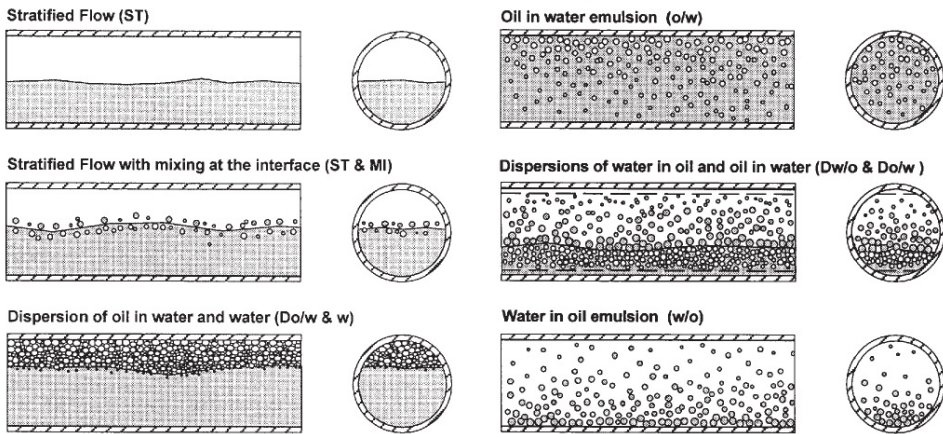


Figure 4.2.1: Horizontal oil-water flow patterns (Trallero et al. 1997)

4.2.2 Result and Discussion

Appendix A contains pictures of the flow pattern from each test point. Looking at these images, the reader can see that six different flow patterns can be identified. One image of each of the six flow patterns can be seen in Fig. 4.2.2. The identified flow patterns are:

- SM – Stratified flow with mixing on the interface
- Do/w – Dispersed oil-in-water
- Dw/o – Dispersed water-in-oil
- Do/w + w – Dispersed oil-in-water with a layer of water at the bottom of the pipe
- Dw/o + o – Dispersed water-in-oil with a layer of oil at the top of the pipe
- Do/w + Dw/o – Dispersed layer of oil-in-water coexisting with a dispersed layer of water-in-oil

Three different flow pattern maps are plotted using excel. One plot is plotted using superficial velocities, see Fig. 4.2.3. Another is plotted using water cut and the velocity of the mixed flow, see Fig. 4.2.4. The last plot is plotted using water cut and the total flow rate, see Fig. 4.2.5. Plotting superficial velocities against each other gives a plot that does not have a square matrix. This is due to the tests matrix, which used mixing flow rates and water cuts. Transforming these values to superficial velocities, did not give the same matrix shape. To get this, the superficial velocities would have to be the variables that is changing when running the experiments.

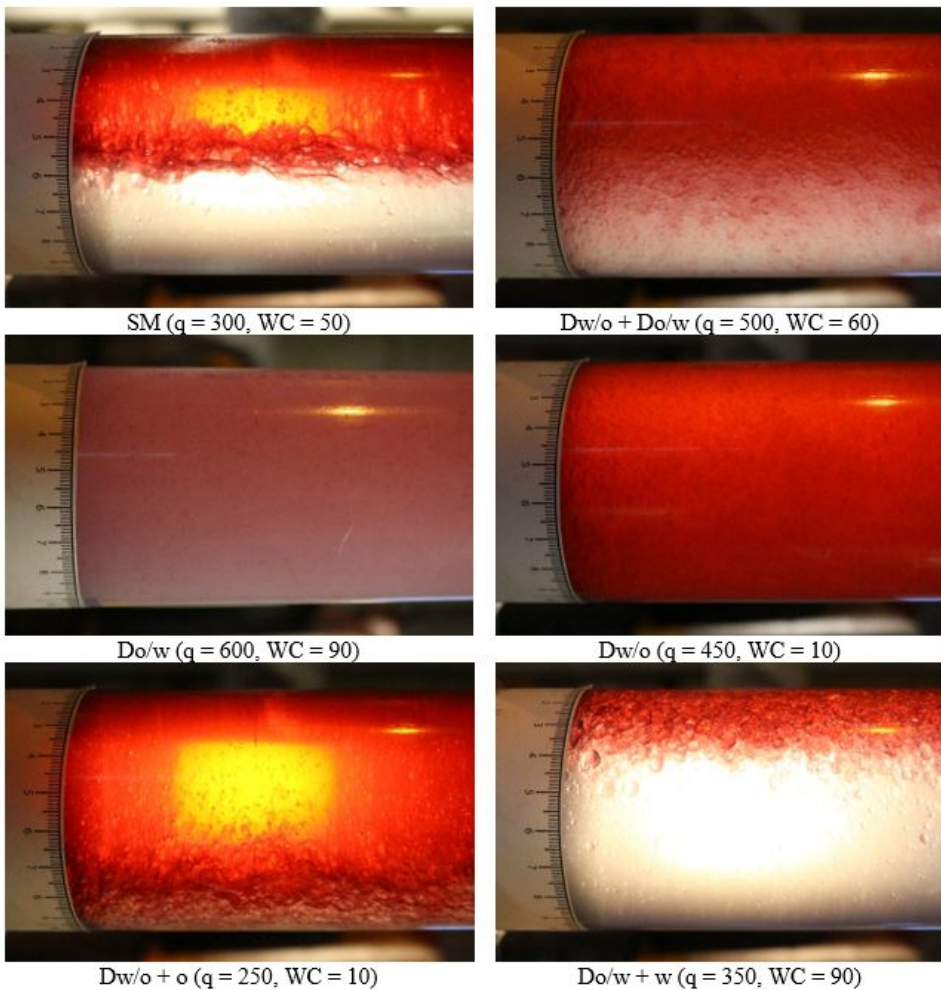


Figure 4.2.2: Images of the different flow patterns that were characterized

Comparing the plot in Fig. 4.2.4 with the plot from Trallero et al. (1997), Fig. 2.5.1b, the reader can see that there is a similar trend between the two flow maps. Due to too high flow rates, a stratified layer was not seen for this experiment so the placement of this flow pattern can not be compared. For both flow pattern maps, one can see that when being in a SM layer, and only increasing the flow rate of oil, the flow pattern will change to Do/w+w and further for even higher flow rates to Do/w. One can also see that when being in a Dw/o and increasing the flow rates of oil, the flow pattern will transform to a Do/w + Dw/o before changing to a Do/w. The flow pattern maps report what would be expected; the flow consists of oil-in-water for low water cuts, and more oil-in-water for higher water cuts. The flow is also getting more mixed for higher flow rates, which is also what one would expect because of the higher energy in the system (see sec. 2.4).

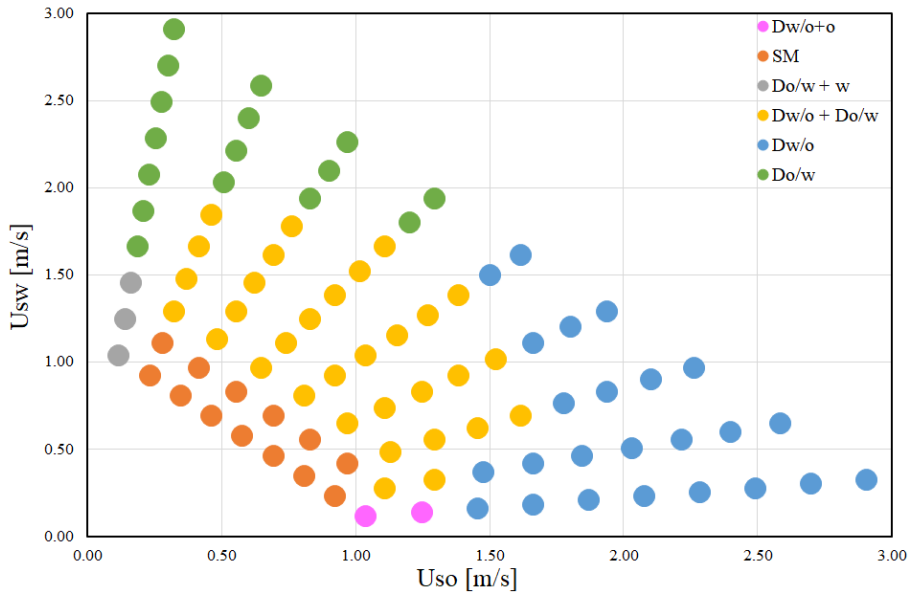


Figure 4.2.3: Flow pattern map plotted for superficial velocities

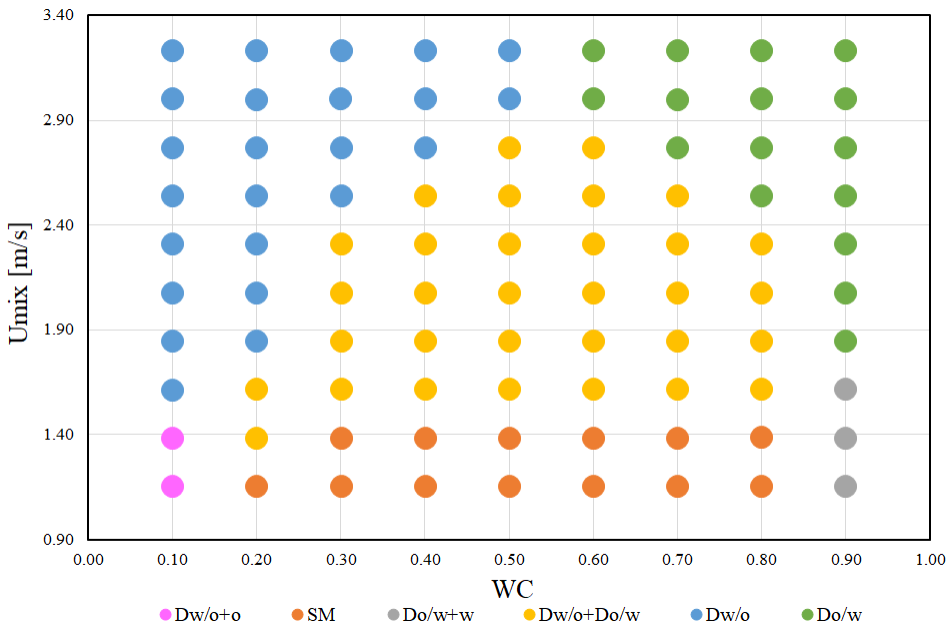


Figure 4.2.4: Flow pattern map plotted for water cut and mixed flow velocity

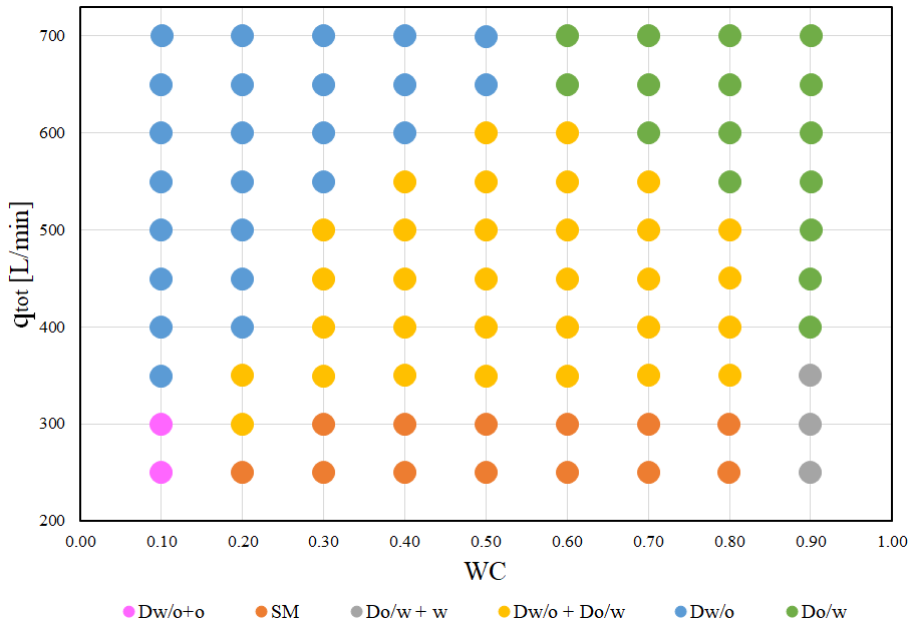


Figure 4.2.5: Flow pattern map plotted for water cut and mixed flow rate

4.2.3 Sources of error

The pictures are interpreted by which flow regime the author can see from the pictures of the flow. Especially for the transition between dispersed oil-in-water and water-in-oil it can be difficult to see the change, so the flow pattern that is plotted close to the transition zones might not be 100% correct.

An error estimate for the apparatus were performed by using equations from sec. 2.7 with equations from calibrations written in sec. 3.3. To calculate the reported error Eq. (2.7.9) is used where $\tau = 1.984$.

The reported error for the different measuring apparatus are:

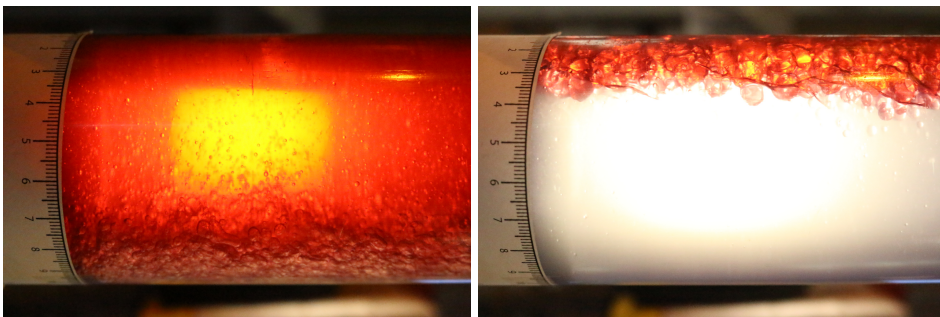
- The error for the temperature measurements was $\pm 0.3^{\circ}\text{C}$
- The error for the density measurements was $\pm 0.54 \text{ kg/m}^3$
- For the flow measurements the largest error was for WC90 for flow rate 700 L/min where the error was $\pm 0.98 \text{ L/min}$. The smallest error was for WC10 for flow rate 250 L/min where the error was $\pm 0.06 \text{ L/min}$

4.3 Characterizing Droplet Size Distribution

The droplet size distribution (DSD) was determined at the inlet of the pipe separator. The distribution was determined for different placements in the pipe for different water cuts, flow rates and valve openings.

4.3.1 Method

A PVM[®] V819 camera from Mettler-Toledo AutoChem was used to find the DSD. The setup of the camera is described in sec. 3.2 and a description of the camera can be seen in sec. 2.3. A 4 mm "hat" was placed on-top of the camera, which means droplets larger than 4 mm ($4000 \mu\text{m}$) can not be seen with the PVM. Due to temperatures close to 20°C it was not used any purge gas for the PVM when running experiments. Tests were performed in two different parts of the pipe, one in the water zone and one in the oil zone. The images that were taken when determining the flow pattern map were used to find the distance the PVM should be placed down in the pipe to make sure the probe would be in a dispersed phase. Test q250-WC10 had the thinnest water layer at the bottom of the pipe. From the picture in Fig. 4.3.1a one can see that the probe should be placed more than 8 cm vertically down in the pipe, to assure the camera records pictures from the dispersed phase. Test q250-WC90 had the thinnest oil layer at the top of the pipe. Looking at the picture in Fig. 4.3.1b one may see that the probe should be placed less than 3 cm vertically down in the pipe, for the probe to be in the dispersed phase. Eq. (4.3.1) together with equations for right triangles were used to find the



(a) Thinnest water layer (q250-WC10)

(b) Thinnest oil layer (q250-WC90)

Figure 4.3.1: Images of the flow used to find how far down in the pipe the probe should be placed

length the PVM should be put in the pipe. A description of the different length can be seen in Fig. 4.3.2. The PVM should be placed 1.1 cm down in the pipe when taking pictures in the top layer, and 7.6 cm in the pipe for tests performed in the bottom of the pipe. The positions were marked on the setup, to get continuous measurements for all experiments.

$$h = (OD/2) * \left(1 - \cos\left(\frac{oh}{OD/2}\right)\right) - \frac{OD - ID}{2} \quad (4.3.1)$$

here H is the vertical distance inside the pipe, and OH is the distance on the outside pipe (what is read on the ruler from the picture of the flow, see Fig. 4.3.1).

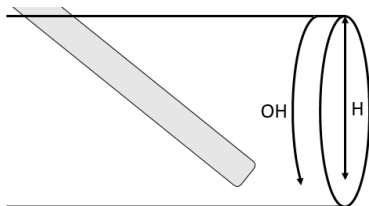


Figure 4.3.2: Measured heights to find the distance to place the PVM in the pipe

Since the oil and water are continuously recirculate in the system, a dispersion of small droplets can started to appear after running tests for some time. This is a result of incomplete separation in the large main separator. To try to avoid the creation of small droplets the experiments were first executed at low flow rates; testing both water cuts at one height, changing height and testing for the two water cuts over again, before increasing to a higher flow rate. The tests were performed for two water cuts, WC30 and WC70, and for two valve openings, 100% open and 50% open, for each of the two heights in the pipe. The tests performed with the valve 100% open were for flow rates 300-700 L/min with a step of 50 L/min, for both water cuts and heights. The tests performed with the valve 50% open were for flow rates 300, 400, 500 and 600 L/min, for both water cuts and heights. Table 4.3.1 show the test matrix for the different test points. Fig. 4.3.3 show the different flow patterns that are tested for the respective flow rates and water cuts.

Table 4.3.1: Test matrix for DSD measurements

Property	Test range	Unit
Flow rate	300-700	L/m ³
Water cut	30 and 70	%
Test points	3 and 8	cm from top of pipe
Valve opening	100 and 50	% open

For each test 240 pictures of the flow were collected, taking an image every 0.5 second. The average temperature in the system when recording the images was 18.4°C. Data from the measurement apparatus were gathered for the same amount of time, logging five points per second. It was visually checked that the flow had stabilized after a parameter was changed, before a new test was performed. Some of the test points gave DSD with less than 500 droplets when using 240 images. Counting 500 droplets is the minimum required value when finding a DSD, see

sec. 3.4.2. A second test was therefore performed, testing for a longer time. The second test recorded 600 images, taking an image every 0.5 second. For this test the average temperature in the system was 20.1°C.

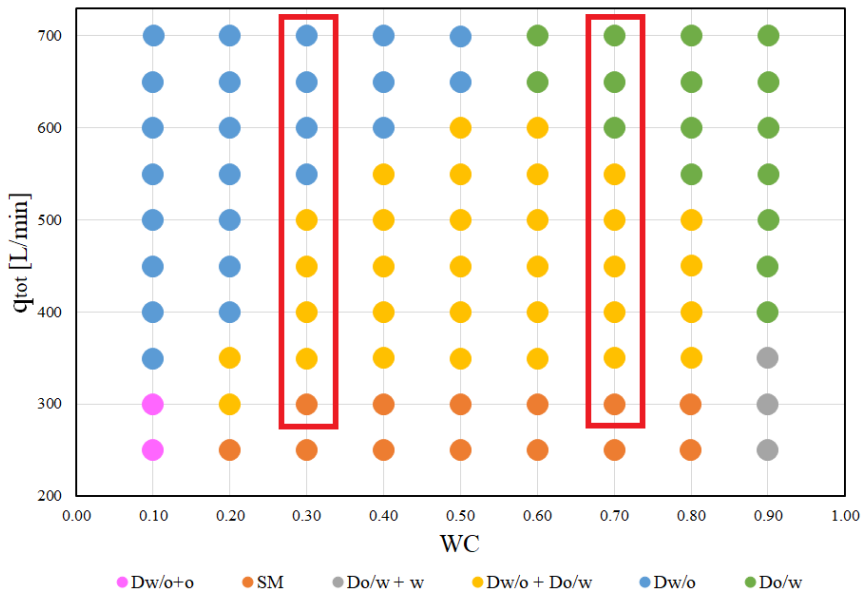


Figure 4.3.3: Tested flow rates and water cut

Two methods were compared to process the images, manual counting and automatic counting using a computational routine. The Matlab routine described in sec. 3.4.1 was used. How the code was edited based on the comparison with the manual counting will be explained in sec. 4.3.2. For the tests with valve 100% open, the experiments with 240 images were used to compare manual counting with counting using the Matlab routine. Measurements from ten test points were compared. For the tests performed with the valve 50% open, four test points were compared. For the tests counted manually with the valve 50% open only 600 droplets were counted for each test point, due to time limitations. When counting the droplets with the valve 50% open, the guidelines from sec. 3.4.2 were not followed a 100%. The edge of the droplets were too difficult to see, so assumptions were made to what size the droplet had. Fig. 4.3.4 shows a picture of the flow with the valve 50% open counted manually. Due to the large number of images and experimental points tested, it will be less time consuming to use the Matlab routine. It was therefore decided to use Matlab routine to process the images to create DSD. To quality control the output of the automatic counting procedure the reported d_{max} was manually compared with images, to see if the droplet the code have reported was a real droplet. The image input to Matlab is half of the original PVM picture, so the picture resolution will be 1.6 $\mu\text{m}/\text{pixel}$.

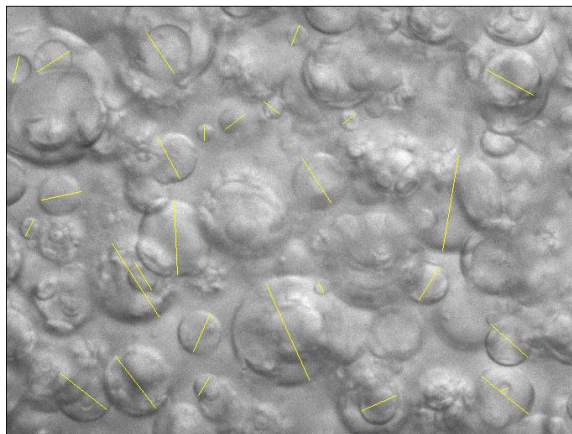


Figure 4.3.4: Droplets from valve 50% open counted manually (q500-WC30-top)

4.3.2 Improvement to Matlab code

When testing the Matlab code, it was noticed that the code overestimated the number of droplets counted. This would give results with large errors. As seen from the first Hough transformation picture in Fig. 3.4.1, several red circles are plotted inside each other. The program has recognized several "phantom droplets", meaning droplets lying inside other droplets that do not exist. These extra circles should therefore be removed to not be in the reported result. However, this correction will also remove the droplets lying inside others for cases where this actually happened, and the recognized droplets do exist. The code was edited so only the droplets that are seen in the original image are counted. The part of the Matlab code that was edited can be seen in Appendix C. A description of how the edited code works can be read in Appendix B. Three possible ways two droplets can be positioned were

Table 4.3.2: Description of different droplet placements

	Description	Want case
Case 1	$L < r_2 < r_1$	Not wanted
Case 2	$r_2 < L < r_1$	Not wanted
Case 3	$r_2 < r_1 < L$	Wanted

recognized, see Table 4.3.2. r_1 and r_2 are the radii of the different droplets, and L is the distance between the center of the droplets. The unwanted scenario appears if the center of one droplet lies inside the other droplet. Case 3 is the only wanted scenario, where L is larger than both r_1 and r_2 so both centers of the droplets lies outside the other. In the other two cases, illustrated in Fig. 4.3.5, L is smaller than both, or one of the droplets radius. This results in one of the droplets lying in, or partly inside the other droplet.

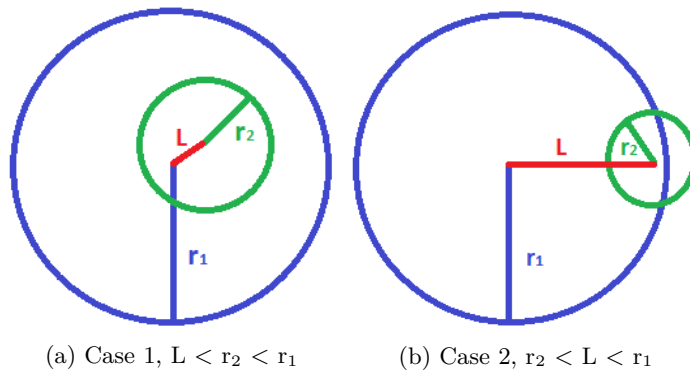


Figure 4.3.5: Unwanted droplet placement scenarios

The edited code was initially placed after the second Hough transformation (after the droplets are found a second time). This gave improvements where the number of droplets displayed on the final picture were reported. However, when comparing the code with manual counting it was found that the code overestimated the droplet sizes. When trying to fit new circles to the black area that were detected, some of the circles that matched using the Hough transformation were larger than the original black circle. Since the code is made to delete all the smaller droplets lying inside the largest drop, this overestimated droplet was the one that was reported. An example of this can be seen in Fig. 4.3.6. From the picture one may see that the largest red circle is overpredicting the droplet size. The black circle on the other hand, is a better representation of the droplet in the original image.

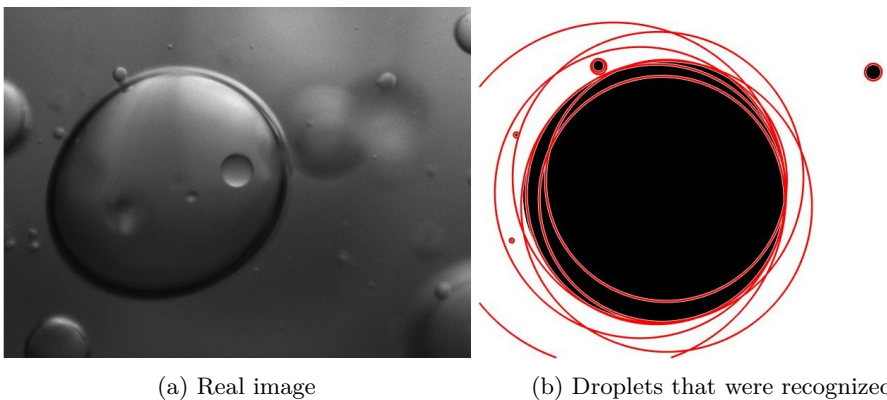


Figure 4.3.6: Example of an overestimated droplet (large red circles) found using the Matlab routine

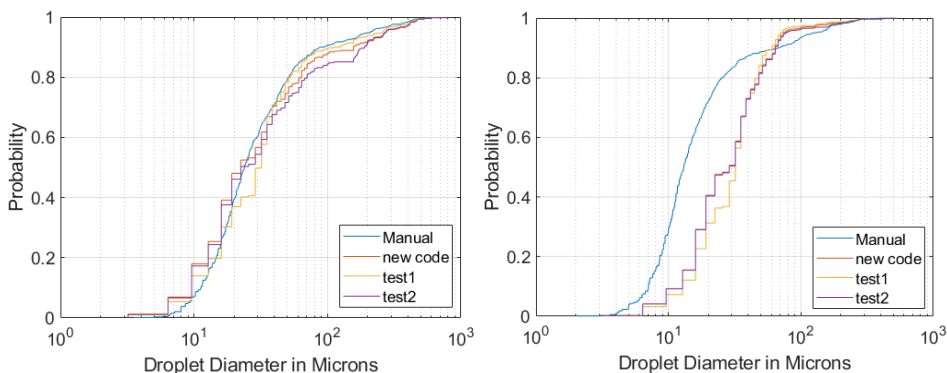
To try to remove the large overestimated droplet sizes, the edited code section was moved higher up in the code. It was placed between the first and second Hough

transformation. The last transformation was not performed, so the black circle would be the final count and the reported size. Changing the location of the edited code worked, where the size of the measured droplets matched better with the droplets from the original image.

After the code was edited it still had some issues. More droplets were counted manually, per picture, than by the code. Especially smaller droplets that were counted manually, were not as well recognized and measured by the code. Using the new edited code, the sensitivity was changed (done from the interface of the program, see Fig. 3.4.2) for different droplet sizes. This was done to see if the change in sensitivity would improve the number of counted droplets and give a more representative DSD. Several tests were performed, where the two sensitivity changes that gave a result that best represented the real image were compared with test performed manually. The three different sensitivities that were compared were:

- new code – code with default sensitivity
- test1 – new code with edited sensitivity to 0.85 for droplet size range 20-39 pixels, and sensitivity of 0.95 for droplet size range 80-99 pixels
- test2 – new code with edited sensitivity to 0.97 for droplet size range 100-139 pixels

The tests were performed using pictures taken from the experiment where 240 images were recorded. Ten test points were compared where droplets were found both manually (using the criteria from sec. 3.4.2) and using the Matlab code to see how the distributions would differ when counting droplets from the same images. Out of the 10 tests, the Matlab counting deviated from the manual counting for two test points. One example of how the graphs deviated can be seen in Fig. 4.3.7b. The other eight tests gave a good fit, similar to the plot in Fig. 4.3.7a.



(a) Example of graphs plotting with small deviations (b) Example of graphs plotting with large deviations

Figure 4.3.7: Matlab routine tested for different sensitivities and compared with manual counting

From the images one may see that the test1 plot is lying closer to the manual count, both for smaller and larger droplet sizes. The graphs from the counting done by Matlab is not as smooth as the graph from manual counting, which could be due to the sensitivity range in the code. All three codes reported the same maximum droplet size. The average percentage difference from the real d_{max} found from manual counting was 16.2%. The d_{32} was also compared for all tests. The results varied allot, varying between an error of 50% to 1% different from manual counting. Test1 gave the smallest average error, 14.76%, for all the tests. This was also the one that gave the best fit on the graphs, and counted the highest numbers of droplets which were closer to the numbers counted manually. The sensitivities that were used in test1 was therefore going to be used.

There were some variation of the d_{max} when compared against manual counting. Three out of the ten tests gave a d_{max} larger than what were counted manually. For some of the test points, layers or large droplets of liquid covered parts of the image. For some of the cases, but not all, the program recognized this as a large droplet which would affect the result. An example of a large droplet that was created by the program can be seen in Fig. 4.3.8.

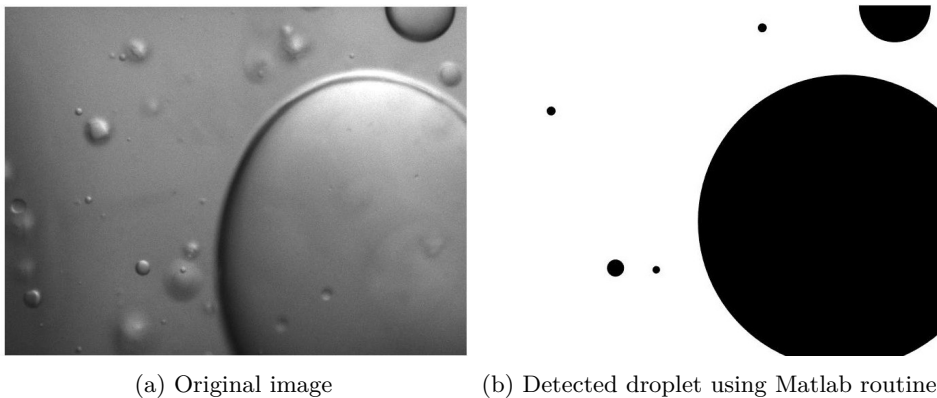


Figure 4.3.8: Example of Matlab detecting and creating an overestimated droplet

These large droplets would not be counted as a droplet when counting manually. First, one can not know how large the droplets really are, and secondly, it seems like there is a layer of liquid, and not a real droplet which should be measured. To avoid these large overestimated droplets, the largest droplet found for a test point should be manually checked to see if the reported d_{max} is a real droplet or not. In the excel file that is saved with the results from the Matlab counting, a matrix containing the image number where the detected droplet is found is reported. This can be used to check the largest droplets manually. One can search for the largest droplet in the excel file and find the picture where it is taken from to see if it is a real droplet. If the droplet found by the program is not a real droplet, the measurement should be deleted.

In addition, to get a more accurate result for d_{max} , the largest droplets could be found manually. One could loop through the pictures taken from the experiments and count the largest droplets. The results could then be included in the results from the Matlab counting. Doing this might result in the same droplets being counted by both the Matlab code, and manually. This might therefore effect the final droplet size distribution. There was not time to see the effect this would make on the final DSD, so this will be written as further work.

It was tried to do other editing to the code as well. The image that is displayed at the interface of the code, displays red circles which is not what is reported. It was tried to display the original image at the end, and also to use the corrected image to do the second Hough transformation over again. This gave an error for the images where there was no droplets to detect. To correct the code is not the main objective of the thesis, so there was no time to study this further. In the code in Appendix C the code that did not work is also added, so it could be improved as further work.

Valve

The Matlab routine was also tested for the measurements performed with the valve 50% open. Fig. 4.3.9 shows an example of the droplets that were recognized by the program. Only a small number of the droplets from the original image has been recognized by the program. With manual counting, see Fig. 4.3.4, 27 droplets were counted compared to six with the Matlab routine.

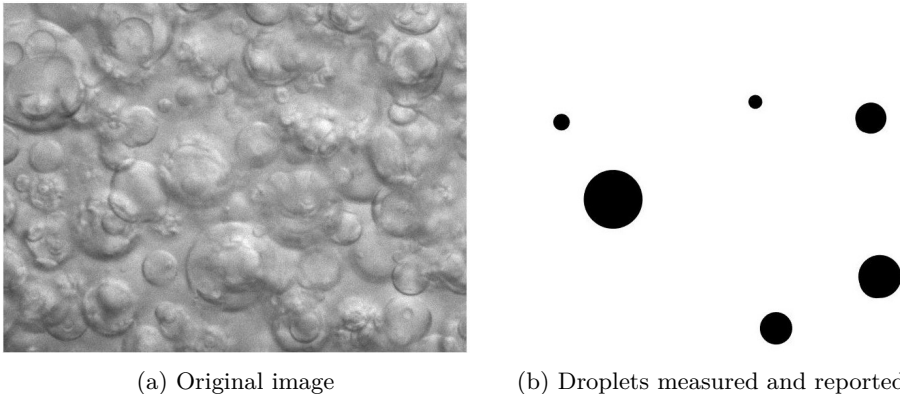


Figure 4.3.9: Example of number of droplets recognized by Matlab using test1 sensitivity (q500-WC30-top).

To compare how the results from Matlab routine varied with the manual counting, the two distributions were plotted in the same plot. The results for the four tests can be seen in Fig. 4.3.10. From the plots, one can see that the two distributions follow the same trend and plots close to each other. For the tests at the top part

of the pipe especially, the graphs plots almost on top of each other.

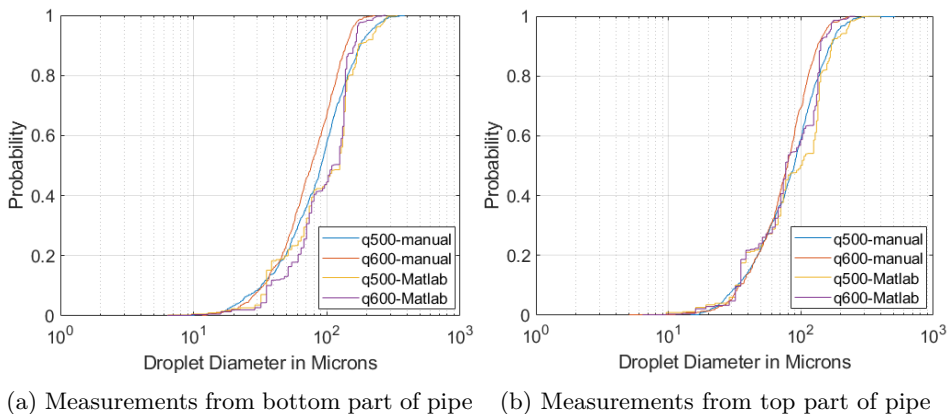


Figure 4.3.10: Comparison of measurements performed manually with measurements using Matlab routine (all tested for WC30)

The number of droplets compared for the two tests vary, where only 600 droplets were counted manually, while more than a thousand droplets were recognized by the program. The d_{max} and d_{32} found from the Matlab routine can also be compared with the results found from manual counting, see Table 4.3.7. From the results one can see that the results are similar with an error varying around 20% (except for d_{32} for q500-top where the error was 50% different).

Table 4.3.3: d_{max} and d_{32} results from Matlab routine from tests with valve 50% open

Flow rate	d_{max}	d_{32}
q500-bottom	336.0	173.3
q500-top	396.8	162.7
q600-bottom	275.2	139.3
q600-top	256.0	130.5

When looking at the results one can see that using the Matlab routine, even though few droplets are counted per picture, will give a fairly good representation of the result. Although the four tests gave similar distributions, the Matlab routine should be compared with more tests. Different sensitivities could be tested, to see if this would affect the number of droplets counted per image. Tests could also be compared with manual counting where more than 600 droplets are counted. There was no time to do this in the thesis work, so this is recommended for further work.

4.3.3 Result and discussion

This section is divided into subsections, where each subsection is reporting and discussing one finding. First the pictures taken with the PVM from the flow will be presented. Secondly, the number of droplets that were counted. Then, the different plots will be discussed, before presenting the d_{max} and d_{32} results. Last, the comparison with the 50% open valve will be presented.

Pictures from the flow

To see what kind of flow pattern that is present for each picture in Fig. 4.3.11 and Fig. 4.3.12, the pictures can be compared and studied together with a side view of each flow in Appendix A and the flow pattern map in Fig. 4.3.3.

Fig. 4.3.11 shows pictures taken in the upper part of the pipe for different water cuts and flow rates. The flow contains more and larger droplets for higher water cuts. For higher flow rates the flow becomes more turbulent, causing the droplets in the dispersed flow being more homogeneously distributed over the total cross section. One might also see a slight variation in the droplets when looking at oil droplets and water droplets. On all the images one will see dispersed water-in-oil, except for WC70 for q600 and q700 where the flow is dispersed oil-in-water. The pictures with oil appear a bit darker, where the oil droplets does not have such a bright circle circumference as the water droplets dispersed in oil. Fig. 4.3.12 shows pictures taken from the bottom part of the pipe for different water cuts and flow rates. The same trend seen at the top part of the pipe can also be seen from the placement at the bottom off the pipe. The flow consists of smaller and less droplets per picture for the lower flow rates. The flow with dispersed water droplets consist of larger droplets that stretch over large parts of the picture. The droplets are also more clear as was seen for the placement at the top of the pipe.

Comparing the images from the top and the bottom of the pipe, the images taken from the bottom have more lines crossing the image for WC30. These lines could come from fluid interfaces and large droplets. A potential cause could be that the probe was not placed low enough in the pipe. For the lower flow rates, the probe could be taking pictures around where the transition between the continuous water and oil layer happened. Larger layers of continuous phase could therefore pass the camera, which could create lines as seen from the pictures. A second cause could be that flow does not have a "free pathway" under the probe. The flow will hit the bottom part of the pipe, which could effect the behavior of the flow around the placement of the camera. A third cause could be that the water droplets are larger than $4000 \mu\text{m}$, and does not fit inside the "hat", or the PVM camera window. An other possible cause could be that large droplets are more deformable (than smaller droplets) and might create lines when stretched.

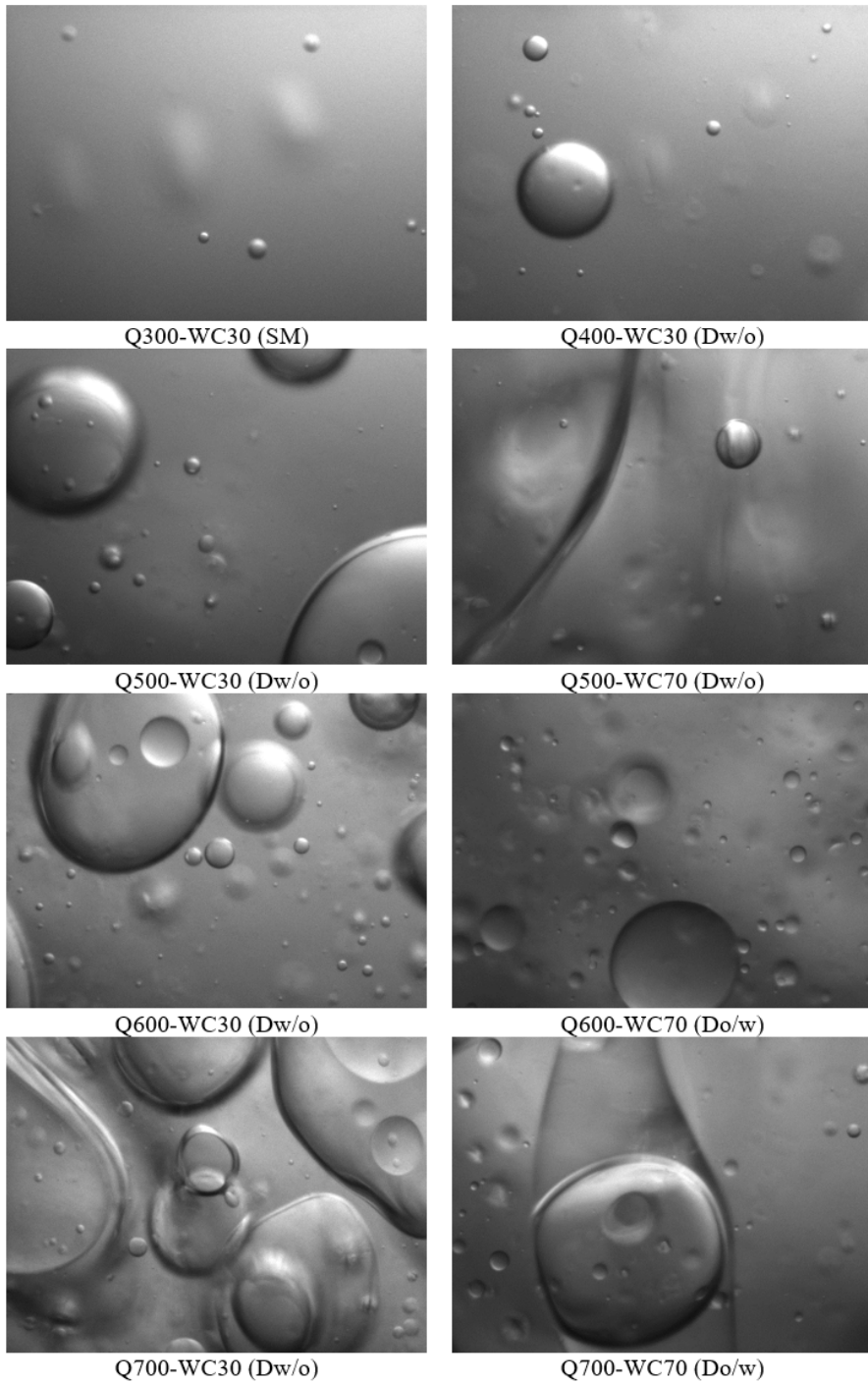


Figure 4.3.11: Images of the flow taken with the PVM at the top part of the pipe

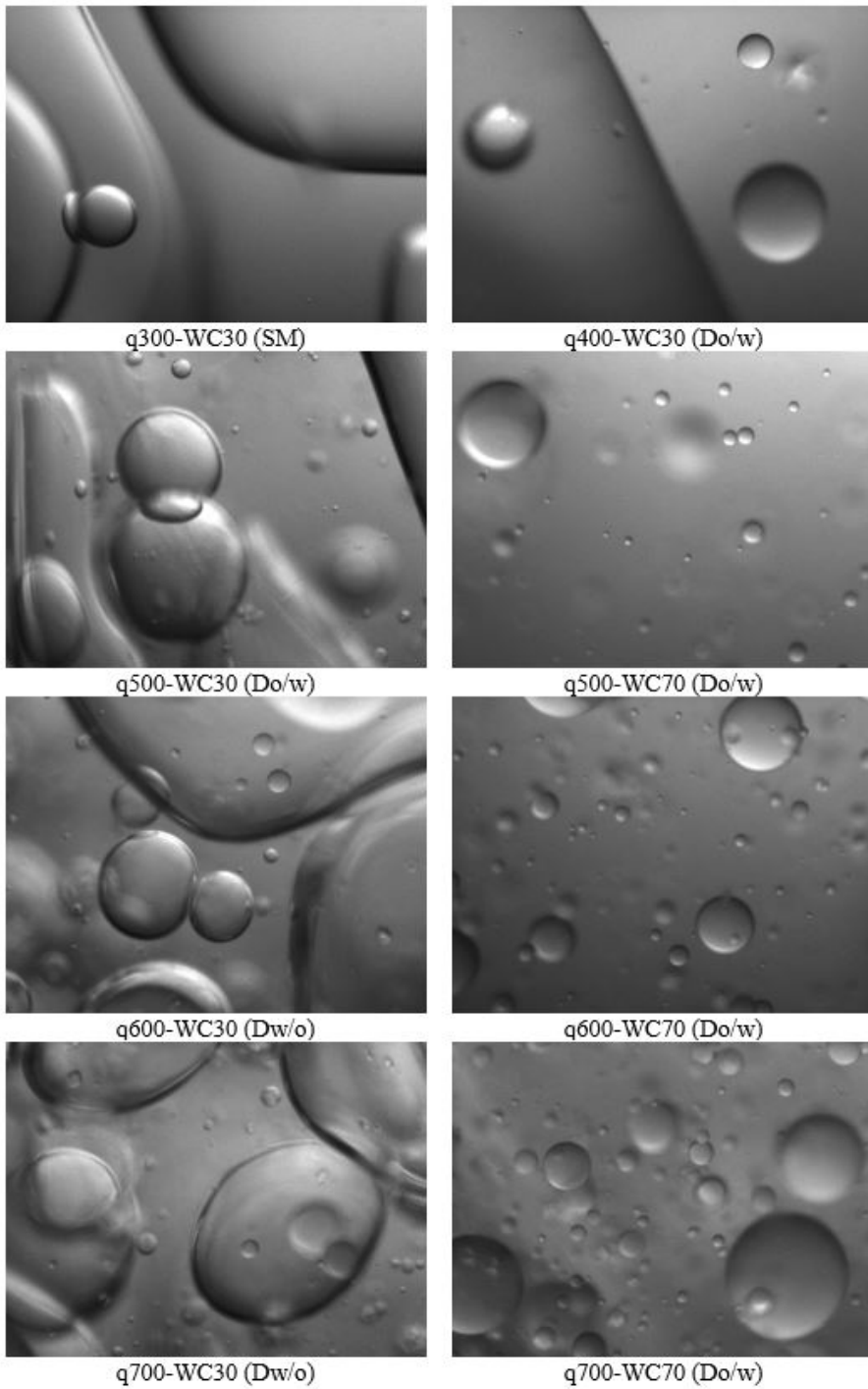


Figure 4.3.12: Images of the flow taken with the PVM at the bottom part of the pipe

Counting

Table 4.3.4 shows the number of droplets that were counted using the Matlab routine. The numbers in black are droplets counted using the first experiment where 240 images were used to get the droplet distributions. Numbers in red is from the second experiment where 600 images were used. From the table one can see that only test q300 has less than 1000 droplets counted, all being over the minimum limit of 500 droplets. The distributions will become more accurate for higher numbers of droplets counted.

Table 4.3.4: Numbers of droplets counted using Matlab routine

Flow rate	Bottom		Top	
	30	70	30	70
300	589	945	970	814
350	1062	1696	1143	1123
400	1482	2771	2645	1945
450	2331	5472	3809	3197
500	2993	1908	1440	1034
550	1242	2842	1445	1568
600	1289	3694	2046	2238
650	1653	3630	1831	2673
700	1689	3883	2017	2888

Plot

As discussed in sec. 2.2.2, there are different ways to present the DSD. Fig. 4.3.13 shows two examples of plot; a normal cumulative plot and a histogram plot. Cumulative plots are better to use when comparing data from different tests, while histograms shows a good representation of the distribution for each test. Since there are a large number of smaller droplet sizes in the system a cumulative log-plot will be used, to better see the difference in smaller droplet sizes.

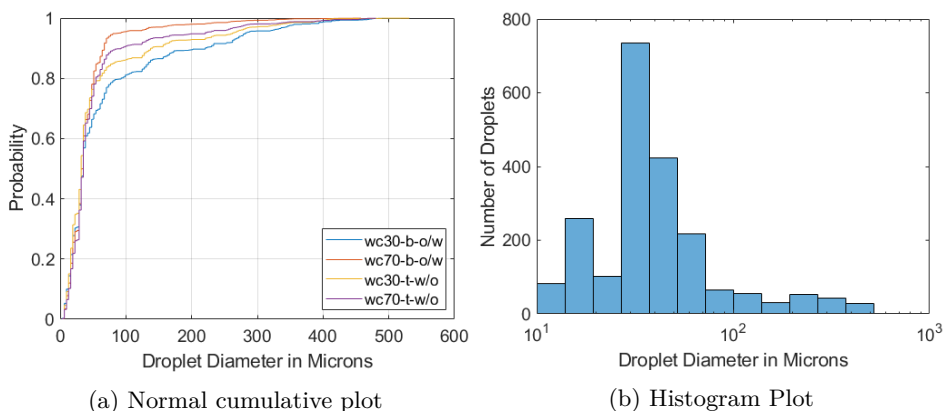


Figure 4.3.13: Different types of DSD plot (q600-WC70-top)

The DSD is plotted for all tested rates on the same figure which gives a good description of how the DSD varies for the different flow rates. Plots were made for the two measured water cuts and for the two positions of the probe. The resulting plots are given in Fig. 4.3.14. Fig. 4.3.15. Fig. 4.3.16 and Fig. 4.3.17.

First, the system consisting of oil droplets dispersed in water will be compared, where the PVM is placed at the bottom of the pipe. For WC30 the flow will consist of dispersed water-in-oil for flow rates higher than 500 L/min. Fig. 4.3.14 shows the plot for WC30 at the bottom of the pipe. The distribution follows the same trend within the droplet size range 40 μm to 300 μm . The distributions are having the same shape of the curves, where the lower flow rates are plotted above the higher ones. In general, the droplet distribution consists of larger droplet sizes for higher flow rates. However, q600 had a larger droplet size distribution than q650 from about 30 μm , and also larger than q700 for a few droplet sizes. For larger droplet diameters, one can see that there is a small gap between q500 and q550 (green and turquoise line). This is where it is expected to see a change in the flow pattern where it goes from $D_{w/o} + D_{o/w}$ to only $D_{w/o}$. This could be a potential cause to the slight shift in the plotted lines. Another potential cause could be that it is where the flow transfers from a dilute to dense system, where the flow is dominated by droplet coalescence that creates larger droplets (see sec. 2.4.2). For the lower part of the graph, from 2-40 μm the flow rates are plotted with the lower flow rates on the top, and the higher on the bottom. The flow rates are plotted in the same area except q300 which consists of smaller droplets. From the flow pattern map (Fig. 4.3.3), one can see that the flow pattern here is stratified with mixing at the interface. There is therefore expected to see less droplets dispersed in this flow pattern, where some of the small droplets seen could be from the small recycled droplets in the closed loop system, see sec. 4.3.1.

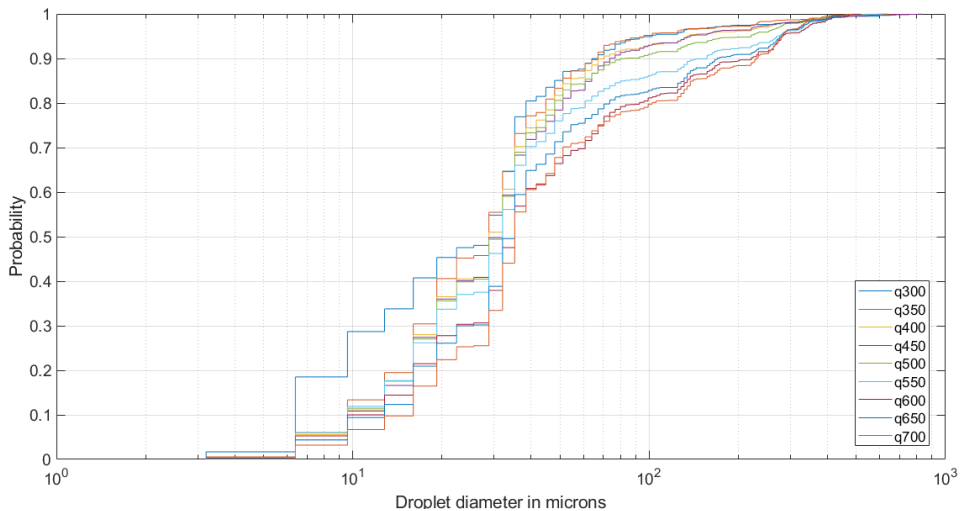


Figure 4.3.14: WC30 bottom of pipe for all flow rates, $D_{w/o}$

Fig. 4.3.15 shows the plot for WC70 at the bottom of the pipe. The system consists of oil droplets dispersed in water, but changes to a dispersion of water droplets in oil for flow rate 550 L/min. One can see that the DSD are, also here, larger for higher flow rates. Around droplet size 40 μm flow rate q500 and q550 starts to consist of smaller droplets sizes than the lower flow rates. The flow rates plot higher up towards the left. From the flow pattern map one could see that it is between 550-600 L/min that the system will change to a pure phase of dispersed oil-in-water. This could explain the deviation from the trend, where the dispersed oil-in-water might consist of smaller droplet sizes before the change to fully dispersed oil-in-water happens. This seems also to be where the change happens from a dilute to a dense systems that can be seen from the gap between q600 and the lower flow rates. Flow rates below 600 L/min might consist of a dilute flow dominated by droplet break-up, while the flow rates above 600 L/min is dominated by droplet coalescence. Flow rate q300 is also plotted a bit higher than the other flow rates for the lower droplet sizes, for this plot as well. Flow rate q600 is following the same trend here, and is not deviating as it was in the WC30 plot.

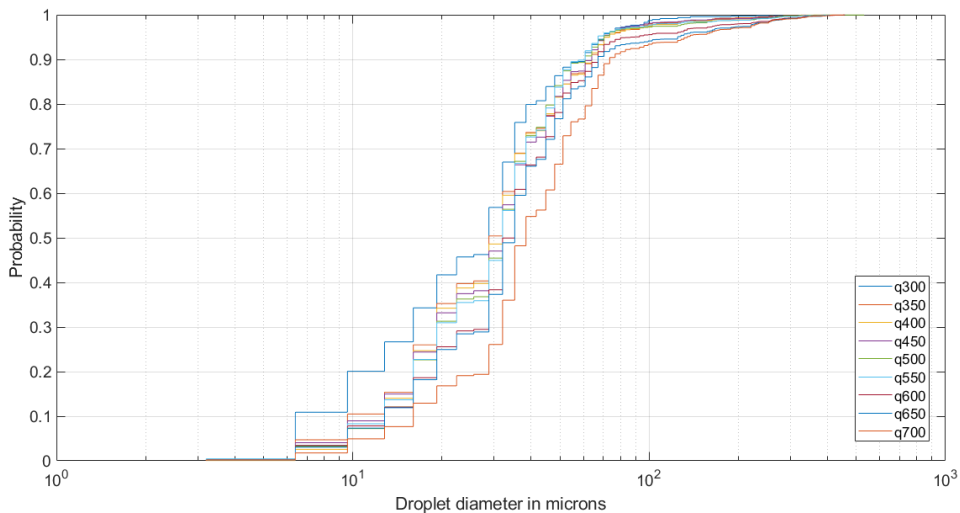


Figure 4.3.15: WC70 bottom of pipe for all flow rates, Do/w

Comparing both graphs one can see that the plots for WC70 at the bottom of the pipe are shifted more towards the left, towards smaller droplet sizes. The plotted lines for WC70 are lying more closely together, with a steeper slope. The droplet size range where the plots cross the 90% line are varying from 60-80 μm for WC70, while for WC30 the droplet sizes are varying between 70-200 μm . The droplet sizes are ergo smaller when there is more water in the system. One reason for this could be that the interface between the oil and water is moved higher up in the pipe for higher water cuts, away from the PVM test point. For the tests with WC30 some large oil droplets could break from the overlying oil layer that created larger

droplets of oil-in-water, than what is naturally dispersed. This effects is not seen for the WC70 case, where only the dispersed droplets is seen. Another reason could be that for the WC30 test, the flow pattern for higher flow rates are dispersed water-in-oil. Due to gravity the larger water droplets will sink towards the bottom of the pipe. This will result in larger water droplets seen when measuring at the bottom of the pipe. The opposite case is seen for the WC70 case, where the dispersed oil droplets might have raised to the top of the pipe and is therefore not measured.

Fig. 4.3.16 shows the plot for WC30 at the top of the pipe. The system consists of water droplets dispersed in oil. The trend seen from the cases with dispersed oil-in-water is not as well represented here, where the droplet size distribution gets larger for higher flow rates. The q400 plot is plotted in the top part of the plot towards the left, meaning it has a higher percentage of smaller droplet sizes than the other flow rates. Around the 70% mark the q600 starts to consist of smaller droplet sizes than q500. The shift where the flow becomes fully dispersed oil-in-water can be seen from the gap between q500 and q550(and q600). The point where the flow changes from a dilute to dense systems seams to be around q450, where one can see a large gap between q450 and q500. The width and slope of the distribution are similar to the one for WC30 at the bottom of the pipe. The thinner point on the graph where the distribution shifts from smaller to larger droplets sizes lies around 60% and 30-40 μm for both plots.

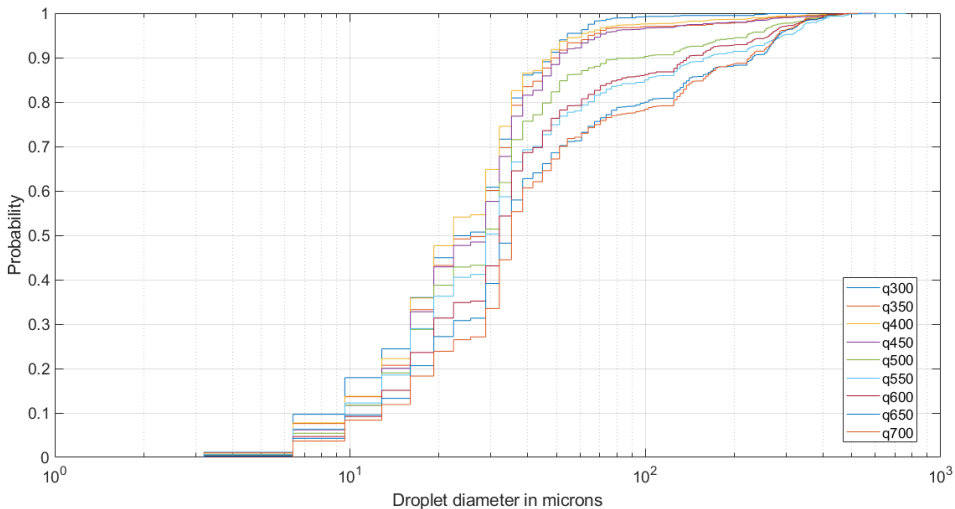


Figure 4.3.16: WC30 top of pipe for all flow rates, D_w/o

Fig. 4.3.17 shows the plot for WC70 at the top of the pipe. The system consists of water droplets dispersed in oil, except for flow rates above 550 L/min where there will be dispersed oil-in-water. As with the plot for the WC30 at the top of the pipe, the trend with increasing droplet sizes for increasing flow rate is not as clearly seen here either. The trend is better for smaller droplet diameters, except around 20-40

μm . Here q400 is plotted higher than the other flow rates, consisting of smaller droplet sizes. For the larger droplet sizes the trend where the lower flow rates are plotted above the higher ones are seen for flow rates up to q450. For flow rates above 450 L/min all the plots are plotted closely together. When looking closely one can see that the turquoise q550 line is plotted at the bottom of the plots, and the dark blue q650 line are plotted on the top of the closely packed lines. The shift in the graph where the flow change from Dw/o + Do/w to Do/w at 550 L/min can not be seen. There is rather a more clear shift between the q450 and higher rates, which might be due to the shift from a dilute to a dense system.

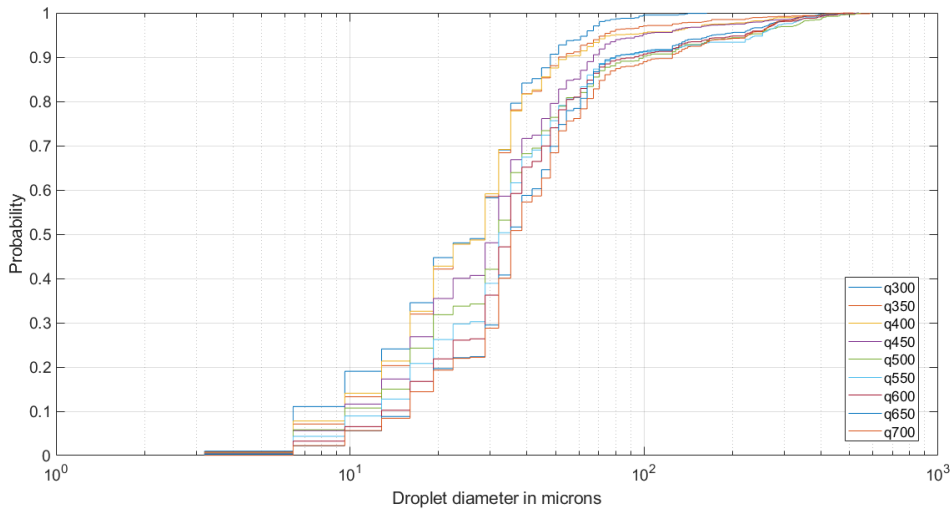


Figure 4.3.17: WC70 top of pipe for all flow rates, Do/w

Comparing both graphs one can see that the two graphs cross the 60% line around droplet size 30-50 μm . The graphs for WC30 plots wider than the graph for WC70, for larger droplet sizes. This trend was also seen from measurements at the bottom of the pipe. The WC30 consists of a larger variation of droplet sizes (50-250 μm at 90%), compared to the WC70 where all the flow rates consists of smaller droplet size (50-100 μm at 90%). When looking at images of the flow (Fig. 4.3.11 and Fig. 4.3.12) one can see that this looks correct. For WC30 droplets stick more together and looks in general larger than the droplets for WC70. The graph for WC70 is wider for the larger droplet sizes, compared to the test performed for WC70 at the bottom of the pipe. This could be because the largest oil droplets will rise in the flow. The camera placed on the top of the pipe will therefore see larger oil droplets, compared to when the camera is placed at the bottom of the pipe. This can also be seen for the WC30 plots, where the plot from the bottom of the pipe is plotted more towards the lower right, compared to the plot from measurements at the top of the pipe.

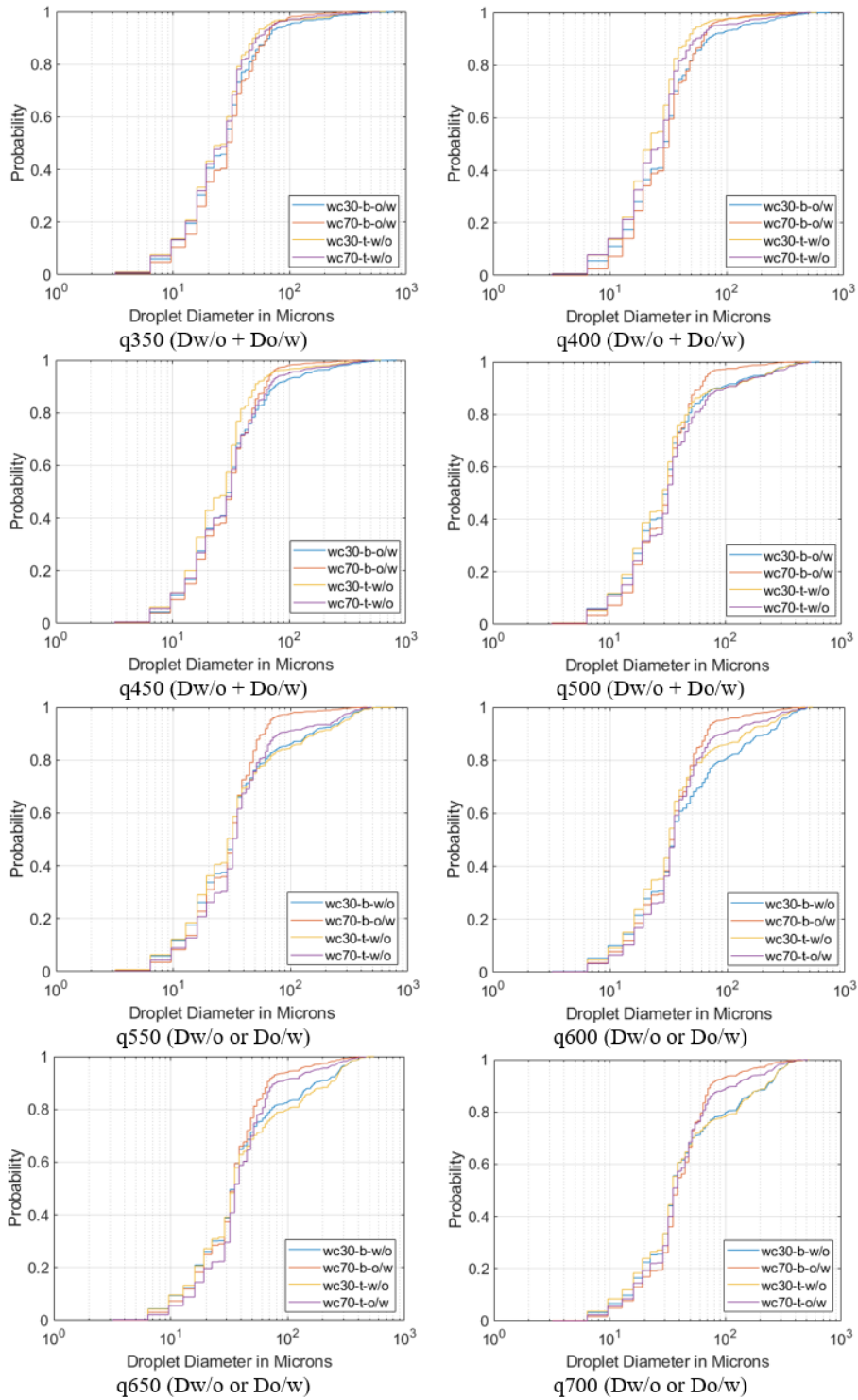


Figure 4.3.18: Cumulative log-plot of all test points for each flow rate 63

Graphs that are plotted for each flow rate, for both water cuts and probe positions can also be compared. These plots can be seen in Fig. 4.3.18, except for the SM flow seen for flow rate 300 L/min. When plotting all test points for each flow rate, one can see how the droplet size distribution varies for each test point. The same trend, where the same test points are plotted in (almost) the same order from top to bottom can be seen for flow rate q550-700. For these test points the WC70 at the bottom of the pipe has the smallest droplet sizes. WC70 is plotted below with a bit larger droplet sizes, and WC30 at both the top and bottom of the pipe are plotted below. The WC30 plots are overlapping or plotting closely together for all flow rates except q600. The gap between the graphs from the top part and the bottom part of the pipe shows a clear difference in DSD for dispersed water-in-oil (WC30), and oil-in-water (WC70). The assumption that the droplets are getting smaller when there is more water in the system (for higher flow rates), is therefore supported. This also means that the droplet sizes of oil-in-water are smaller than the ones for water-in-oil. For the lower flow rates, q350-450, all the test points are plotted more closely together, where the WC30 plots are plotted (slightly) higher than the WC70. The WC70 at the bottom of the pipe (orange line) starts to deviate and plot above the other test points for increased flow rates from flow rate q450. WC70 at the top of the pipe starts to deviate from the others at q550. After this point, both water cuts at both test points in the pipe plot close together. From this one can assume that the flow is getting better mixed and droplets being more uniform spread across the pipe cross section for higher flow rates.

Diameters

In this subsection the d_{max} and the d_{32} will be discussed. The largest droplet diameters found for each test point can be seen in Table 4.3.5. How the d_{max} varied with flow rate is plotted in Fig. 4.3.19.

Table 4.3.5: Results for d_{max} for all test points

Flow rate	Bottom		Top	
	30	70	30	70
300	688.0	422.4	352.0	163.2
350	780.8	380.8	665.6	585.6
400	758.4	390.4	592.0	521.6
450	828.8	412.8	608.0	537.6
500	643.2	531.2	531.2	544.0
550	611.2	448.0	761.6	492.8
600	518.4	457.6	531.2	480.0
650	473.6	406.4	544.0	464.0
700	480.0	454.4	524.8	515.2

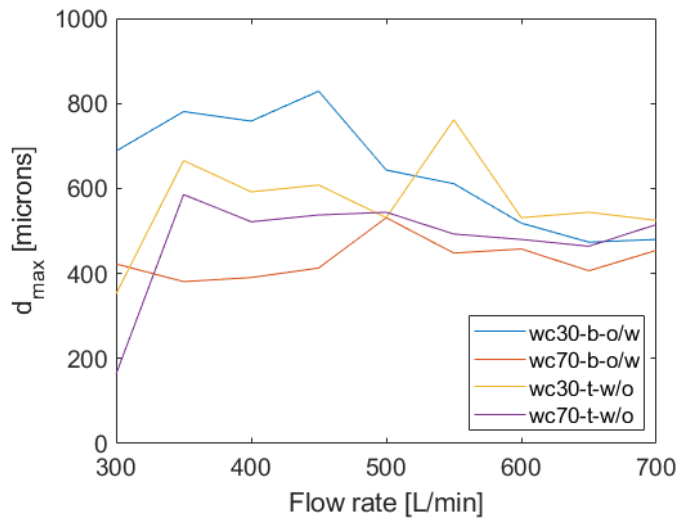


Figure 4.3.19: Total flow rate plotted against d_{max}

As seen from Fig. 4.3.19 there is not a clear trend for how the d_{max} vary with flow rate. It would be expected that the droplet size would decrease with higher flow rates, due to stronger forces in the system that will break-up the droplets (see sec. 2.2.4). All the different test points, except WC70 at the bottom of the pipe has a trend where the droplet size is, in general, decreasing (except a few point which have a higher peak). The test point WC70 at the bottom of the pipe on the other hand has a slight increase from both sides up to q_{500} . Both the WC70 plots have a peak at q_{500} . This is one test point before q_{550} , where the transition of flow pattern happens. The plots of WC30 does not peak in the same point. The test performed at the bottom of the pipe peaks at q_{450} , which is also one test point before the flow pattern transition. The test performed at the top part of the pipe on the other hand, has the highest droplet size for the point after the transition have occurred. For the tests performed in the top of the pipe, both water cuts has the smallest d_{max} for the SM layer. This is not the case for the tests performed at the bottom of the pipe. When comparing the largest droplet sizes, for the same water cut one would expect the largest droplet sizes to be at the bottom of the pipe for WC30. The water droplets dispersed in the oil, would sink towards the bottom of the pipe due to gravity. This is not seen here, where all the measurements from the top of the pipe has the largest droplet sizes. The trend is better seen for the WC70 case, where all the test points from the top of the pipe has larger droplet diameters, than the measurements at the bottom of the pipe.

The calculated Sauter mean diameter, d_{32} , for each test point can be seen in Table 4.3.6. How the d_{32} varied with flow rate is plotted in Fig. 4.3.20.

Table 4.3.6: Results for d_{32} for all test points

Flow rate	Bottom		Top	
	30	70	30	70
300	393.8	129.0	113.4	56.2
350	394.7	123.5	285.5	296.8
400	337.4	136.5	266.0	263.5
450	366.1	137.8	288.5	272.6
500	288.2	165.6	284.9	311.0
550	301.2	166.3	324.7	273.4
600	290.7	193.6	273.9	268.0
650	277.5	197.8	277.5	237.1
700	262.6	191.1	265.2	238.9

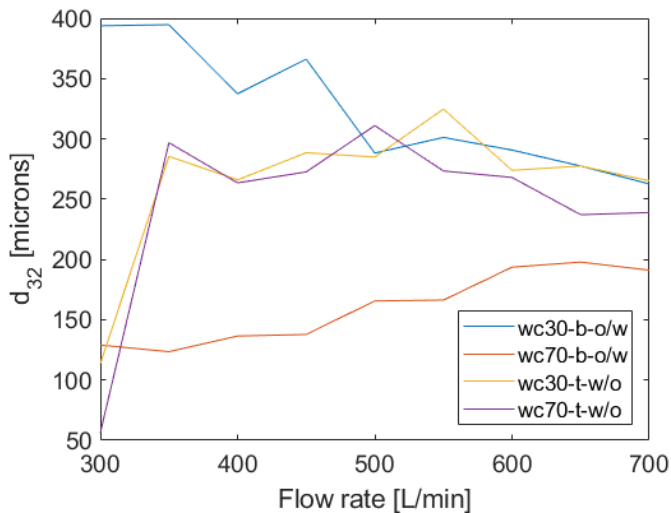


Figure 4.3.20: Total flow rate plotted against d_{32}

Looking at the plot in Fig. 4.3.20 one can see that there is not a common trend for all the different test points. The tests performed in the top of the pipe has a similar trend, compared to the tests performed at the bottom of the pipe. The peak in the plot for both WC30 plots is at the same flow rate as where the d_{max} peaked. This is not the case for the WC70 plots. When comparing how the d_{32} change with the cumulative log-plots (Fig. 4.3.14, 4.3.15, 4.3.16 and 4.3.17) one can see a trend. From Fig. 4.3.20 one can see that the WC70 from the top of the pipe has the highest d_{32} for q500. Looking at Fig. 4.3.17 one can see that the q500 is plotted fare to the low right (for larger droplet sizes), meaning it has a large

amount of large droplets in the distribution. Looking at Fig. 4.3.16 one can see that the q550, which has the highest d_{32} for the two WC30 tests, is plotted more towards the right than what the natural trend would expect. For droplet diameters larger than $300 \mu\text{m}$ the q550 is plotted to the far right, meaning it has the largest droplet diameters for all flow rates.

Both the d_{max} and d_{32} result did not give a good trend for the different test points. A reason for this could be that the Matlab routine does not work well for the largest droplet diameters, see sec. 4.3.2. Since the d_{32} is including the d_{max} measurements, the d_{32} will also be affected by the inaccurate measurement of d_{max} . A second reason could be that there are too many disturbances from the mixing point of the oil and water and down to where the flow is measured. This could affect the development of fully pipe flow, where the droplets might not be created purely from the pipe flow, but rather at the mixing point. The measured maximum droplet sizes were much smaller than $4000 \mu\text{m}$. Hence, the droplets that were larger would not fit in the 4 mm gap in the "hat" and would therefore not be seen. The large layers of liquid seen on several images from the flow could indicate that there were droplets larger than $4000 \mu\text{m}$ present in the flow.

Valve opening of 50%

Looking at Fig. 4.3.21 one can see that the flow is changing flow pattern when the valve is 50% open. The flow upstream (right side of) the valve is stratified with a clear separation between the oil and water layer. Downstream the valve (left side) the flow is completely dispersed, where the whole pipe is filled with a (milky-) red fluid flow.

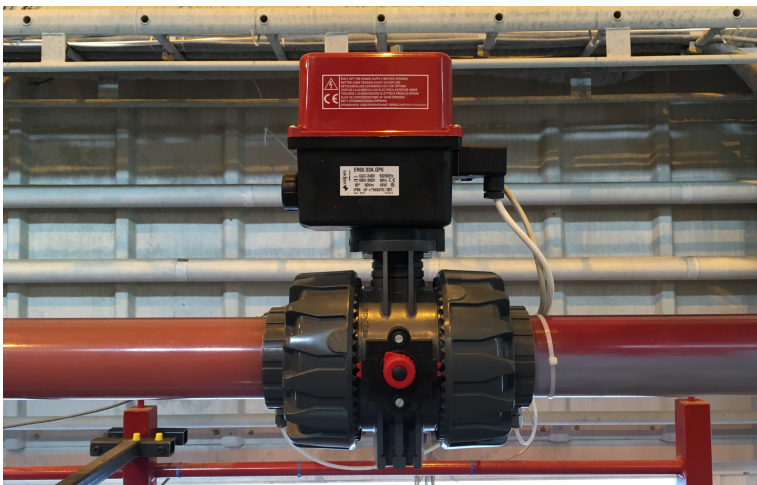


Figure 4.3.21: Change in flow system when using ball valve 50% open. Flow direction is from right to left.

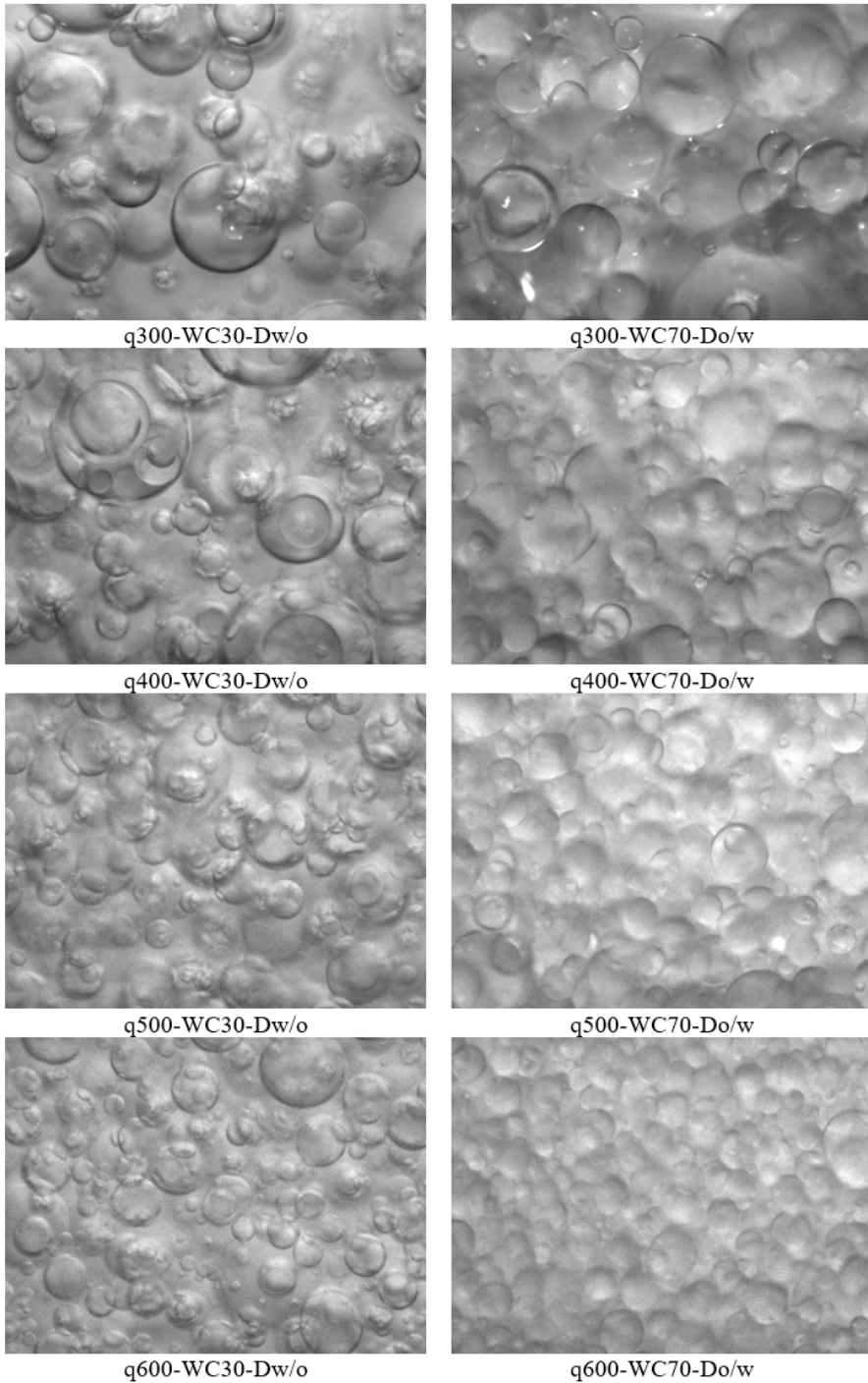


Figure 4.3.22: Images taken of the flow with 50% valve opening, with the PVM at the bottom of the pipe

Fig. 4.3.22 shows pictures taken from the flow with the PVM camera at the bottom of the pipe (images from the top of the pipe look similar). From the images one may see that the droplets are more uniform in size, compared to the pictures of the flow with the valve fully open (Fig. 4.3.11 and Fig. 4.3.12). There are also significantly more droplets per pictures for the pictures taken with the valve 50% open. There is a trend where the number of droplets per image increase, while the size of the droplets decreases for higher flow rates. This follows the trend mention in sec. 2.2.4. One may see that the water droplets dispersed in oil, on these pictures as well, has a more clear edge. The droplets are easier to distinguish, than from the images with oil droplets in water.

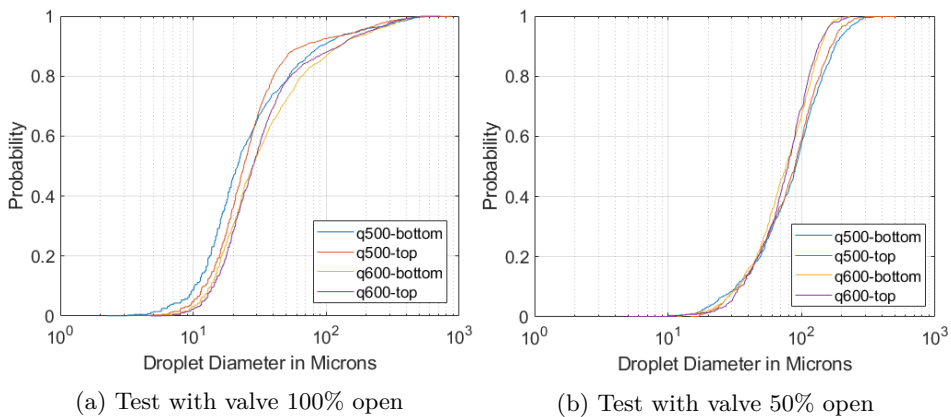


Figure 4.3.23: DSD for valve 50% and 100% open. Tested for WC30 at different places in the pipe, both tests counted manually.

Fig. 4.3.23 shows the DSD found manually for different flow rates and placement in the pipe tested for WC30 for both valve openings. Looking at the two plots one may see that the graph for the flow with the valve 50% open plots more closely together, than the plots with the valve 100% open. This indicates that the general DSD are more similar and does not vary as much for different flows with the valve 50% open. A gap can be seen between q500 and q600, for valve opening 50%, where plots starts to split and plot further apart from droplet sizes around $70 \mu\text{m}$. Hence, the two test points for each flow rate plots closely together.

Fig. 4.3.24 shows a comparison of the manual counting, using the valve 100% open and 50% open, for the two test points in the pipe. In sec. 2.2.3 it was mentioned that due to higher shear stress in the valve, the droplets created should be smaller in size, than if there was no valve present. One can see that for both points the DSD for the measurements with the valve 50% open consists of larger droplets than when the vale is fully open. This could be because of stable droplets that coagulate after passing the valve, or the flow could be promoting drop-drop coalescence. The flow system is possibly a dense system, due to the large coagulating forces acting in the flow that creates the larger droplet sizes. It is also seen that, as mentioned

in the discussions above, the tests with the valve fully open creates larger droplets sizes for higher flow rates, while the opposite is seen for the tests with the valve partly open.

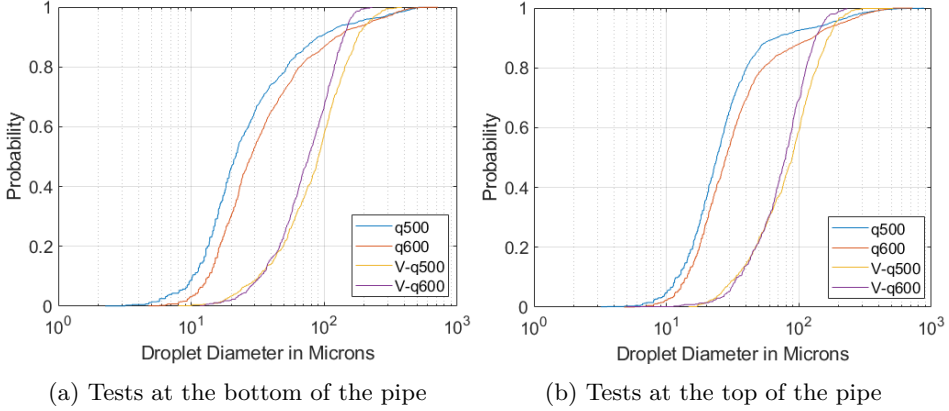


Figure 4.3.24: Comparing how the droplet size distributions vary with the valve 50% open and 100% open. Labels with V refers to valve being 50% open, and labels without a V is with the valve 100% open.

The results for the largest droplets in the system, and the d_{32} can be seen in Table 4.3.7. Comparing with the results for the valve 100% open for d_{max} in Table 4.3.5 and for d_{32} in Table 4.3.6, one can see that the maximum droplet diameter is smaller for the droplets created from the valve. This can also be seen from Fig. 4.3.24, where the droplets with the valve fully open is plotted further towards the right around 90%, both places in the pipe. Even though the droplets with the valve 50% open is plotted more towards the right, towards larger droplet sizes in Fig. 4.3.24, one can see from the d_{32} measurement that the average droplet size is smaller. The steeper curve in the figure also indicates that the droplets size are more uniformly distributed, with less variations in the droplet size when the valve is 50% open. Using the valve, the general droplet size will get larger, which could benefit the separation process, since larger droplets need shorter settling time, see sec. 2.1. Even though the droplets are larger in size, there is also a lot more droplets present in the flow, which might again take longer time to separate.

Table 4.3.7: d_{max} and d_{32} from manual counting droplets from experiment with valve 50% open for WC30.

Flow rate	d_{max}	d_{32}
q500-bottom	382.1	161.2
q500-top	512.8	118.7
q600-bottom	229.1	118.9
q600-top	231.3	170.2

4.3.4 Sources of error

An error estimate for the apparatus were performed by using equations from sec. 2.7 together with equations from calibrations in sec. 3.3. The reported error is using Eq. (2.7.9) where $\tau = 1.984$ for the tests using 240 images, and $\tau = 1.962$ for the tests using 600 images.

Errors for tests using 240 images:

- The error for the temperature measurements was $\pm 0.3^{\circ}\text{C}$
- The error for the density measurements was $\pm 0.54 \text{ kg/m}^3$
- For the flow measurements the smallest error for the apparatus was found for the tests performed at the top of the pipe. The largest error was for WC70 measured at the bottom of the pipe for flow rate 700 L/min where the error was $\pm 0.75 \text{ L/min}$. The smallest error was for WC30 measured at the top of the pipe for flow rate 300 and 350 L/min where the error was $\pm 0.03 \text{ L/min}$

Errors for tests using 600 images:

- The error for the temperature measurements was $\pm 0.3^{\circ}\text{C}$
- The error for the density measurements was $\pm 0.54 \text{ kg/m}^3$
- For the flow measurements the error was identical for the top and bottom tests, except for q500 and q550. The largest error was for WC30 measured at the top of the pipe for flow rate 500 L/min where the error was $\pm 0.69 \text{ L/min}$. The smallest error was for both test points for WC30 and flow rate 300 L/min where the error was $\pm 0.14 \text{ L/min}$

Valve

The very closely packet and a bit more blurry images makes it more difficult to accurately count the droplet size manually. The guidelines in sec. 3.4.2 is not followed as strict, where one have to guess the size of the droplets to be able to count any droplets at all. In this results the DSD is more of a guideline rather than being 100% accurate.

Errors for tests using 600 images:

- The error for the temperature measurements was $\pm 0.3^{\circ}\text{C}$
- The error for the density measurements was $\pm 0.54 \text{ kg/m}^3$
- For the flow measurements the error was identical for the top and bottom tests. The largest error was for WC70 for flow rate 600 L/min where the error was $\pm 0.69 \text{ L/min}$. The smallest error was for test WC30 for flow rate 300 L/min where the error was $\pm 0.14 \text{ L/min}$

Chapter 5: Numerical Modeling

Four statistical distributions were used to represent the experimental data gathered in chapter 4. The models are tested for two sets of data. The first data is from the measurements that were performed at SINTEF multiphase laboratory. The description of the setup was explained in sec. 1.1.2. The second data is from the experiments performed in sec. 4.3.

5.1 Method

The method and parameters used when comparing the numerical functions and models with real data in Matlab are explained below.

5.1.1 Log-Normal Distribution

To test the LND both the real data points and the LND were plotted in the same plot. The number weighted distribution was tested, putting $b = 3$ when finding d_0 , to get the number weighted distribution. The graphs were plotted with a logarithmic x-axis. The two graphs had different y-axis values so the plots were plotted with two different y-axis. The d_{32} and d_{43} could also be compared to see if the model gave a good fit, but since the LND is based on these values, this would give the same results and can therefore not be compared.

5.1.2 Upper-Limit Log-Normal Distribution

Both the real data (v -parameter) and the ULLN function was plotted together to see how well the function fitted with the data. The v parameter was found from the following equation:

$$v_n = \frac{\sum_{i=1}^n \frac{\pi}{6} d_i^3}{V_{total}} \quad (5.1.1)$$

where n is the number of droplets with diameter smaller than d and V_{total} is the total volume from all droplets in the distribution.

To create the ULLN function, first the droplet diameter was plotted against $100v$. Polynomial functions were tested to see which gave the best fit to the data points. The function that gave the best fit, for all the different tests was used. When the cubic equation gave the best fit, it was seen that the fitted curve crossed the 90th percentile line in two points for some test points. An example of this can be seen in Fig. 5.1.1. In these cases it was manually checked that the correct value was used in the calculation.

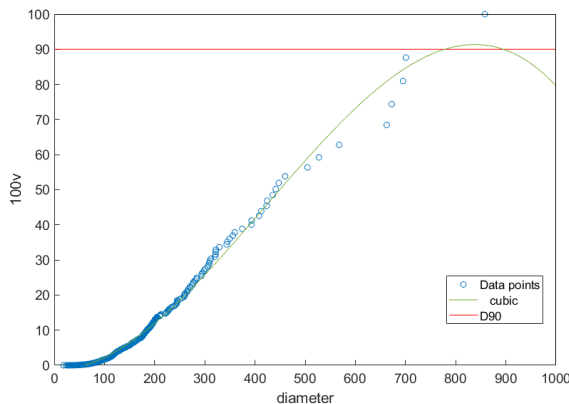


Figure 5.1.1: Cubic equation crossing the 90th percentile in two points (SINTEF 100 mbar, WC50)

To find the different percentiles first the *polyfit* function was used, to get the polynomial. Further *fsolve* was used to find the different percentiles for the polyfit equation. For some of the test points the d_{max} value that was found using Eq. (2.6.9) was smaller than the d_{max} from the used data. In these cases imaginary numbers were created when calculating z for the largest diameters. For these cases the points containing these imaginary numbers were not used to find the cumulative volume fraction (Eq. (2.6.4)) since this gave an error. The points was neither used when plotting the graphs. To plot graphs a logarithmic x-axis was used.

To see how well the ULLN graph fits with the measured data, not only by looking at the graph, an error estimate was performed. The difference in the calculated y-value to the real value was tested for every point using Eq. (5.1.2). The average of all the values were then calculated and reported. An error estimation was also performed to see how the calculated d_{max} and d_{32} value varied from the one from the data, using the same equation.

$$\text{error} = \left(\sum_{i=1}^n \frac{\text{measured value}_i - \text{real value}_i}{\text{real value}_i} \right) \quad (5.1.2)$$

where n is the number of measurements.

5.1.3 Hinze and Brauner - breakage models

To compare Hinze and Brauner models, Abduvayt et al. (2006) values (for n and C_f) from table 3 in Xu et al. (2010) were used for n and C in Eq. (2.6.13). Using these values gave the smallest error for the different maximum droplet diameters. The parameter \tilde{C}_H is put equal to one. The model does not take into account the different parts in the pipe the probe is placed. It returns the largest droplet that can be found in a system for each water cut.

5.1.4 Droplet breakup over restrictions

The model does not consider the influence of the water cut in the droplet breakup process. It provides the maximum droplet diameter as a function of the pressure drop. The reported diameter is the maximum diameter that can be created in the system, meaning the measured diameters should be smaller. The Δp_{perm} input to the model were taken from the experimental measurements, and put equal to the measured pressure drop over the valve. The model was not used for the NTNU data, since the pressure drop was not measured for these experiments.

5.2 Results and discussion

5.2.1 SINTEF Data

Log-Normal Distribution

The real data points were plotted using histograms, plotted with logarithmic bin size with 30 steps between each decade. The measurements did not fit well with a log normal distribution.

The test for a pressure drop of 25 mbar did not exhibit a LND shape. The peak in the LND plot was always shifted towards the right, towards larger droplet sizes compared to the real values. For the higher water cuts, the width of the real distribution was wider than the LND. The fit was better for larger droplet sizes, than for smaller ones. This could be because the plots are plotted with a logarithmic x-axis, where the step size becomes larger towards higher droplets sizes. The larger steps could therefore mask the variance better than the smaller droplet sizes. Images showing both a fairly good fit for WC10, and a bad fit for WC60 for pressure drop 25 mbar can be seen in Fig. 5.2.1.

For the 100 mbar test both the real data and the LND peaked around the same values. The LND tangent more of the histogram bar from the real values, compared to the 25 mbar test. The fit was better for lower water cuts, compared to the higher ones. The best fit was for WC10, where the corners of the histogram is tangent

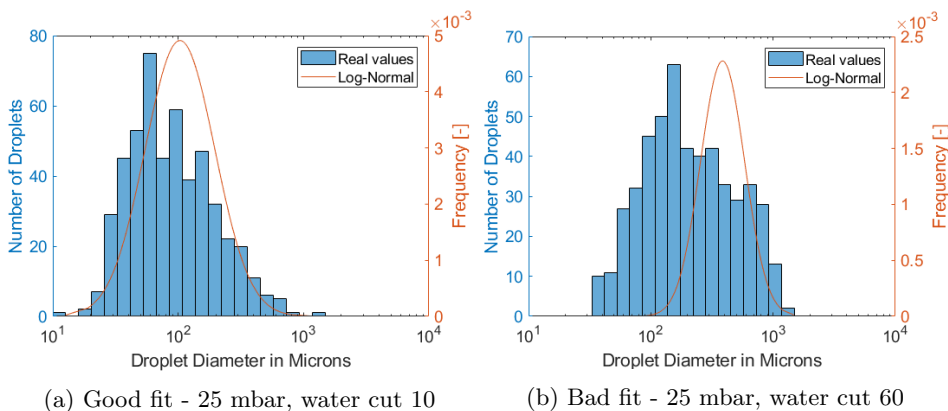


Figure 5.2.1: Comparing Log-Normal Distribution with real data for pressure drop 25 mbar

the LND graph, and almost the whole graph is fitted inside. The plots also peak in the same point, around $60 \mu\text{m}$. The 500 mbar test did also have a better fit for lower water cuts. The graphs peaked around the same droplet diameter, but for higher water cuts the peak in the LND shifted towards the right. All the graphs, except WC60, had almost all the histograms plotted inside the LND plot, but it did not tangent the graph as well as the 100 mbar plots. The plot that gave the best fit for the 100 mbar and 500 mbar test can be seen in Fig. 5.2.2

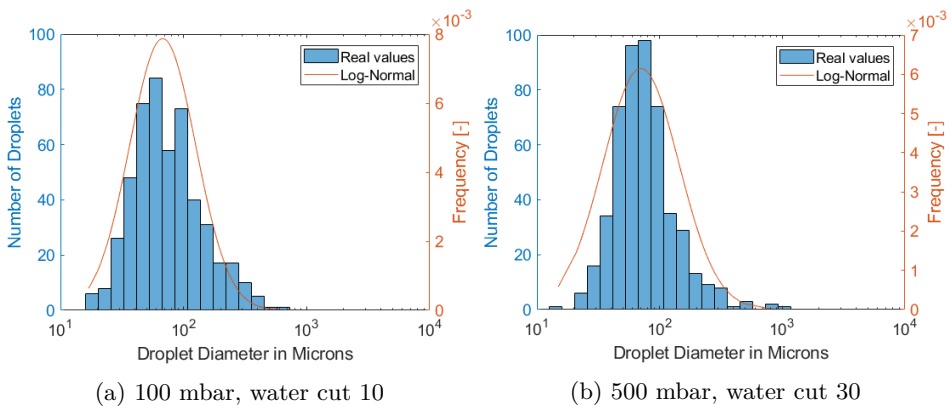


Figure 5.2.2: Best LND fit for 100 mbar and 500 mbar

Upper-Limit Log-Normal Distribution

An example of how the cubic equation gave a good fit to the plotted data can be seen in Fig. 5.2.3.

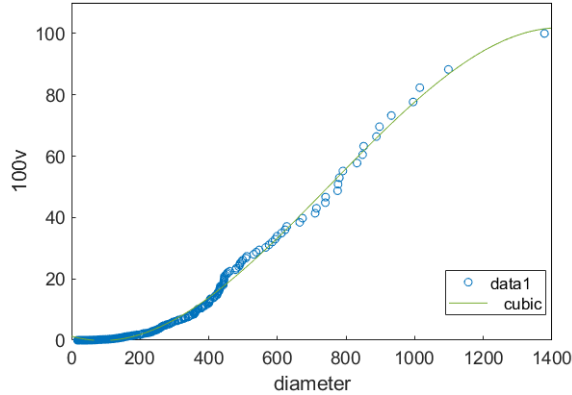


Figure 5.2.3: Cubic fitted curve to droplet diameter vs $100v$ (25 mbar, WC50)

The best fit was given for test point 25 mbar with water cut 50 where the error was 0.206. The largest deviation was for test point 500 mbar, water cut 30 where the error was 14.888. Images of the two test can be seen in Fig. 5.2.4.

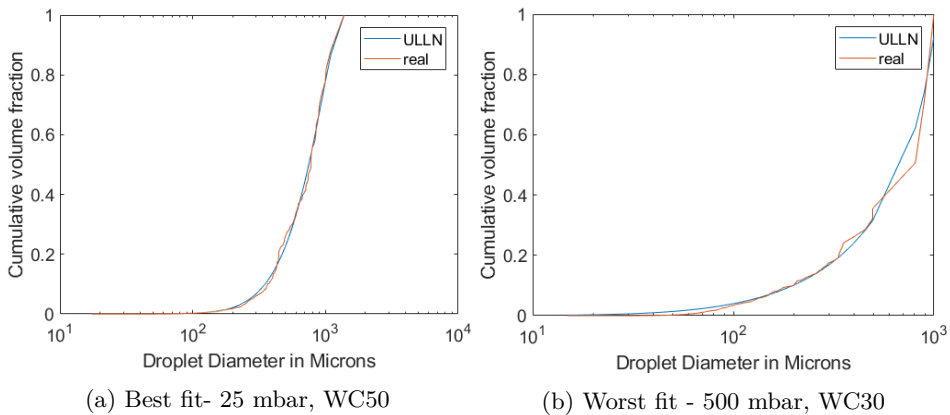


Figure 5.2.4: Best and worst fit using ULLN

The comparisons with the d_{max} and d_{32} gave the following result:

- The best fit for d_{max} was 0.005 for 25 mbar - WC60.
- The worst was 0.297 for test 100 mbar - WC50.
- For the d_{32} the best fit was 0.007 for 25 mbar - WC60.
- The worst was 0.110 for test 500 mbar - WC10.

Droplet breakup over restrictions

The results for the modeled and real measured diameters can be seen in Table 5.2.1.

Table 5.2.1: Comparison of measured maximum droplet diameter with modeled, for different pressures, all values in μm

Pressure	Measured	Modeled
25 mbar	1549.2	1981.3
100 mbar	1301.4	747.7
500 mbar	1498.8	310.7

As reported in Ellertsen (2017) some coalescence was seen from the beak-up of droplets over the valve, to the measuring point. This could explain why the measured diameter for the 100 mbar and 500 mbar test were higher than the modeled. For the 25 mbar test the modeled diameter was larger than the measured. It would be expected that the droplets for this test also would coagulate. A reason why this was not seen could be that it was not counted infinite amount of droplets, so the largest droplet in the system might not have been measured. An other reason could be that the droplet did not fit in the gap in the Cauty camera. Fossen & Schümann (2017) performed similar experiments, where it can be seen from Fig. 5 and Fig. 6 in the paper that the droplet size have the same ratio as what was found here.

5.2.2 NTNU Data

Log-Normal Distribution

The real data points were plotted using histograms, plotted with logarithmic binsize with 15 steps between each decade. The measurements did only give a good fit for the test performed at the bottom of the pipe at WC70. An example of one bad and a good fit for the data can be seen in Fig. 5.2.5.

For the bad fit, all LND graphs were plotted towards the right (see Fig. 5.2.5b) of the real distribution, except the flow rate 300 L/min for test WC70 and WC30 at the top of the pipe, which was plotted more towards the left. For the bottom test for WC70 all the flow rates from 450 L/min and higher had a fairly good fit, as can be seen in Fig. 5.2.5a. The peak in the plot is lying in the same area as the peak from the real data, just slightly shifted to the side. For the largest droplet diameters, one can also see that the graph is tangent to the histogram.

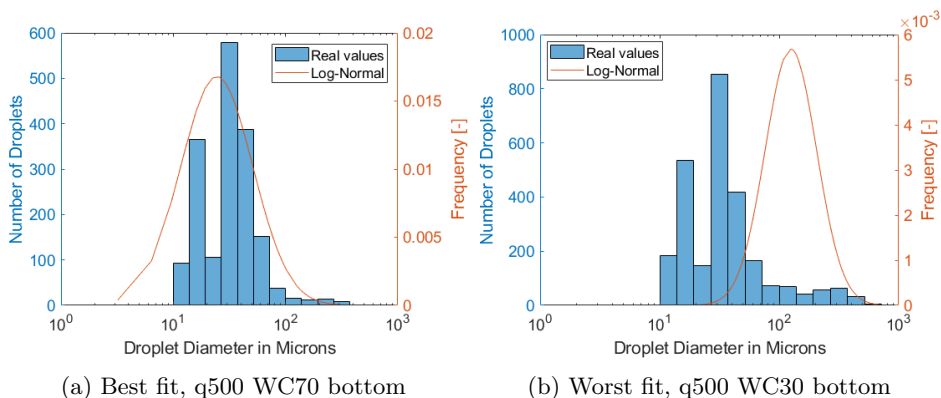


Figure 5.2.5: Best and worst fit using LND

Upper-Limit Log-Normal Distribution

Both the square and the cubic polynomial equation gave a good fit for the data, as can be seen for test q500-WC30-bottom in Fig. 5.2.6.

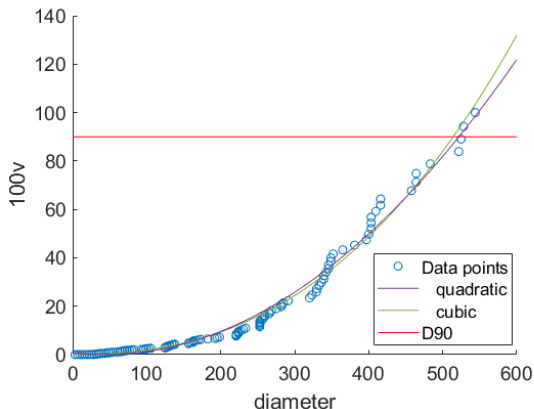


Figure 5.2.6: Comparing quadratic and cubic fit to data (q500-WC30-bottom)

To find which equation to use, bot equations were used to plot the ULLN. The error for how the calculated d_{max} vary from the real, and how much the graph deviated from the real data was compared. The cubic equation gave the smallest total error for the d_{max} , while the error for how the graphs deviated was slightly larger for the cubic than the square equation. Based on the findings, it was decided to use the cubic equation for further calculations.

Fig. 5.2.7 shows the graph that gave the best and the worst fit. The best fitted graph had and error of 0.54 while the worst fitted graph had an error of 52.9.

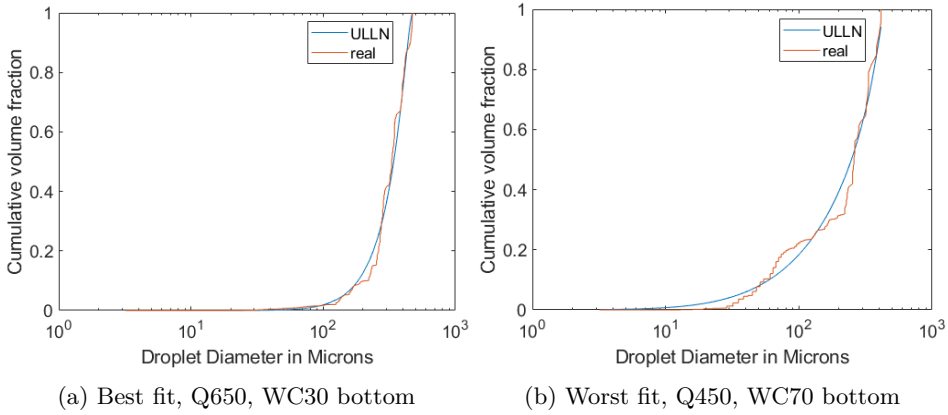


Figure 5.2.7: Best and worst fit using ULLN

Looking at the total error for the different test points, the WC30 bottom test had the smallest total error for both the graph, the d_{max} and d_{32} . The largest error was for the bottom WC70 test.

Hinze and Brauner - breakage models

It is assumed that the flow is oil continuous, with dispersed water droplets for WC30 (c_o), and opposite, with a water continuous flow with oil droplets for WC70 (c_w). Table 5.2.2 shows the results for the different models at different temperatures, reported in μm . As written in sec. 2.2.4, according to literature it is assumed that the droplet sizes will decrease for higher flow rates. This trend can be seen from the results from the Hinze and Brauner models.

Table 5.2.2: Maximum droplet diameter using Hinze and Brauner model, all values in μm

Flow rate L/min	Hinze		Brauner		Temp. °C
	30 c_o	70 c_w	30 c_o	70 c_w	
300	595.4	451.5	17876.8	27610.1	20.1
350	555.2	419.9	16670.5	25675.7	20.1
400	522.6	394.3	15691.6	24109.9	20.1
450	495.4	373.0	14876.0	22808.3	20.1
500	472.3	354.9	14182.0	21703.6	20.1
500	472.3	354.9	14183.6	21704.9	18.4
550	452.3	339.4	13584.0	20751.6	18.4
600	434.8	325.7	13058.8	19918.0	18.4
650	419.4	313.7	12593.5	19189.8	18.4
700	405.5	302.9	12177.6	18522.6	18.4

From table 5.2.2, one can see that the droplet sizes are getting smaller for each flow rate for both models. One can also see that the temperature is affecting the result, where the effect is larger for the Brauner model, than for the Hinze model.

Comparing with the reported d_{max} in Table 4.3.5, one can see that the d_{max} found using the Brauner model, is larger than all the d_{max} from the data. Looking at the Hinze model, there is more variations. For WC30 (c_o) all the d_{max} from the data is larger than the d_{max} found from Hinze, except for q300 measured at the top of the pipe. For WC70 (c_w) measured at the top of the pipe the q300 is the only test point where the diameter is smaller than the Hinze diameter. For WC70(c_w) only flow rate 300-400 L/min in the bottom of the pipe is smaller than Hinze model. All the reported diameters for the Hinze model are below 4000 μm . For the Brauner model, this is not the case. This means that the largest droplet sizes that could be created in a dense flow (using this model) might not have been seen when using the 4 mm "hat" on the PVM. This could also explain the large lines across the images seen in Fig. 4.3.11 and Fig. 4.3.12. This could therefore be droplets that does not fit in the gap between the "hat" and the camera lens.

Chapter 6: Conclusion

This report has looked at droplet size distribution characterization, and compared measured data with numerical functions and models. Four different experiments were performed. First, the interfacial tension and the viscosity of the used oil and water was found. Second, the flow pattern map for the inlet of the system was determined. Third, the droplet size distribution for different water cuts, valve openings, flow velocities at two placements in the pipe were found. Last, two sets of data (one from NTNU and one from SINTEF) were compared with statistical distributions and models.

Regarding the computational routine for automatic counting of droplet size, the following conclusions are given:

- The output of the automatic droplet counting routine was compared against manual counting. The initial agreement was not satisfactory regarding number of droplets, maximum diameter and distribution.
- Two modifications were made in the code that significantly improved the results of the routine: first, a logic was added before the Hough transformation to remove phantom droplets detected inside bigger droplets and second the sensitivities were adjusted manually for some droplet size ranges.
- The reported maximum droplet diameter was not in agreement with the real size from the pictures. The Matlab routine overestimated the size and reported droplets that were not real droplets. The largest reported droplet sizes had to be checked manually for each test point.

For the droplet size distribution measurements the following conclusions are given:

- For measurements performed with the valve fully open the DSD got larger for flow rates in the higher range.
- The droplet sizes were smaller when more water was present in the system.
- The droplet sizes for oil-in-water were smaller than the droplet sizes for water-in-oil.
- When the valve was partially open, it produced a droplet distributions with a smaller d_{max} and d_{32} compared to the fully open position. However, the

cumulative droplet size distributions were shifted towards the right when the valve was partially open. This means there were more droplets seen in the flow, with a more uniform droplet size.

For the numerical modeling, the following conclusions are given:

- The Log-Normal Distribution fairly represented the SINTEF data.
- The Log-Normal Distribution did not match the data gathered at NTNU.
- The ULLN function gave a better fit than the LND for all test points for both the SINTEF and NTNU experiments.
- Comparing the maximum droplet diameter, the NTNU flow systems can better be described using Brauner's dense model, rather than Hinze's dilute model.
- The droplet breakup over restriction model gave a smaller droplet sizes than what was seen in the system for pressure drop 100 mbar and 500 mbar tested with the SINTEF data. This was assumed to be due to coagulation in the system. The modeled diameter for the 25 mbar pressure drop was larger than the measured.

Chapter 7: Recommendations for Further Work

- Quantify the effect of the temperature on the fluid viscosity and consider this variation when processing the results.
- To perform modifications and improvements to the Matlab routine for automatic counting of droplets, such as:
 - The displayed picture on the "screen" should be updated to show the circles that are actually measured and reported.
 - The reported pictures using the Matlab code could be saved for each run. This would make it easier to find the places where Matlab overpredict droplet sizes or see how many droplets that are counted for each picture.
 - To include an input field to enter the image size. This will spare the user to have to adjust the ratio $\mu\text{m}/\text{pixel}$ manually.
 - The name of the saved excel file and where to save it could be specified from the interface so this does not have to be done manually for each test.
 - The program could be coded to run on a sequence. The program could open different folders with images and run through the images before opening a new folder, run through these pictures and so on.
 - The code should be tested for more measurements performed with the valve 50% open. Different sensitivities should also be tested, to see how this affects the counting.
- The measured droplet sizes can further be compared with the separation efficiency to see how the droplet size effect the separation performance.
- The tests measured with the Matlab routine could be counted manually to see if the results are accurate, and to see how well the code worked for all test points.

- Experiments could be performed with a different gap size on the "hat" to see if larger droplet sizes would be detected.
- The largest droplet diameters for all the test points could be found manually to see how well the d_{max} found with the Matlab routine match the real one.
- It is recommended to measure manually d_{max} for all test points and use this number to recalculate the DSD and d_{32} .
- The model for droplet breakup over restriction could be tested for the NTNU measurements performed with a valve.
- Perform experiments to find the DSD at other heights in the pipe to see if this would effect the result.

Bibliography

- Amundsen, L. (2011), An experimental study of oil-water flow in horizontal and inclined pipes, PhD thesis, Norwegian University of Science and Thecnology.
- Angeli, P. & Hewitt, G. (2000a), ‘Flow structure in horizontal oil–water flow’, *International Journal of Multiphase Flow* **26**(7), 1117 – 1140.
URL: <http://www.sciencedirect.com/science/article/pii/S0301932299000816>
- Angeli, P. & Hewitt, G. F. (2000b), ‘Drop size distributions in horizontal oil-water dispersed flows’, *Chemical Engineering Science* **55**(16), 3133 – 3143.
URL: <http://www.sciencedirect.com/science/article/pii/S0009250999005850>
- Arirachakaran, S., Oglesby, K., Malinowsky, M., Shoham, O. & Brill, J. P. (1989), ‘An analysis of oil/water flow phenomena in horizontal pipes’, *Society of Petroleum Engineers* .
- Ballard, D. (1981), ‘Generalizing the hough transform to detect arbitrary shapes’, *Pattern Recognition* **13**(2), 111 – 122.
URL: <http://www.sciencedirect.com/science/article/pii/0031320381900091>
- Boxall, J. A., Koh, C. A., Sloan, E. D., Sum, A. K. & Wu, D. T. (2010), ‘Measurement and calibration of droplet size distributions in water-in-oil emulsions by particle video microscope and a focused beam reflectance method’, *Industrial & Engineering Chemistry Research* **49**(3), 1412–1418.
- Brauner, N. (2003), Liquid-liquid two-phase flow systems, in V. Bertola, ed., ‘Modelling and Experimentation in Two-Phase Flow’, Springer Vienna, Vienna, pp. 221–279.
URL: https://doi.org/10.1007/978-3-7091-2538-0_5
- Brennen, C. E. (2005), *Fundamentals of Multiphase Flow*, Cambridge University Press, Cambridge. Chapter 7 - Flow Patterns.
URL: <http://resolver.caltech.edu/CaltechBOOK:2005.001>
- Cengel, Y. A. & Cimbala, J. M. (2014), *Fluid Mechanics, Fundamentals and Applications*, McGraw-Hill.
- Corke, P. (2011), *13.2 Line Features*, Springer Berlin Heidelberg, Berlin, Heidel-

BIBLIOGRAPHY

- berg, pp. 361–365.
URL: https://doi.org/10.1007/978-3-642-20144-8_12
- Ellertsen, E. K. (2017), ‘Experimental study of oil-water pipe flow and separation’. Project Report delivered as part of Petroleum Geosciences and Engineering 5 years Master’s degree program, course TPG4560.
- Emerson (2014), ‘Importance of flow measurement for separators’. Accessed 25.11.17, Picture is edited by Author.
URL: <https://www.emersonprocessxperts.com/2014/01/importance-of-flow-measurement-for-separators/>
- ExxonMobil (2016), ‘Safety Data Sheet - EXXSOLTM D60 Solvent’. Accessed 25.04.18.
URL: [https://www.chemical.net/content/images/uploaded/sds/Exxsol%20D60%20\(12560-g\).pdf](https://www.chemical.net/content/images/uploaded/sds/Exxsol%20D60%20(12560-g).pdf)
- Farr, R. S. (2013), ‘Random close packing fractions of lognormal distributions of hard spheres’, *Powder Technology* **245**, 28 – 34.
URL: <http://www.sciencedirect.com/science/article/pii/S0032591013002660>
- FMC Technologies (2018), ‘Special separator solutions’. Accessed 15.13.18.
URL: <http://www.fmctechnologies.com/en/SeparationSystems/Technologies/SpecialSeparatorSolutions.aspx>
- Fossen, M. & Schümann, H. (2017), ‘Experimental study of the relative effect of pressure drop and flow rate on the droplet size downstream of a pipe restriction’, *Journal of Dispersion Science and Technology* **38**(6), 826–831.
URL: <http://dx.doi.org/10.1080/01932691.2016.1207184>
- Frohn, A. & Roth, N. (2000), *Dynamics of Droplets*, Springer, Berlin, Heidelberg.
- Greaves, D., Boxall, J., Mulligan, J., Montesi, A., Creek, J., Sloan, E. D. & Koh, C. A. (2008), ‘Measuring the particle size of a known distribution using the focused beam reflectance measurement technique’, *Chemical Engineering Science* **63**(22), 5410 – 5419.
- Human benchmark (2018), ‘Reaction time tester’. Tested 25.04.18.
URL: <https://www.humanbenchmark.com/tests/reactiontime/>
- JM Canty Inc (2017), ‘Canty inflowTM particle analyzer manual’.
- Karabelas, A. J. (1978), ‘Droplet size spectra generated in turbulent pipe flow of dilute liquid/liquid dispersions’, *AIChE Journal* **24**(2), 170–180.
URL: <http://dx.doi.org/10.1002/aic.690240203>
- Kline, S. & McClintock, F. (1953), ‘Describing uncertainties in single-sample experiments’, *Mechanical Engineering* pp. 3–8.
- Kowalczyk, P. B. & Drzymala, J. (2016), ‘Physical meaning of the sauter mean diameter of spherical particulate matter’, *Particulate Science and Technology* **34**(6), 645–647.

- Krüss (2010), ‘Determining the surface tension of liquids by measurements in pendant drops’. Accessed 03.06.18.
URL: https://warwick.ac.uk/fac/cross_fac/sciencecity/programmes/internal/themes/am2/booking/dropshapeanalyser/kruss-tn316-en.pdf
- Lovick, J., Mouza, A., Paras, S., Lye, G. & Angeli, P. (2005), ‘Drop size distribution in highly concentrated liquid–liquid dispersions using a light back scattering method’, *Journal of Chemical Technology and Biotechnology* **80**(5), 545–552.
- Malvern-Instruments (2015), ‘A basic guide to particle characterization’. Accessed 02.03.18.
URL: https://www.cif.iastate.edu/sites/default/files/uploads/Other_Inst/Particle%20Size/Particle%20Characterization%20Guide.pdf
- Merck (2018), ‘105230 | Oil red O (c.i. 26125)’. Accessed 27.04.18.
URL: http://www.merckmillipore.com/NO/en/product/Oil-red-O-C.I.-26125,MDA_CHEM-105230?ReferrerURL=https%3A%2F%2Fwww.google.no%2F
- Mettler-Toledo (2009), *PVM[®] V819 System Manual*, 0030819 REV G edn, Mettler-Toledo AutoChem.
- Mettler-Toledo (2017), ‘Particleview v19’. Accessed 06.11.17.
URL: https://www.mt.com/gb/en/home/products/L1_AutochemProducts/FBRM-PVM-Particle-System-Characterization/PVM/ParticleView-V19-PVM-Technology.html
- Mugele, R. A. & Evans, H. D. (1951), ‘Droplet size distribution in sprays’, *Industrial & Engineering Chemistry* **43**(6), 1317–1324.
URL: <https://doi.org/10.1021/ie50498a023>
- Norsk olje og gass (2017), ‘Miljørapport 2017’.
- Nädler, M. & Mewes, D. (1995), ‘The effect of gas injection on the flow of immiscible liquids in horizontal pipes’, *Chemical Engineering and Technology* **18**(3), 156–165.
URL: <http://dx.doi.org/10.1002/ceat.270180303>
- O’Rourke, A. M. & MacLoughlin, P. (2005), ‘A comparison of measurement techniques used in the analysis of evolving liquid–liquid dispersions’, *Chemical Engineering and Processing: Process Intensification* **44**(8), 885 – 894.
- Paolinelli, L., Rashedi, A. & Yao, J. (2017), ‘Characterization of droplet sizes in large scale oil–water flow downstream from a globe valve’, *International Journal of Multiphase Flow* .
URL: <http://www.sciencedirect.com/science/article/pii/S0301932217302756>
- Rawle, D. A. (2017), ‘Basic principles of particle size analysis’. Accessed 08.02.18.
- Rivera, R. M. (2011), Water separation from wellstream in inclined separation tube with distributed tapping, PhD thesis, Norwegian University of Science and Tech-

BIBLIOGRAPHY

- nology, Faculty of Engineering Science and Technology, Department of Petroleum Engineering and Applied Geophysics.
- Sahimi, M. (2012), *Flow and Transport in Porous Media and Fractured Rock: From Classical Methods to Modern Approaches*, Wiley-VCH Verlag GmbH & Co. KGaA, Weinheim, Germany.
- Schlumberger (2017), 'Flow regime'. Accessed 22.11.17.
URL: http://www.glossary.oilfield.slb.com/Terms/f/flow_regime.aspx
- Schümann, H. (2016), Experimental investigation of transitional oil-water pipe flow, PhD thesis, Norwegian University of Science and Technology.
- Schümann, H., Khatibi, M., Tutkun, M., Pettersen, B. H., Yang, Z. & Nydal, O. J. (2015), 'Droplet size measurements in oil–water dispersions: A comparison study using FBRM and PVM', *Journal of Dispersion Science and Technology* .
- Simmons, M. & Azzopardi, B. (2001), 'Drop size distributions in dispersed liquid–liquid pipe flow', *International Journal of Multiphase Flow* **27**(5), 843 – 859.
URL: <http://www.sciencedirect.com/science/article/pii/S0301932200000550>
- Skjefstad, H. & Stanko, M. (2017), 'Subsea water separation: a state of the art review, future technologies and the development of a compact separator test facility', *18th International Conference on Multiphase Technology* .
- Speight, J. G. (2014), 'The chemistry and technology of petroleum'.
- SUBPRO (2017), 'Subsea production and processing (SUBPRO)'. Accessed 09.11.17.
URL: <https://www.ntnu.edu/subpro/>
- Table, T.-V. (2018), 'T-value table'. Accessed 05.06.2018.
URL: <http://www.ttable.org/>
- Trallero, J., Sarica, C. & Brill, J. (1997), 'A study of oil-water flow patterns in horizontal pipes', *Society of Petroleum Engineers* **12**(03), 165 – 172.
- Van der Zande, M. J. & Van den Broek, W. (1998), 'Break-up of oil droplets in the production system'.
URL: <https://www.semanticscholar.org/paper/Break-up-of-Oil-Droplets-in-the-Production-System-Zande/9cdb8a4ca7f1f34db5c9adbddc93e920406107f5>
- Van der Zande, M. J. & Van den Broek, W. (1999), 'The effect of tubing and choke valve on oil-droplet break-up'.
URL: <https://www.semanticscholar.org/paper/The-Effect-of-Tubing-and-Choke-Valve-on-Oil-drople-Zande/7dc2ed1afa9868e20bbf275475903d79f8a559f6>
- Walsh, J. M. (2016), 'Savvy separator series: The effect of shear on produced water treatment'. Accessed 09.11.17.
URL: <https://www.spe.org/en/ogf/ogf-article-detail/?art=25>

Ward, J. P. & Knudsen, J. G. (1967), 'Turbulent flow of unstable liquid-liquid dispersions: Drop sizes and velocity distributions', *AIChE Journal* **13**(2), 356–365.

URL: <http://dx.doi.org/10.1002/aic.690130229>

Wheeler, A. J. (2010), 'Introduction to engineering experimentation'.

Xu, B., Liu, D., Xu, G., Zhang, X. & Bi, L. (2013), 'A measurement method for contact angle based on hough transformation', *Measurement* **46**(3), 1109 – 1114.

URL: <http://www.sciencedirect.com/science/article/pii/S0263224112003958>

Xu, J.-y., Li, D.-h., Guo, J. & Wu, Y.-x. (2010), 'Investigations of phase inversion and frictional pressure gradients in upward and downward oil-water flow in vertical pipes', *International Journal of Multiphase Flow* **36**(11), 930 – 939.

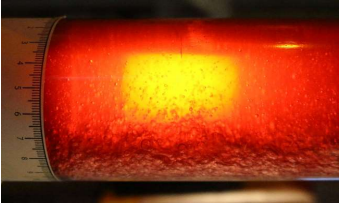
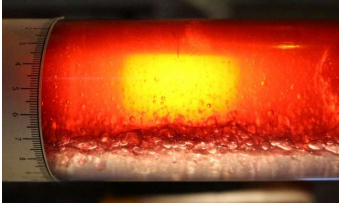
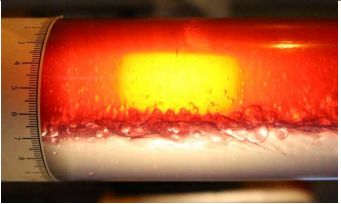
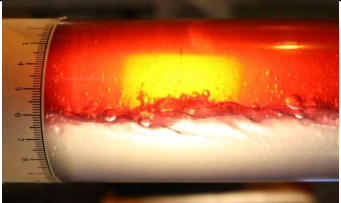





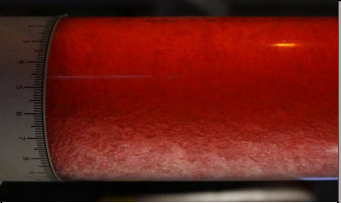


URL: <http://www.sciencedirect.com/science/article/pii/S0301932210001424>

Appendices

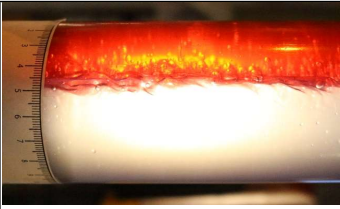

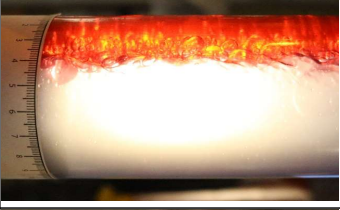




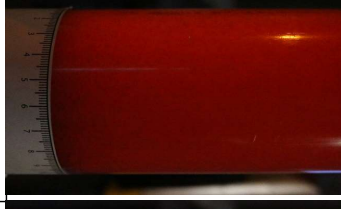


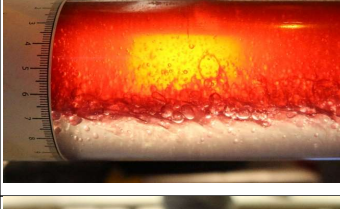

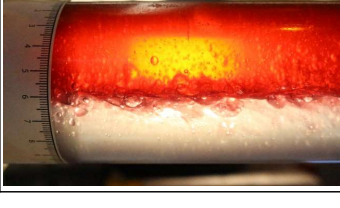

Appendix A: Pictures of Flow

An overview of the pictures that were taken for each test point when creating the flow pattern map are shown in this appendix. Pictures are from water cut range 10-90 and flow rate 250-700 L/min.

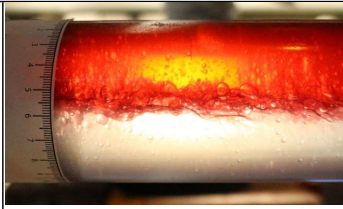





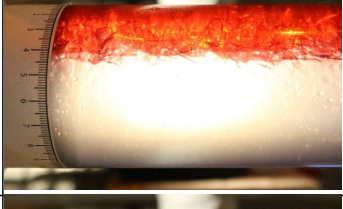

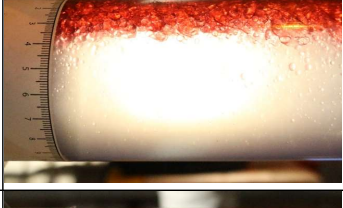

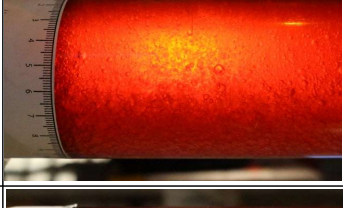



A. Images of the flow

Flow rate	Wc	Picture	Flow pattern
250	10		Dwo+O
250	20		SM
250	30		SM
250	40		SM
250	50		SM
250	60		SM
500	10		Dwo
500	20		Dwo
500	30		Dwo + Dow
500	40		Dwo + Dow
500	50		Dwo + Dow
500	60		Dwo + Dow











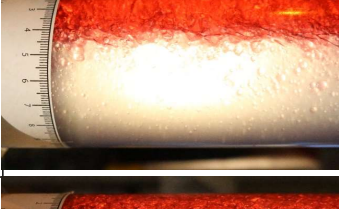

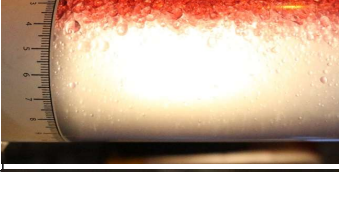

A. Images of he flow

250	70		SM	500	70		Dwo + Dow
250	80		SM	500	80		Dwo + Dow
250	90		Dwo + W	500	90		Dwo
300	10		Dwo+O	550	10		Dwo
300	20		Dwo + Dow	550	20		Dwo
300	30		SM	550	30		Dwo
300	40		SM	550	40		Dwo + Dow









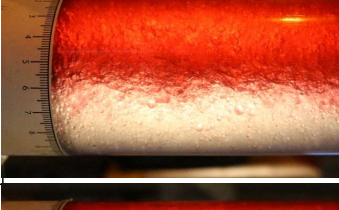

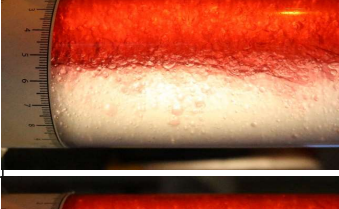



A. Images of he flow

300	50		SM	550	50		Dwo + Dow
300	60		SM	550	60		Dwo + Dow
300	70		SM	550	70		Dwo + Dow
300	80		SM	550	80		Dow
300	90		Dow + W	550	90		Dow
350	10		Dwo	600	10		Dwo
350	20		Dwo + Dow	600	20		Dwo













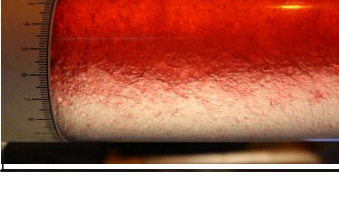

A. Images of he flow

350	30		Dwo + Dow	600	30		Dwo
350	40		Dwo + Dow	600	40		Dwo
350	50		Dwo + Dow	600	50		Dwo + Dow
350	60		Dwo + Dow	600	60		Dwo + Dow
350	70		Dwo + Dow	600	70		Dow
350	80		Dwo + Dow	600	80		Dow
350	90		Dow + W	600	90		Dow









A. Images of he flow

400	10		Dwo	650	10		Dwo
400	20		Dwo	650	20		Dwo
400	30		Dwo + Dow	650	30		Dwo
400	40		Dwo + Dow	650	40		Dwo
400	50		Dwo + Dow	650	50		Dwo
400	60		Dwo + Dow	650	60		Dow
400	70		Dwo + Dow	650	70		Dow

A. Images of he flow

400	80		Dwo + Dow	650	80		Dwo
400	90		Dwo	650	90		Dwo
450	10		Dwo	700	10		Dwo
450	20		Dwo	700	20		Dwo
450	30		Dwo + Dow	700	30		Dwo
450	40		Dwo + Dow	700	40		Dwo
450	50		Dwo + Dow	700	50		Dwo

A. Images of he flow

450	60		Dwo + Dow	700	60		Dow
450	70		Dwo + Dow	700	70		Dow
450	80		Dwo + Dow	700	80		Dow
450	90		Dow	700	90		Dow

Appendix B: User manuals

B.1 Matlab program

To start the program open the folder in Matlab and type in *guide* in the command window. Open the file *Droplet_GUI_V3.fig*. The program takes in a single picture or a series of pictures. The pictures have to be a *.bmp* file, named from 0 and up, with picture dimensions 680 x 512 pixels. To convert images to the right format and file type e.g. the program IrfanView can be used. All the pictures that are going to be analyzed have to lie in the same folder as the program. Before running the program different parameters can be changed like; type of edge fining method where Canny is the most powerful, but also uses a bit longer time. The fudge factor can be changed, which adjusts the threshold levels on the pictures. The line-fill factor will fill in gaps to complete incomplete edges. The sensitivity for each droplet size (which droplet sizes the program should recognize) can also be regulated. In addition, picture resolution ($\mu\text{m}/\text{pixel}$), weighting method and the number of bins can also be adjusted.

(Reference: Matlab routine user-guide.)

B.2 Edited part of the Matlab code

These lines is part of the edited code: Defining variables in line 123-129 before looping through the pictures. After finding the droplets the first time using Hough transformation, the code was edited in line 231-280. A matrix called CIRCLES_VECTOR is created, which consists of rows for each circle that were detected with columns [centre point x, centre point y, radius]. The code starts at the top row, and compares the radius of the droplet with all the rows below. If the criteria is met, the row of the smallest droplet is removed. This is done for each row, where in the end, all rows have been compared with each other. When the code has looped through all the rows, the final matrix is imported to a new matrix, CIRCLES_VEC_3. CIRCLES_VEC_3 is a 5000x4 matrix consisting of zeros, with columns [centre point x, centre point y, radius, image number]. The counts that keep track of which row that contain information in CIRCLES_VEC_3 is then

updated. With the new code, line 340 has to be removed. After looping through all the images, the empty rows consisting of zeros in matrix `CIRCLES_VEC_3` is deleted. The vector `CIRCLES` is then made, which consists of all the rows from `CIRCLES_VEC_3`, but only the three first columns. This is done in line 348-351. `CIRCLES` is used further in the code and reported on the interface in the end. Using the new code, line 353 can be removed, where in the original code the first row in `CIRCLES` is deleted. Line 362 - 412 consists of the code that first was tested, if this will be further edited. At the end, line 506-510 is used to display the wanted matrices in the excel sheet.

Appendix C: Matlab Code

This Appendix contains the Matlab codes that were used for modeling and calculations for this thesis work.

Section C.1 - The section of the Matlab routine that was edited and described in sec. 4.3.2

Section C.2 - Code to get matrix with data for different flow rates

Section C.3 - Log-Normal Distribution

Section C.4 - Upper-Limit Log-Normal Distribution

Section C.5 - Hinze and Brauner breakage models

Section C.6 - Droplet breakup over restrictions

C.1 Matlab routine that was edited

```

1      %-----Eddit code-----%
2      CIRCLES_VECTOR = [centers , radii]; % keep midpoints and add picture
          number
3      [Row_num,~] = size(CIRCLES_VECTOR);% number of rows for picture i
4      Rn = Row_num + Rn;                % updating the last row
5      temp_vec_vec = CIRCLES_VECTOR;    % creating a temporary matrix to
          update result
6      x=1;                               % defining first row in matrix
7      while x <= Row_num                 % looking through each row
8          y = x+1;
9          while y <= Row_num             % comparing with the other rows
10             Vec = sqrt((temp_vec_vec(y,1)-temp_vec_vec(x,1))^2+...
11                 (temp_vec_vec(y,2)-temp_vec_vec(x,2))^2);% distance
                  between points
12             if Vec < temp_vec_vec(x,3) || Vec < temp_vec_vec(y,3)% check
                  if vec is smaller than R1 or R2
13                 if temp_vec_vec(x,3) <= temp_vec_vec(y,3)
14                     temp_vec_vec(x,:) = []; % deleting R1
15                     y=x;
16                 elseif temp_vec_vec(x,3) > temp_vec_vec(y,3)
17                     temp_vec_vec(y,:) = []; % deleting R2
18                     y=y-1;
19                 end
20             [Row_num,~] = size(temp_vec_vec);
21         end
22         y=y+1;
23     end
24     x=x+1;
25 end
26 [Rows,~] = size(temp_vec_vec);
27 CIRCLES_VEC_3(Matrix_update:(Matrix_update+Rows-1),:) = ...
28     [temp_vec_vec , ones(Rows,1).*i]; % updating matrix
29 Matrix_update = Matrix_update + Rows;
30 Final = Matrix_update;                % start of empty rows
31 Row_hold = Rn+1;
32
33 %-----Kode 4 (not working)-----%
34 %     centers = temp_vec_vec(:,1:2);
35 %     radii = temp_vec_vec(:,3);
36 %     Bilde=ones(size(BWsdil));
37 %     figure('name','new_identified_circles','numbertitle','off'), imshow(
          Bilde);
38 %     elem1=size(Rows);
39 %     if elem1(1)==0
40 %     else
41 %         for c=1:elem1
42 %             rectangle('Position',[centers(c,1)-radii(c),centers(c,2)
          -radii(c),2*radii(c),2*radii(c)],'Curvature',[1,1],'FaceColor','k')
43 %         end
44 %     end
45 %     Bilde=getframe;
46 %     Bilde=rgb2gray(Bilde.cdata);
47 %     Bildeh=fspecial('disk',1);
48 %     Bilde=imfilter(Bilde,Bildeh);
49 %     figure, imshow(Bilde);
50 %-----%

```

C.2 Function to get data from flow rates

```
1 function matrix = values(Q)
2 % [30 bottom, 70 bottom, 30 top, 70 top]
3     switch Q
4         case 250
5             load ('Q250.mat')
6             matrix = Q250';
7         case 300
8             load ('Q300.mat')
9             matrix = Q300';
10        case 350
11            load ('Q350.mat')
12            matrix = Q350';
13        case 400
14            load ('Q400.mat')
15            matrix = Q400';
16        case 450
17            load ('Q450.mat')
18            matrix = Q450';
19        case 500
20            load ('Q500.mat')
21            matrix = Q500';
22        case 550
23            load ('Q550.mat')
24            matrix = Q550';
25        case 600
26            load ('Q600.mat')
27            matrix = Q600';
28        case 650
29            load ('Q650.mat')
30            matrix = Q650';
31        case 700
32            load ('Q700.mat')
33            matrix = Q700';
34     end
35 end
```

C.3 Log-Normal Distribution

```

1  Q = 300; % The wanted test flowrate
2  mat = values(Q); % [30 bottom, 70 bottom, 30 top, 70 top]
3  b_wc30 = sort(mat(1,:)); % Water cut 30 in bottom pipe
4  b_wc70 = sort(mat(2,:)); % Water cut 70 in bottom pipe
5  t_wc30 = sort(mat(3,:)); % Water cut 30 in top pipe
6  t_wc70 = sort(mat(4,:)); % Water cut 70 in top pipe
7  % Deleting NaN values
8  b_wc30(isnan(b_wc30)) = [];
9  b_wc70(isnan(b_wc70)) = [];
10 t_wc30(isnan(t_wc30)) = [];
11 t_wc70(isnan(t_wc70)) = [];
12 %-----Calculations-----%
13 Q_test = b_wc30; % Test point
14 WC = '30-b'; % To create right figure name
15
16 k = length(Q_test);
17 D32 = sum(Q_test.^3)/sum(Q_test.^2); % Sauter mean
18 D43 = sum(Q_test.^4)/sum(Q_test.^3); % De Brouckere mean
19 SD = sqrt(log(D43/D32)); % Sigma/width of distribution
20 b = 3; % 0,1,2,or 3 for the volume, surface
21 %%% ,diameter, or number-weighted
22 D0 = ((D32*D43)^0.5)*(D32/D43)^b; % Reference diameter
23 xlog = logspace(1,3,15); % To create log scale
24 lnf = zeros(1,500); % Log-normal function
25
26 for i =1:k
27     lnf(i) = (1/(SD*sqrt(2*pi)*Q_test(i)))*...
28         exp(-((log(Q_test(i)/D0))^2/(2*SD^2)));
29 end
30 %-----Plotting figures-----%
31 figure('Name',[ 'Q', num2str(Q), ' WC', WC], 'NumberTitle', 'off');
32 yyaxis left
33 histogram(Q_test, xlog)
34 ylabel('Number of Droplets')
35 hold on
36 yyaxis right
37 plot(Q_test, lnf)
38 ylabel('Frequency [-]')
39 hold off
40 set(gca, 'xscale', 'log')
41 xlabel('Droplet Diameter in Microns')
42 legend('Real values', 'Log-Normal')
43 set(gca, 'FontSize', 14)

```

C.4 Upper-Limit Log-Normal Distribution

```

1  Q = 300; % The wanted test flowrate
2  mat = values(Q); % [30 bottom, 70 bottom, 30 top, 70 top]
3  b_wc30 = sort(mat(1,:)); % Water cut 30 in bottom pipe
4  b_wc70 = sort(mat(2,:)); % Water cut 70 in bottom pipe
5  t_wc30 = sort(mat(3,:)); % Water cut 30 in top pipe
6  t_wc70 = sort(mat(4,:)); % Water cut 70 in top pipe
7  % Deleting NaN values
8  b_wc30(isnan(b_wc30)) = [];
9  b_wc70(isnan(b_wc70)) = [];
10 t_wc30(isnan(t_wc30)) = [];
11 t_wc70(isnan(t_wc70)) = [];
12 %-----Calculations-----%
13 Q_test = b_wc30; % Wanted test point
14 WC = '30-b'; % To create right figure name
15 k = length(Q_test); % Length of test vector
16 k_plot = k-1; % Length of lnf and plot vector
17
18 %Vectors
19 lnf = zeros(1,k); % Log-normal function
20 v = zeros(1,k); % Cumulative distribution
21 z = zeros(1,k);
22
23 %Finding volume weighted vectors
24 weight_sum = sum((pi/6)*Q_test.^3); % Total weight of all vectors
25 Q_weight = (pi/6)*Q_test.^3; % Volume weighted vector
26
27 %%%-----Finding values using Mugele(1951)-----%%
28 for j = 1:k
29     v(j) = (sum(Q_weight(1:j))/weight_sum); % To get 100v multiply with
30     100
31 end
32 %-----Plot to find the best fit equation-----%
33 figure('Name',[ 'Q = ',num2str(Q), ' ', WC = ',WC'], 'NumberTitle','off');
34 scatter(Q_test,100.*v)
35 ylabel('100v')
36 xlabel('diameter') % Label when plotting 100v vs diameter
37 set(gca,'FontSize',14)
38 hline = reline([0 90]);
39 hline.Color = 'r';
40 legend('Data points','D90')
41 %-----Calculating values-----%
42 % Change the last number in equation "pol" for another degree fit
43 % Calculating percentiles
44 pol = polyfit(Q_test(1:k),100*v,3); % Returns coefficients from function
45 D10 = fsolve(@(x) pol(1)*x^3+pol(2)*x^2+pol(3)*x+pol(4)-10,100);
46 D50 = fsolve(@(x) pol(1)*x^3+pol(2)*x^2+pol(3)*x+pol(4)-50,100);
47 D90 = fsolve(@(x) pol(1)*x^3+pol(2)*x^2+pol(3)*x+pol(4)-90,100);
48
49 % Other values
50 Dmax = max(Q_test); % Fom measurements
51 D32 = sum(Q_test.^3)/sum(Q_test.^2); % Fom measurements
52 dmax = D50*((D50*(D90+D10)-(2*D90*D10))/(D50^2-D90*D10)); % Calculated
53 a_dmax = (dmax-D50)/D50;
54 v90 = D90./(dmax-D90);
55 v50 = D50./(dmax-D50);
56 delta = 0.394/log10(v90/v50);
57 d32 = dmax/(1+a_dmax*exp(1/(4*delta^2))); % Calculated

```

C.4. Upper-Limit Log-Normal Distribution

```

57
58 for o = 1:k
59     z(o) = log((a_dmax*Q_test(o))/(dmax-Q_test(o)));
60 end
61 for i =1:k_plot
62     lnf(i)= 1-(0.5*(1-erf(delta*z(i))));% Cumulative volume fraction
63 end
64 %-----Compare calculated values with real values-----%
65 % d90 = Q_test(round(k*0.90)); % Test to see how it varies with "real"
66 % d10 = Q_test(round(k*0.10));
67 % a_Dmax = (Dmax-D50)./D50; % a-parameter using real Dmax
68 %-----Calculating errors-----%
69 error_graph =sum(abs((lnf-v)./v))/k;% Finding average error
70 error_dmax = 100*(dmax-Dmax)/Dmax; % Error for how Dmax vary from dmax
71 error_d32 = 100*(d32-D32)/D32; % Error for how D32 vary from d32
72
73 %Printing the results%
74 sprintf(['Average error graph = ',num2str(error_graph),' for test Q' ,...
75         num2str(Q), ' WC', num2str(WC)])
76 sprintf(['Error dmax = ',num2str(error_dmax),' percent for test Q=' ,...
77         num2str(Q), ' WC=', num2str(WC)])
78 sprintf(['Error d32 = ',num2str(error_d32),' percent for test Q=' ,...
79         num2str(Q), ' WC=', num2str(WC)])
80 %-----Plotting figures-----%
81 figure('Name',[ 'Q', num2str(Q), ' ', WC', num2str(WC) ] ,...
82        'NumberTitle','off');
83 plot(Q_test(1:k_plot),lnf(1:k_plot))% Plots Droplet D vs function(cdf)
84 hold on
85 plot(Q_test(1:k_plot),v(1:k_plot)) % Plots diameter vs volume fraction d<x
86 legend('ULLN','real')
87 xlabel('Droplet Diameter in Microns')
88 ylabel('Cumulative volume fraction')
89 set(gca,'FontSize',14)
90 set(gca,'xscale','log')

```

C.5 Hinze and Brauner breakage models

```

1 Q = 300; % The wanted test flowrate [L/min]
2 mat = values(Q); % [30 bottom, 70 bottom, 30 top, 70 top]
3 b_wc30 = sort(mat(1,:)); % Water cut 30 in bottom pipe
4 b_wc70 = sort(mat(2,:)); % Water cut 70 in bottom pipe
5 t_wc30 = sort(mat(3,:)); % Water cut 30 in top pipe
6 t_wc70 = sort(mat(4,:)); % Water cut 70 in top pipe
7 % Deleting NaN values
8 b_wc30(isnan(b_wc30)) = [];
9 b_wc70(isnan(b_wc70)) = [];
10 t_wc30(isnan(t_wc30)) = [];
11 t_wc70(isnan(t_wc70)) = [];
12 %-----Parameters to cahnge-----%
13 Q_test = b_wc30; % Test point
14 T = 18.40; % Test temperature
15 WC = 0.30; % Water cut to test. Contionous phase:
16 %%% Oil = WC30, water = WC70
17 %-----Calculating-----%
18 q_m = Q/(1000*60); % Mixed flow rate [m^3/s]
19 rho_w = -0.004*T^2-0.11*T+1025.4; % Density of water [kg/m3]
20 rho_o = -0.732*T+806.29; % Oil density [kg/m3]
21 visc_o = 1.4095*10^-3; % Oil viscosity 10^-3[cP]->[kg/m*s]
22 visc_w = 0.9934*10^-3; % Water viscosity 10^-3[cP]->[kg/m*s]
23 sigma = 11.41*10^-3; % Interfacial tension[mN/m] --> 10^-3N/m
24 D = 67.8*10^-3; % Diameter of pipe [m]
25 Ch = 1; % Constant
26 A = pi*(D/2)^2; % Area of pipe [m2]
27
28 if WC == 0.30 %Oil contionous
29 rho_c = rho_o; % Density contonous phase[kg/m3]
30 u_c = q_m/A*(1-WC); % Speed of oil in the system [m/s]
31 eta_c = visc_o; % Viscosity continous [kg/m*s]
32 Cf = 4.154e7; % 4.154e7 3.403 57.1e1 6.642e4 2.617
33 n = 1.867; % 1.867 0.667 1.066 1.579 0.738
34 elseif WC == 0.70 %Water contionous
35 rho_c = rho_w; % Density contonous phase[kg/m3]
36 u_c = q_m/A*WC; % Speed of water in the system [m/s]
37 eta_c = visc_w; % Viscosity continous [kg/m*s]
38 Cf = 9.078e7; % 9.078e7 1.786e1 6.677e1 1.287e3 4.828e4
39 n = 1.822; % 1.822 0.658 0.834 1.177 1.401
40 end
41 %-----Calculations-----%
42 format long g % Displays without potential
43 dmax_real = max(Q_test); % Dmax from measured data [microns]
44 We = rho_c*u_c^2*D/sigma; % Weber number
45 rho_m = rho_w*WC + rho_c*(1-WC); % Mixture density
46 Re_m = rho_m*u_c*D/eta_c; % Reynolds number for mixed fluid
47 f = Cf*Re_m^-n; % Friction factor
48 %-----Calculate dmax [m]-----%
49 dmax_hinze = (0.55*We^-0.6*f^-0.4*D)*10^6; % [microns]
50 dmax_brauner = (2.22*Ch*We^-0.6*(rho_m*f/(rho_c*(1-WC)))^-0.4*...
51 (WC/(1-WC))^0.6)*10^6; % [microns]
52 %-----Calculating errors-----%
53 error_h = (dmax_hinze-dmax_real)*100/dmax_real; % Error using Hinze [%]
54 sprintf(['Hinze error is ',num2str(error_h),...
55 ' prosentag larger/smaller than the real'])
56 error_b = (dmax_brauner-dmax_real)*100/dmax_real;% Error using Brauner[%]
57 sprintf(['Brauner error is ',num2str(error_b),...

```

58 ' prosentag larger/smaller than the real '])

C.6 Droplet breakup over restrictions

```

1  %-----Input data-----%
2  p      = 25;                % Pressure to test [mbar]
3  IFT    = 11.41*10^-3;      % 10^-3[mN/m] -> [N/m] = [kg/s^2]
4  T      = 22;                % Test temperature
5  rho_w  = -0.004*T^2-0.11*T+1025.4;% Water density
6  rho_o  = -0.732*T+806.29;  % Oil density
7  rho_c  = rho_o;            % Density contonous phase(oil)[kg/m3];
8  DP_perm = p*100;           % 100 [mbar] -> 1 [Pa] = [kg/m*s^2]
9  D_pipe = 67.8*10^-3;       % Diameter of pipe 10^-3 [mm] ->[m]
10 U_mix  = 100;              % Mixed flow velocity [m/s]
11 Dx_perm = 2.5*D_pipe;      % Length of orfice zone [m]
12 D0     = 10.65*10^-3;      % Orifice opening diameter 10^-3[mm]->[
    m]
13 Up     = U_mix*(D_pipe/D0)^2; % Mean velocity in the pipe [m/s]
14 %-----Calculations-----%
15 E = (DP_perm*Up)/(rho_c*Dx_perm); % Average Energy dissipation [m^2/s^3]
16 dmax = (IFT/rho_c)^0.6*E^(-0.4)*10^6;% Maximum diameter 10^-6[m]->[microns
    ]
17 disp(['dmax = ',num2str(dmax), ' microns for test DP = ',num2str(p)])

```


Appendix D: Density experiment

Tests were performed in the Reservoir lab at NTNU to find how the density varied with temperature for the oil and distilled salt water. The samples were taken from the rig on the date 24-01-18.

Method

Tests were performed by measuring the densities at four different temperatures for both the oil and water solution. Tests were executed using a pycnometer with a thermometer, see Fig. D.0.1. The empty pycnometer with the thermometer was put on a scale and the scale was tared. The pycnometer was taken off the scale, filled with liquid and the outside was dried before putting it back on the scale. The measured weight, and temperature of the liquid were recorded. Since the same pycnometer was used, the volume the pycnometer contains was the same for all tests = 50.006 cm^3 . To regulate the temperature of the liquid, the liquid was put in a water bath to get a desired temperature.



Figure D.0.1: Pycnometer filled with oil

Results and discussion

The results of how the density varied with temperature can be seen in Table D.0.1. From the results one can see that it can not be found a linear approximation for how the density change with temperature. The method of measurement is not accurate enough.

Table D.0.1: Results from density measurements

Temp.[°C]	Weight [g]	Density [kg/m ³]
Water		
17.4	51.048	1020.08
20.6	51.071	1021.30
24.4	51.054	1020.96
24.9	51.031	1020.50
Oil		
18.8	40.196	803.82
21.4	39.469	789.29
23.2	40.114	802.18
24.8	40.258	805.06

Errors

The temperature has a reading error of about $\pm 0.2^\circ\text{C}$, due to very small lines on the thermometer. The scale has a error of ± 0.001 g. There are also some errors if the equipment are not fully dried, so some small droplets might be in the pycnometer, or not all the liquid has been dried of the glass. The scale did not stabilize for a long time when the filled pycnometer was put back on, so it was difficult to read of the weight and get an accurate result.

Appendix E: PDF's

This Appendix contains different kinds of PDFs.

Section E.1 - Risk Assessment performed on the compact inline separator before experiments were started

Section E.2 - Hagenbach constant

Section E.3 - Technical drawings of PVM camera mount made by Noralf Vedvik

Section E.4 - Manufacturer's certificate for capillary viscometer

E.1 Risk Assessment

NTNU	Risikovurdering			Utarbeidet av	Nummer	Dato
				HMS-avd.	HMSRV2603	22.03.2011
HMS				Godkjent av		Erstatter
				Rektor		01.12.2006

Enhet: Forsøkshall

Linjeleder: Erlend Våtevik

Deltekere ved kartleggingen (m/ funksjon): Milan Stanko, Ellen Kristine Ellertsen, Håvard Slettajøll Skjefstad
(Ansv. veileder, student, evt. medveileder, evt. andre m. kompetanse)

Risikovurderingen gjelder hovedaktivitet: Ellen Kristine Ellertsen, Masteroppgave: Experimentental study o finline oil-water separation in pipe

Signaturer: Ansv.veileder: 

Student: 

Dato: 12.09.17

ID nr	Aktivitet fra kartleggings-skjemaet	Mulig uønsket hendelse/ belastning	Vurdering av sannsynlighet (1-5)	Vurdering av konsekvens:				Risiko-Verdi (menneske)	Kommentarer/status Forslag til tiltak
				Menneske (A-E)	Ytre miljø (A-E)	Økt/ materiell (A-E)	Om-dømme (A-E)		
1	Arbeid i høyden	Falle ned trapp, 2,5 m	3	B	A	A	A	GUL	Sette opp skilt, holde i rekkværk
2	Støy i labb	Blir sliten, øreproblemer, miste hørselen	3	B	A	A	A	GUL	Bruke hørselsvern ved støy
3	Lekasje olje	Skli på olje	2	A	A	A	A	GRØNN	Utstyr for å vaske, makere områder med søl, grav
3	Lekkasje olje	Innhalere, svimmelhet hodepine	2	A	B	A	A	GRØNN	Ha ventilasjon, <i>maske</i>
3	Lekkasje olje/vann	Sprut i øyne og irritert hud	2	A	B	A	A	GRØNN	Bruke briller, ha tilgjengelig øyeksyllingsvann, <i>maske</i>
4	Brannfare	Lekk olje kan starte å brenne	2	C	C	B	B	GUL	Ha brannslukking, alarm tilgjengelig
5	Høy temperatur på utstyr	Små brannskader på hud	2	B	A	A	A	GRØNN	Markere utstyr som blir varmt, kann berøre med varmesikkert beskyddelsesutstyr

NTNU	Kartlegging av risikofylt aktivitet			Utarbeidet av	Nummer	Dato
				HMS-avd.	HMSRV2601	22.03.2011
HMS				Godkjent av		Erstatler
				Rektor		01.12.2006

Enhet: Forsøkshall

Linjeleder: Erlend Våtevik

Deltakere ved kartleggingen (m/ funksjon): Milian Stanko (veileder), Ellen Kristine Ellertsen (student), Håvard Slettahjell Skjefstad (PhD)
(Ansv. veileder, student, evt. medveiledere, evt. andre m. kompetanse)

Kort beskrivelse av hovedaktivitet/hovedprosess: Masteroppgave: Experimentel study o finline oil-water separation in pipe

Er oppgaven rent teoretisk? (JA/NEI): NEI «JA» betyr at veileder innestår for at oppgaven ikke inneholder noen aktiviteter som krever risikovurdering. Dersom «JA»: Beskriv kort aktiviteten i kartleggingskjøremat under. Risikovurdering trenger ikke å fylles ut.

Signaturer: Ansv. veileder:  Student: Ellen Kristine Ellertsen

Dato: 12.09.17

ID nr.	Aktivitet/prosess	Ansv. ansvarlig	Eksisterende dokumentasjon	Eksisterende sikringstiltak	Lov, forskrift o.l.	Kommentar
1	Arbeide i høyden	Student + andre i labben				Sette på skilt ved trapp
2	Støy i labben	Student + andre i labben		Høreklodder	Lov for støy, kapp. 2	Ta på hørselvern
3	Lekasje	Student + andre i labben		Briller, værneklær, værne sko, øyeskyling, grav for olje	Kap. 3 arbeid med kjemikalier	Bruke værnebriller, øyeskyling, Grav så olje ikke renner rundt, utstyr for vaske opp, masker
4	Brannfare	Student + andre i labben		Brannvarsler, slukningsutstyr		Ha tilgang på slukningsutstyr
5	Høye temp. på utstyr?	Student + andre i labben		Varmesikre hansker, beskyttende klær		Merke utstyr som blir varmt, bruk varmebeskyttende utstyr

E.2 Hagenbach constant

Tabelle der Hagenbach-Korrekturen für:

Viskosimeter nach Cannon-Fenske

Steigrohrviskosimeter,
Typ-Nr. 511..., 519..

Korrektionssekunden¹:

Table of Hagenbach corrections for:

Viscometers Cannon-Fenske

Reverse-Flow Viscometers,
Type No.: 511..., 519..

Correction seconds¹:

Tableau de la correction Hagenbach pour:

Viscosimètres selon Cannon-Fenske

Viscosimètres à tube ascendant,
No. de réf.: 511..., 519..

Secondes de correction¹:

Durchflußzeit (s) Flow time (s) Durée de passage (s)	<i>Vi benigne</i> 25	50	Kapillare Nr. / Capillary No. / Tube capillaire No.	75	100	150
50	(4,61)*	(2,11)*	0,66	0,24	0,06	—
60	(3,20)*	1,46	0,46	0,16	0,04	—
70	(2,35)*	1,07	0,34	0,12	0,03	—
80	(1,80)*	0,82	0,26	<u>0,10</u>	0,02	—
90	1,42	0,65	0,20	0,07	—	—
100	1,15	0,53	0,16	0,06	—	—
110	0,95	0,43	0,14	0,05	—	—
120	0,80	0,37	0,11	0,04	—	—
130	0,68	0,31	0,10	0,03	—	—
140	0,59	0,27	0,08	0,03	—	—
150	0,51	0,23	0,07	0,03	—	—
160	0,45	0,21	0,06	0,02	—	—
170	0,40	0,18	0,06	—	—	—
180	0,36	0,16	0,05	—	—	—
190	0,32	0,15	0,04	—	—	—
200	0,29	0,13	0,04	—	—	—
220	0,24	0,11	—	—	—	—
240	0,20	0,09	—	—	—	—
260	0,17	0,08	—	—	—	—
280	0,15	0,07	—	—	—	—
300	0,13	0,06	—	—	—	—
350	0,09	0,04	—	—	—	—
400	0,07	0,03	—	—	—	—

* Für Präzisionsmessungen sollten die in Klammern stehenden Korrektionssekunden nicht zur Anwendung kommen. Gegebenenfalls ist ein Viskosimeter mit einer engeren Kapillare zu verwenden.

* For precision measurements the correction seconds stated in parentheses should not be applied. A selection of a viscometer with a smaller capillary diameter is suggested.

* Les secondes de correction entre parenthèses ne sauraient être utilisées pour les mesures de précision. Le cas échéant, il est à utiliser un viscosimètre avec un tube capillaire d'un diamètre plus petit.

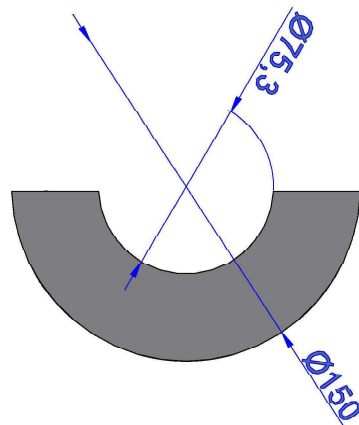
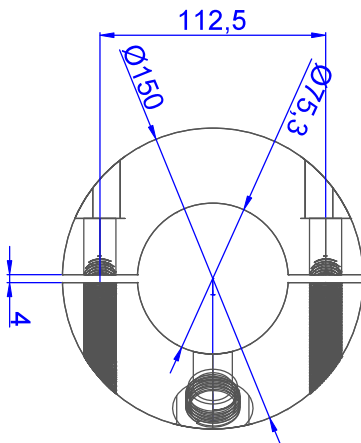
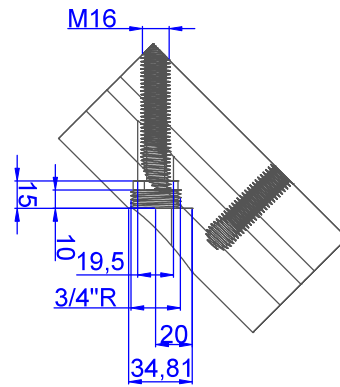
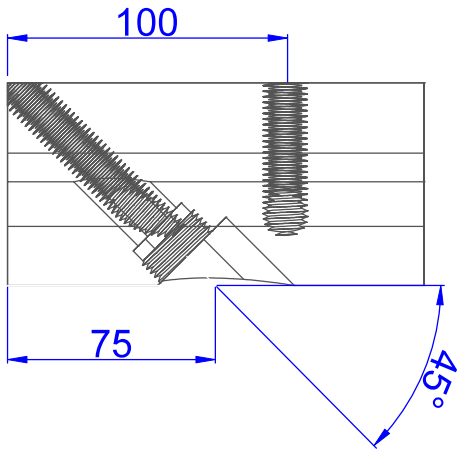
¹ Die angegebenen Korrektionssekunden beziehen sich auf die jeweilige Soll-Konstante.

¹ The correction seconds stated are related to the respective theoretical constant.

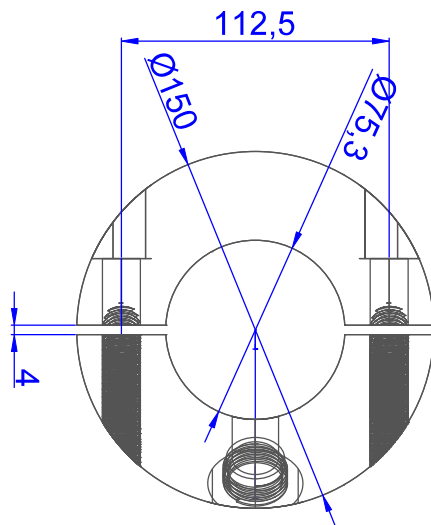
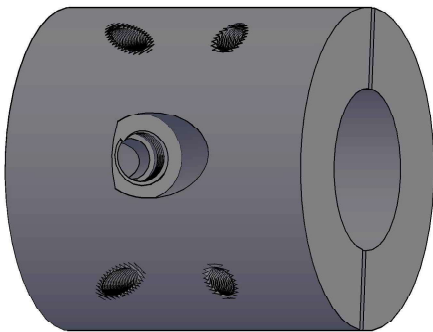
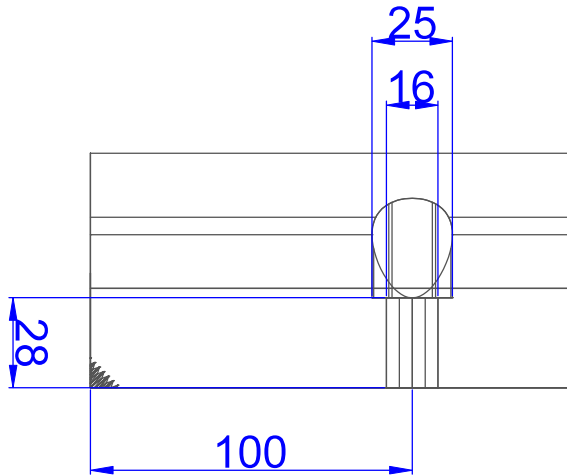
¹ Les secondes de correction indiquées se réfèrent à la constante théorique respective.

Typ-Nr. Typ-Nr. No. de ref.	Kapillare Nr. Capillary No. Tube capillaire No.	Kapillare Ø l (mm) Capillary I. D. (mm) Tube capillaire Ø int. mm	Konstante K (Richtwert) Constant K approx. Constante K environ	Meßbereich mm ² /s (cSt) (Richtwert) Measuring range mm ² /s (cSt) approx. Limites de mesure mm ² /s (cSt) environ
... 00	25	0,31	0,002	0,4 bis/to/à 1,6
... 03	50	0,42	0,004	0,8 bis/to/à 3,2
... 01	75	0,54	0,008	1,6 bis/to/à 6,4
... 10	100	0,63	0,015	3 bis/to/à 15
... 13	150	0,78	0,035	7 bis/to/à 35
... 20	200	1,02	0,1	20 bis/to/à 100
... 23	300	1,26	0,25	50 bis/to/à 200
... 21	350	1,48	0,5	100 bis/to/à 500
... 30	400	1,88	1,2	240 bis/to/à 1200
... 33	450	2,20	2,5	500 bis/to/à 2500
... 40	500	3,10	8	1600 bis/to/à 8000
... 43	600	4,00	20	4000 bis/to/à 20000

E.3 Camera mount



E.3. Camera mount



E.4 Capillary Viscometer Certificate

Translation of the legally binding german version.

Traduction de la version allemande légale.

MANUFACTURER'S CERTIFICATE FOR CAPILLARY VISCOMETER

(Manufacturer's certificate M according to
DIN 55 350, Part 18)

CERTIFICAT DU FABRICANT ET TUBE VISCOSIMETRIQUE CAPILLAIRE

(Certificat du fabricant M selon DIN 55 350, Partie 18)

Subject: Cannon-Fenske reverse flow viscometer for opaque liquids for the determination of the kinematic viscosity according to ISO/DIS 3105, ASTM D 2515/D and NF T 60-100.

Objet: Viscosimètre Cannon-Fenske type à écoulement inversé pour liquides opaques pour la détermination de la viscosité cinématique selon ISO/DIS 3105, ASTM D 2515/D et NF T 60-100.

Manufacturer: SI Analytics GmbH, Mainz

Fabricant: SI Analytics GmbH, Mainz

Viscometer: Type and capillary no.: 511 03 / 50
Apparatus no.: 1060755

Viscosimètre: No. de type et de capillaire: 511 03 / 50
No. d'appareil: 1060755

This viscometer is suitable to determine the kinematic viscosity of newtonian liquids according to ISO/DIS 3105, Annex C. The viscometer constants K_1 and K_2 refer to the timing marks during the visual survey of the meniscus passage. They come to

Ce viscosimètre est approprié pour la détermination de la viscosité cinématique de liquides newtoniens selon ISO/DIS 3105, Annex C. Les constantes K_1 et K_2 sont valables pour des index rotatifs avec une saisie visuelle du passage du ménisque. Elles sont de

$$K_1 = 0,003771 \text{ mm}^2/\text{s}^2$$

$$K_2 = 0,002763 \text{ mm}^2/\text{s}^2.$$

They were determined by using comparative measurements with reference viscometers, of which the constants were determined at the Physikalisch-Technischen Bundesanstalt, D-38116 Braunschweig.

Elles ont été déterminées par des mesures de comparaison avec des viscosimètres étalons dont les constantes ont été déterminées auprès de la Physikalisch-Technischen Bundesanstalt, D-38116 Braunschweig.

The instrument constants K_1 and K_2 are valid for liquids with a surface tension of 20 to 30 mN/m and an acceleration of the fall of 9.8105 m/s². For temperatures up to 100 °C it is not required to pay attention to the heat expansion of the viscometer. The kinematic viscosity ν within mm²/s of liquids can be calculated using the instrument constants in the equation:

Les constantes K_1 et K_2 de l'instrument sont valables pour des liquides avec une tension de surface de 20 à 30 mN/m et avec une accélération de la pesanteur de 9.8105 m/s². Dans le cas de températures jusqu'à 100 °C, il n'est pas nécessaire de tenir compte de la dilatation thermique du viscosimètre. La viscosité cinématique ν en mm²/s de liquides peut être calculée à l'aide des constantes de l'instrument selon l'équation:

$$\nu = K_1 \cdot t_1,$$

$$\nu = K_2 \cdot t_2,$$

whereby t_1 and t_2 are the flow times in seconds which were corrected -if necessary- according to ISO/DIS 3105, Part 6.2.

t_1 et t_2 sont les temps d'écoulement en secondes qui ont été corrigés -si nécessaire- selon ISO/DIS 3105, Partie 6.2.

The relative uncertainty of the mentioned numerical values of K_1 and K_2 comes to 1,2 % at a confidence level of 95 %.

L'insécurité relative des valeurs numériques de K_1 et K_2 indiquée est de 1,2 % dans le cas d'un niveau de confiance de 95 %.

It is required to check the instrument constants in regular intervals. In particular any change to the viscometer, for example when using liquids that corrode glass or a glass blowing repair took place, makes a new determination of the instrument constants absolutely necessary.

Il est nécessaire de contrôler les constantes de l'instrument en intervalles réguliers. Une nouvelle détermination des constantes de l'instrument devient absolument nécessaire lors de toute modification du viscosimètre, par exemple, en raison de l'utilisation de liquides qui attaquent le verre, ou dans le cas de réparations par un souffleur de verre.

SI Analytics GmbH, Hattenbergstraße 10, D-55122 Mainz

This certificate was prepared mechanically and is valid without signature.

Ce certificat a été établi mécaniquement et est valable sans signature.

The document may only be duplicated if no changes were

Le document ne peut être reproduit que sans correction.